Augmented Taylor-Hood Elements for Incompressible Flow

Masterarbeit im Studiengang „Mathematik"

Institut für Numerische und Angewandte Mathematik
Georg-August-Universität Göttingen

vorgelegt von

Daniel Arndt

Betreuer:

Prof. Dr. Gert Lube

Zweitgutachter:

Dr. Timo Heister

Göttingen, den 11. März 2013

Contents

List of Figures

List of Tables

Introduction

In this thesis we examine an augmented Taylor-Hood element on quadrilateral or hexahedral meshes. This modification consists in adding elementwise constant functions to the pressure space. We want to understand the resulting finite element pair in terms of stability, mass conservation and performance. In particular we analyze the behavior when applied to incompressible flow, namely the Stokes and Navier-Stokes equations.

Motivation

The flow of fluids is a omnipresent phenomenon in our environment and daily life. Physically these motions are governed by the Navier-Stokes equations. They are for example used for forecasting the weather, calculating storm damages in forests, water flows or in the construction of the wings of airplanes.

In many cases the considered fluid can be assumed to be incompressible. This means that the the material density remains constant within a parcel of fluid which moves with the fluid velocity. A mathematical equivalent is that the divergence of the velocity vanishes due to the conservation of mass. In this thesis we consider the resulting incompressible Navier-Stokes equations and in a previous step the Stokes equations as a simplification for the situation when advective forces are negligible compared to viscous forces. In particular, we are interested in the influence of the incompressibility constraint on numerical results.

In a finite element approach all the equations are only stated in a weak formulation. Although on a continuous level this equivalent, the discretized formulation does not imply that the numerical velocity solution is pointwise solenoidal. Nevertheless, the construction of many discretizations for incompressible flow problems relies on this property. For that reason it is desirable to fulfill this requirement at least locally. This can be ensured by choosing a discrete pressure ansatz space containing elementwise constant functions. In particular in this case the approximation space is discontinuous.

In many flow problems solutions with discontinuous pressure occur, e.g. two-phase flows. In the so-called continuum surface force model [BKZ92] the right-hand side is discontinuous in the resulting Navier-Stokes equation along the interface of the phases. This leads to a discontinuous pressure solution with poor interpolation accuracy whenever the finite element interpolants are continuous across the interface. Thus, a discontinuous pressure ansatz space combined with a mesh that is aligned along the interface improves the results much [GR07].

Outline

First of all in Section 1 we define finite element methods and state the assumptions that we want to impose on the triangulation. Furthermore, we define the polynomial spaces that are used for the approximation in this thesis.

Section 2 is then devoted to the Stokes problem. We extend the inf-sup stability of the pair $\mathcal{P}_{k+1}/(P_k + P_0)$ on simplicial meshes (proved by Boffi et al. in [BCGG12]) to our element pair on quadrilateral and hexahedral meshes in space dimensions $d = 2, 3$. Afterwards we obtain some convergence results and confirm the optimality numerically. Finally, we discuss our implementation into the finite element library `deal.II`.

We construct suitable methods for solving a Poisson equation using the element $(\mathcal{Q}_k + \mathcal{Q}_0)$ in Section 3. This kind of problem often occurs when one discretizes incompressible flow problems. In this thesis we need the result for constructing a preconditioner for the Navier-Stokes problem.

Finally, the full incompressible Navier-Stokes equations are considered in Section 4. We state the details of our implementation and especially discuss the construction of a suitable preconditioner. A channel flow is considered as testcase and the resulting statistics are compared with reference data using a turbulence model by Verstappen.

1 Finite elements

The *finite element method* (FEM) is a special version of Ritz-Galerkin method that is characterized by the following properties:

- The domain Ω is divided into polyhedral fragments called elements.

- The numerical solution is a linear combination of ansatz functions with support on few of these elements.

- In order to obtain the numerical solution the problem has to be stated in a variational (or weak) formulation.

In [Giv01] the finite element method is declared to one of the top 10 algorithms of the 20th century in computational mechanics and thus one of the most used techniques for numerically solving partial differential equations.
We use this technique in order to approximate the solution of the considered incompressible flow problems.

The following mathematical description of finite elements is based on [GR86, p. 95-109].

Definition 1.1 (Finite element)**.** A *finite element* is a triple $(K, \mathcal{P}, \Sigma_K)$ satisfying

- $K \subset \mathbb{R}^n$ is a closed, convex, polyhedral set with a Lipschitz-continuous subset and $\operatorname{meas}(K) \neq 0$.

- The space of shape functions $\mathcal{P}_K$ is finite dimensional linear function space with dimension d on K.

- The set of degrees of freedom (dofs) Σ_K consists of d linear independent functionals $\sigma_i, i = 1, \ldots, d$ on $\mathcal{P}_K$. Each $p \in \mathcal{P}_K$ is uniquely determined by the d values $\sigma_i(p), i = 1, \ldots, d$.

1.1 Triangulation

For the construction of finite elements spaces we need a decomposition of the domain Ω into finite elements. In this thesis the triangulations consist either of triangular or quadrilateral resp. hexahedral elements. In order to classify certain types of decompositions of Ω we define on each element K the quantities h_K, ρ_K and σ_K by

$$h_K = \inf\{\operatorname{diam}(B), B \subset K \text{ is a ball}\}$$

$$
\rho_K = \begin{cases} \sup\{\operatorname{diam}(B), B \supset K \text{ is a ball}\} & \text{simplicial triangulation } \mathcal{T}_h \\[2ex] 2 \min_{1 \le i \le 2^d} \sup\{\operatorname{diam}(B), B \supset S_i \text{ is a ball}\} & \begin{array}{l} \text{quadrilateral or hexahedral} \\ \text{triangulation } \mathcal{T}_h \end{array} \end{cases}
$$

$$
\sigma_K = h_K/\rho_K \ge 1.
$$

where S_i is the d-simplex spanned by the d neighboring edges of vertex a_i.

With these definitions we are able to specify a given decomposition with respect to greatest diameter of an element.

Definition 1.2 (Triangulation). A decomposition $\mathcal{T}_h = \{K_i\}_{i=1,\dots,n}$ of the domain Ω in finitely many elements K_i satisfying

$$
\overline{\Omega} = \bigcup_{i=1}^{n} K_i,
$$

$$
h_K \le h \qquad \forall K \in \mathcal{T}_h
$$

is called *triangulation.*

Furthermore, the triangulations that we want to consider in this thesis have to satisfy the following regularity assumption.

Definition 1.3 (Admissibility). A triangulation $\mathcal{T}_h$ of Ω is *admissible* if the intersection between two distinct elements is

- empty,

- a common vertex,

- a common side $(d \ge 2)$

- or a common face $(d = 3)$.

Additionally, we want to characterize a family of triangulations $\{\mathcal{T}_h\}_h$ with respect to h_K, ρ_k and σ_K.

Definition 1.4 (Regularity and uniformity).

1. A family $\{\mathcal{T}_h\}_h$ of triangulations is said to be *regular* if

$$
\sigma_K \le C_1 \qquad \forall K \in \mathcal{T}_h. \tag{1.1}
$$

where $C_1 > 0$ is a constant independent of h.

2. If in addition there exists a constant $C_2 > 0$ independent of h such that

$$C_2 h \leq h_K \leq C_1 \rho_K \qquad \forall K \in \mathcal{T}_h, \tag{1.2}$$

then $\mathcal{T}_h$ is called *uniformly regular* or *quasi-uniform*.

If not stated more precisely, we assume all triangulations in this thesis to be regular. In particular this means that we do not consider anisotropic elements. For approximation results in that case we refer to the monograph [Ape99] by Thomas Apel.

1.2 Polynomial spaces

After defining the triangulations we now consider the ansatz functions that we want to use on each element. We distinguish here between simplicial (triangular resp. tetrahedral) and quadrilateral resp. hexahedral elements.

In the case of simplicial elements we consider the following space.

Definition 1.5 (Space of polynomials)**.** Let $\{e_i, 1 \leq i \leq d\}$ denote the standard unit vectors in $\mathbb{R}^d$. Then the *space of polynomials* of order $k \in \mathbb{N}_0$ on the reference cell $\hat{K} = \mathrm{conv}\{e_i : 1 \leq i \leq d\}$ is defined by

$$\mathcal{P}_k = \mathrm{span}\left\{ \prod_{i=1}^{d} x_i^{\alpha_i} : \sum_{i=1}^{d} \alpha_i \leq k \right\}. \tag{1.3}$$

For quadrilateral or hexahedral elements we use the following product polynomial space.

Definition 1.6 (Space of tensor product polynomials)**.** The *space of tensor product polynomials* of order $k \in \mathbb{N}_0$ on the reference cell $\hat{K} = [0,1]^d$ is defined by

$$\mathcal{Q}_k = \mathrm{span}\left\{ \prod_{i=1}^{d} x_i^{\alpha_i} : \max_{i=1}^{d} \alpha_i \leq k \right\}. \tag{1.4}$$

In order to define the used function spaces on arbitrary elements, we need to have a mapping from the reference cell that transforms the polynomial spaces adequately.

In the case of simplicial elements there exists exactly one invertible affine-linear mapping $F_K \in \mathcal{P}_1$ that maps the reference cell $\hat{K}$ onto a generic simplicial element $K = \mathrm{conv}\{a_i \in \mathbb{R}^d, 1 \leq i \leq d+1\}$ where

$$F_K(e_i) = a_i, \quad 1 \leq i \leq d+1. \tag{1.5}$$

Similarly there exists exactly one invertible multilinear mapping $F_K \in \mathcal{Q}_1$ that maps the reference cell $\hat{K}$ to a generic quadrilateral resp. hexahedral element $K = \mathrm{conv}\{a_i \in \mathbb{R}^d, 1 \leq i \leq 2^d\}$ where

$$F_K(e_i) = a_i \quad 1 \leq i \leq 2^d. \tag{1.6}$$
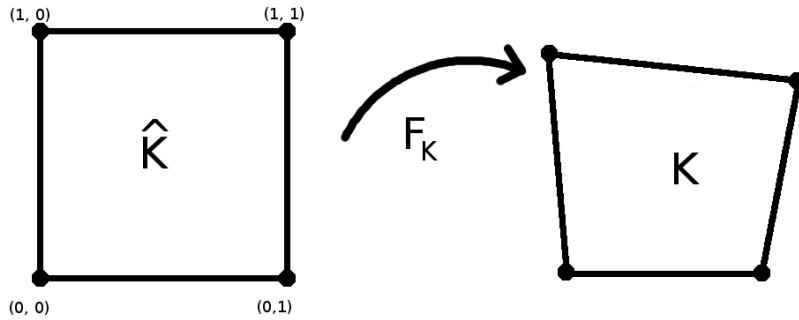
Figure 1.1: Bilinear mapping F_K from the reference cell $\hat{K}$ to the quadrilateral element K

Finally, we are able to describe the mapped polynomial spaces $\mathcal{R}_k(K)$ that are defined by

$$\mathcal{R}_k(K) = \{r = \hat{r} \circ F_K^{-1}, \, \hat{r} \in \mathcal{R}_k\} \tag{1.7}$$

where $\mathcal{R}_k$ is either the space of polynomials $\mathcal{P}_k$ or the space of tensor product polynomials $\mathcal{Q}_k$ and F_K the respective mapping from the reference cell.

Remark 1.7. Since the polynomial space $\mathcal{P}_k$ is invariant under affine linear mappings, the mapped space can in the case of simplicial elements equivalently be described as

$$\mathcal{P}_k = \mathrm{span}\left\{\prod_{i=1}^{d} x_i^{\alpha_i} : \sum_{i=1}^{d} \alpha_i \leq k\right\}. \tag{1.8}$$

Remark 1.8. In the case of quadrilateral or hexahedral elements the mapped space $\mathcal{Q}_k(K)$ is in general *not* a space of polynomials. This stems from the fact that the mapping F_K is affine multilinear and in general not affine linear. Just for parallelotops F_K is affine linear. Because also $\mathcal{Q}_k$ is invariant under affine linear transformations, in this case the mapped space can equivalently be described as

$$\mathcal{Q}_k = \mathrm{span}\left\{\prod_{i=1}^{d} x_i^{\alpha_i} : \max_{i=1}^{d} \alpha_i \leq k\right\}. \tag{1.9}$$

However, in general we can only assume to have polynomials on the reference cell.

2 Stokes equations

In a domain Ω we consider the Stokes equations

$$
\begin{aligned}
-\nu \Delta \boldsymbol{u} + \nabla p &= \boldsymbol{f} & &\text{in } \Omega \\
\operatorname{div} \boldsymbol{u} &= 0 & &\text{in } \Omega \\
\boldsymbol{u} &= 0 & &\text{on } \partial\Omega
\end{aligned}
\tag{2.1}
$$

that describe incompressible flow in which advective inertial forces are neglectable compared to viscous forces. $\boldsymbol{u}$ is the velocity of the fluid, p the pressure and f an external force that drives the motion. Finally, ν denotes the kinematic viscosity that expresses the ration of the inertial to viscous forces.

In order to solve these equations we consider the weak formulation:

$$
\begin{aligned}
&\text{Find } (\boldsymbol{u}, p) \in \boldsymbol{V} \times Q \text{ such that} \\
&\quad a(\boldsymbol{u}, \boldsymbol{v}) + b(\boldsymbol{v}, p) = \boldsymbol{f}(\boldsymbol{v}) \quad \forall \boldsymbol{v} \in \boldsymbol{V} \\
&\quad\quad\quad\quad\quad\; b(\boldsymbol{u}, q) = 0 \quad\quad \forall q \in Q
\end{aligned}
\tag{2.2}
$$

where $\boldsymbol{f} \in [H^{-1}(\Omega)]^d$ and the bilinear forms $a(\cdot, \cdot)$ and $b(\cdot, \cdot)$ are given by

$$
\begin{aligned}
a(\boldsymbol{u}, \boldsymbol{v}) &= \nu \int_\Omega \nabla \boldsymbol{u} : \nabla \boldsymbol{v} \, dx \\
b(\boldsymbol{u}, p) &= -\int_\Omega p \operatorname{div} \boldsymbol{u} \, dx.
\end{aligned}
\tag{2.3}
$$

Since only the derivative of the pressure p appears in the equations, we have to impose an additional constraint in order to achieve uniqueness. Therefore, we choose as pressure solution space $Q = L_0^2(\Omega) := \{q \in L^2(\Omega) : \int_\Omega q \, dx = 0\}$. The velocity has to be weakly differentiable and we want to find a velocity solution in $\boldsymbol{V} = [H_0^1(\Omega)]^d$. Then we get the following existence and uniqueness result.

Theorem 2.1. *Let $\Omega \subset \mathbb{R}^d$ be a bounded and connected open subset with Lipschitz-continuous boundary Γ. Then there exists for each $\boldsymbol{f} \in [H^{-1}(\Omega)]^d$ a unique pair $(\boldsymbol{u}, p) \in [H_0^1(\Omega)]^d \times L_0^2(\Omega)$ that solves (2.1) and (2.2).*

Proof. cf. [GR86, Theorem 5.1] □

Remark 2.2. A crucial part in the proof is to show that the choice of spaces $\boldsymbol{V} \times Q$ satisfies the inf-sup condition

$$
\exists \beta > 0 : \inf_{\substack{q \in Q \\ q \neq 0}} \sup_{\substack{\boldsymbol{v} \in \boldsymbol{V} \\ \boldsymbol{v} \neq 0}} \frac{b(\boldsymbol{v}, q)}{\|\boldsymbol{v}\|_{\boldsymbol{V}} \|q\|_Q} \geq \beta.
\tag{2.4}
$$

The discrete counterpart (2.10) is of similar importance for the discrete case.

Next we are interested in solving the Stokes problem numerically using finite elements defined in Section 1. Therefore, we choose a regular triangulation $\mathcal{T}_h$ and finite dimensional spaces $\boldsymbol{V}_h$ and Q_h. For this problem we restrict ourselves to the case of conforming elements, i.e. $\boldsymbol{V}_h \subset \boldsymbol{V}$ and $Q_h \subset Q$. The discretized Stokes problem then reads:

Find $(\boldsymbol{u_h}, p_h) \in \boldsymbol{V}_h \times Q_h$ such that
$$
\begin{aligned}
a(\boldsymbol{u_h}, \boldsymbol{v_h}) + b(\boldsymbol{v_h}, p_h) &= (\boldsymbol{f}, \boldsymbol{v_h})_{[L^2(\Omega)]^d} \quad &&\forall \boldsymbol{v}_h \in \boldsymbol{V}_h \\
b(\boldsymbol{u_h}, q_h) &= 0 &&\forall q_h \in Q_h.
\end{aligned}
\tag{2.5}
$$

A common choice of the finite element spaces is the Taylor-Hood pair of order $k \in \mathbb{N}_{>0}$
$$
\begin{aligned}
\boldsymbol{V_h} &= \{\boldsymbol{v} \in H_0^1(\Omega)^d : \boldsymbol{v}|_K \in \mathcal{Q}_{k+1}(K)^d \quad \forall K \in \mathcal{T}_h\} \\
Q_h &= \{q \in L_0^2(\Omega) \cap C(\overline{\Omega}) : q|_K \in \mathcal{Q}_k(K) \quad \forall K \in \mathcal{T}_h\}.
\end{aligned}
\tag{2.6}
$$

It is well-known that these elements satisfy a discrete inf-sup condition (cf. Remark 2.11) and that there is a unique numerical solution (cf. Theorem 2.12). But in general we cannot expect the numerical solution to be more than globally mass conservative, i.e.
$$
\int_\Omega \operatorname{div} \boldsymbol{u}_h \, dx = 0.
\tag{2.7}
$$

At the same time, using elementwise constant elements ($\mathcal{Q}_0$) for the pressure and $\mathcal{Q}_1$ elements for the velocity leads to a better approximation for the incompressibility. Testing the divergence constraint with the indicator function $\mathbf{1}_K \in Q_h$ yields
$$
\int_K \operatorname{div} \boldsymbol{u}_h \, dx = 0 \qquad \forall K \in \mathcal{T}_h
\tag{2.8}
$$

and the numerical solution is locally mass conservative. However, the $\mathcal{Q}_1/\mathcal{Q}_0$ element is in general not stable [BBF08]. Thus the variational formulation has to be stabilized in order to get reasonable results.

In the next subsection we will examine an element pair that is stable and locally mass conservative. Furthermore, it is not much more expensive than the Taylor-Hood element meaning that the resulting linear system is not much larger.

2.1 Inf-sup stability for the $\mathcal{Q}_{k+1}/(\mathcal{Q}_k + \mathcal{Q}_0)$ element

In [BCGG12] Boffi, Cavallini, Gardini and Gastaldi have shown based on the inf-sup stability of the Taylor-Hood pair $\mathcal{P}_{k+1}/\mathcal{P}_k$ that the element coupling $\mathcal{P}_{k+1}/(\mathcal{P}_k + \mathcal{P}_0)$

defined by

$$\boldsymbol{V_h} = \{\boldsymbol{v} \in H_0^1(\Omega)^d : \boldsymbol{v}|_K \in \mathcal{P}_{k+1}(K)^d \quad \forall K \in \mathcal{T}_h\}$$
$$Q_h = \{q \in L_0^2(\Omega) : q = q_k + q_0, q_k \in C(\overline{\Omega}), q_k|_K \in \mathcal{P}_k(K), q_0|_K \in \mathcal{P}_0(K) \quad \forall K \in \mathcal{T}_h\}.$$
$$(2.9)$$

is stable on simplicial meshes. In this section we want to prove in a analogous way that this result also holds for the case of quadrilateral or hexahedral elements.

It turns out that the following inf-sup condition is essential for the solvability of the discretized Stokes problem.

Definition 2.3 (Inf-sup condition). The pair $(\boldsymbol{V_h}, Q_h)$ is said to fulfill the *inf-sup condition* if there exists $\beta > 0$ independent of h such that

$$\inf_{\substack{q_h \in Q_h \\ q_h \neq 0}} \sup_{\substack{\boldsymbol{v_h} \in \boldsymbol{V_h} \\ \boldsymbol{v_h} \neq 0}} \frac{b(\boldsymbol{v_h}, q_h)}{\|\boldsymbol{v_h}\|_{\boldsymbol{V}} \|q_h\|_Q} \geq \beta, \tag{2.10}$$

Instead of showing the stability directly we make use of the macroelement technique introduced by Stenberg in [Ste84].

Definition 2.4 (Macroelement). A *macroelement* M is a polytope which is the union of adjacent elements. Two macroelement $M, \widehat{M}$ are said to be equivalent if there exists a mapping $F_M : \widehat{M} \to M$ such that

1. F_M is continuous and invertible.

2. If $\widehat{M} = \bigcup_{j=1}^m \widehat{K}_j$ where $\widehat{K}_j$ are the elements defining $\widehat{M}$, then $K_j = F_M(\widehat{K}_j)$ are the elements of M.

3. $F_M|_{\widehat{K}_j} = F_{K_j} \circ F_{\widehat{K}_j}^{-1} \quad \forall j \in \{1, \ldots, m\}$ where F_K denotes the affine mapping from the reference element to a generic element K.

For a macroelement M we introduce the following discrete spaces $\boldsymbol{V_{0,M}}$ and Q_M

$$\boldsymbol{V_{0,M}} = \{\boldsymbol{v} \in H_0^1(M)^d : \exists \boldsymbol{w} \in \boldsymbol{V_h} \text{ with } \boldsymbol{v} = \boldsymbol{w}|_M\}$$
$$Q_M = \{q|_M \text{ with } q \in Q_h\}$$
$$(2.11)$$

and also the space of spurious pressure modes on M

$$N_M = \{q \in Q_M : \int_M q \operatorname{div} \boldsymbol{v} \, dx = 0 \quad \forall \boldsymbol{v} \in \boldsymbol{V_{0,M}}\}. \tag{2.12}$$

Using this definitions we get some easy to check criteria for the inf-sup condition.

Theorem 2.5. *Let $\mathcal{M}_h$ be a macroelement partition of the elements of $\mathcal{T}_h$ such that*

(H1) *for each $M \in \mathcal{M}_h$ the space N_M is one-dimensional and consists of functions which are constant on M;*

(H2) *each $M \in \mathcal{M}_h$ belongs to an equivalence class of macroelements;*

(H3) *the number of equivalence classes of macroelements is finite and independent of h;*

(H4) *each element $K \in \mathcal{T}_h$ is contained in a finite number N of macroelements $M \in \mathcal{M}_h$, with N independent of h;*

(H5) *the inf-sup condition between V_h and the space of elementwise constant pressure functions $\mathcal{Q}_0$ holds true.*

Then the choice of spaces $\boldsymbol{V_h}$ and Q_h satisfies the inf-sup condition.

Proof. This is a consequence of Proposition 4.8 and Remark 4.7 in [BBF08]. $\square$

We now consider the following approximation spaces that are based on these polynomial spaces.

$$\boldsymbol{V_h} = \{\boldsymbol{v} \in H_0^1(\Omega)^d : \boldsymbol{v}|_K \in \mathcal{Q}_{k+1}(K)^d \quad \forall K \in \mathcal{T}_h\} \tag{2.13}$$

$$Q_h = \{q \in L_0^2(\Omega) : q = q_k + q_0, q_k \in C(\overline{\Omega}), q_k|_K \in \mathcal{Q}_k(K), q_0|_K \in \mathcal{Q}_0(K) \quad \forall K \in \mathcal{T}_h\}. \tag{2.14}$$

We first treat here the three-dimensional case.

Proposition 2.6. *Define a macroelement partition $\mathcal{M}_h$ by grouping together, for each internal vertex x_0, those vertex elements that touch x_0. Then for the three-dimensional case ($d = 3$) the space of spurious pressure modes N_M is one-dimensional, consisting of globally constant functions in M for each $M \in \mathcal{M}_h$.*

Proof. First of all we consider the polynomial $\tilde{w} = 4x(1 - x)(1 - y)(1 - z) \in \mathcal{Q}_2$ on the reference cell. The properties of interest are:

(P1) The value of $\tilde{w}$ on the plane $\{y = 0\}$ just depends on x and z.

(P2) On the plane $\{z = 0\}$ $\tilde{w}$ only varies with x and y.

(P3) The function vanishes on the four planes $\{x = 0\}$, $\{x = 1\}$, $\{y = 1\}$ and $\{z = 1\}$.

(P4) $\tilde{w}$ is linear with respect to y and z individually.

(P5) $\tilde{w}(x, y, z) \geq 0 \quad \forall (x, y, z) \in [0, 1]^3$.

(P6) $\tilde{w}(x, y, z) = \tilde{w}(x, z, y) \quad \forall (x, z) \in [0, 1]^2$.

Let x_0 be an arbitrary internal vertex and consider the associated macroelement $M \in \mathcal{M}_h$. A generic hexahedron element $K_0 \in \mathcal{T}_h$ of M has three edges $e_i, i = 1, 2, 3$ that meet at x_0. We choose a coordinate system in such a way that e_1 lies on the x-axis.

We want to prove that ∇p vanishes on K_0 due to the macroelement condition (2.12). Therefore, consider the set $\mathcal{A} = \{K_0, \dots, K_n\}$ of elements in $\mathcal{T}_h$ that share e_1. Obviously each $K \in \mathcal{A}$ has exactly two faces with other elements in $\mathcal{A}$ in common. Next we denote by $\boldsymbol{F_i}$ an invertible bilinear mapping from K_i to the reference cell that satisfies:

- The two faces of K_i which are in common with other elements in $\mathcal{A}$ are mapped to the $\{z = 0\}$ and $\{y = 0\}$ plane.

- $\boldsymbol{F_i}$ is the identity on e_1.

- Vertices are mapped onto vertices.

Now we are able to construct a polynomial for a given $q \in Q_M$ that gives us the desired property:

$$\boldsymbol{w}|_{K_i} = \left((\tilde{w} \circ \boldsymbol{F_i^{-1}}) \left. \frac{\partial p}{\partial x} \right|_{K_i}, 0, 0 \right) \quad i = 1, \dots, n,$$

$$\boldsymbol{w}|_K = \boldsymbol{0} \qquad\qquad\qquad\qquad \forall K \in \mathcal{T}_h \setminus \mathcal{A}. \tag{2.15}$$

The constructed polynomial vanishes in $M \setminus \mathcal{A}$ and is continuous in $K_i \cup (M \setminus \mathcal{A})$ due to properties (P1)-(P3). The continuity of ∇p on the faces between elements in $\mathcal{A}$ in all tangential directions then ensures together with properties (P1) and (P2) the continuity of $\boldsymbol{w}$ on these interfaces and finally in the whole set M.

Due to the fact that $\boldsymbol{F_i}$ preserves the x-direction, $\frac{\partial p}{\partial x} \circ \boldsymbol{F_i}$ is of the form

$$\frac{\partial p}{\partial x} \in \text{span}\{x^r y^s z^t, 0 \leq r \leq k - 1, 0 \leq s, t \leq k\} \tag{2.16}$$

in K_i. The function $\tilde{w} \circ \boldsymbol{F_i^{-1}} \circ \boldsymbol{F_i} = \tilde{w}$ is quadratic in x and linear in y and z due to property (P4). Therefore, we get

$$\left((\tilde{w} \circ \boldsymbol{F_i^{-1}}) \left. \frac{\partial p}{\partial x} \right|_{K_i} \right) \circ \boldsymbol{F_i} \in \text{span}\{x^r y^s z^t, 0 \leq r, s, t \leq k + 1\} = \mathcal{Q}_{k+1}. \tag{2.17}$$

Thus, we have the desired result

$$\boldsymbol{w} \in \boldsymbol{V_{0,M}} \tag{2.18}$$

and are allowed to test the macroelement condition (2.12) with this function. This yields

$$
\begin{aligned}
0 = \int_M q \operatorname{div} \boldsymbol{w}\, dx &= \sum_{i=1}^n \left(\int_{\partial K_i} q\, \boldsymbol{w} \cdot \boldsymbol{n}\, dx - \int_{K_i} \nabla q \cdot \boldsymbol{w}\, dx \right) \\
&= \sum_{i=1}^n \int_{K_i} (\tilde{w} \circ \boldsymbol{F_i^{-1}}) \left(\left. \frac{\partial q}{\partial x} \right|_{K_i} \right)^2
\end{aligned} \tag{2.19}
$$

where $\int_{\partial K_i} q\, \boldsymbol{w} \cdot \boldsymbol{n}\, dx$ disappears due to the choice of $\boldsymbol{w}$. The function $(\tilde{w} \circ \boldsymbol{F_i^{-1}})$ is non-negative in K_i for all $i = 1, \dots, n$ because of (P5). Hence, we can conclude that the first component of ∇q vanishes. The same argumentation can then be applied to the edges e_2 and e_3. This gives us that $\nabla q_k|_{K_i}$ disappears and therefore that q is elementwise constant in M.

All that is left, is to show that q is constant in M.
Consider two neighboring elements K^+ and K^- in M and let $q^\pm$ be the constant pressures. We now choose a coordinate system in which the interface Γ between K^+ and K^- lies in the xy-plane. By $\boldsymbol{F_\pm}$ we denote an invertible bilinear mapping from the reference cell to $K^\pm$, that reduces to the identity in the xy-plane and maps vertices onto vertices. Furthermore, we consider the function $\tilde{u} = x(1-x)y(1-y)(1-z) \in \mathcal{Q}_2$. Then we are able to define the function $\boldsymbol{u}$ by

$$
\begin{aligned}
\boldsymbol{u}|_{K^\pm} &= (0, 0, \tilde{u} \circ \boldsymbol{F_\pm}), \\
\boldsymbol{u}|_K &= \boldsymbol{0} \qquad \forall K \in \mathcal{T}_h \setminus (K^+ \cup K^-)
\end{aligned} \tag{2.20}
$$

Since $\tilde{u}$ vanishes on all faces except for the xy-plane $\boldsymbol{u}$ is continuous in M and is by definition an element of $\mathcal{Q}_2(K^+ \cup K^-)$.
This gives the inclusion

$$\boldsymbol{u} \in \boldsymbol{V_{0,M}} \tag{2.21}$$

and we are allowed to test the macroelement condition (2.12) with it

$$0 = \int_M q \operatorname{div} \boldsymbol{u}\, dx = q^+ \int_{K^+} \operatorname{div} \boldsymbol{u}\, dx + q^- \int_{K^-} \operatorname{div} \boldsymbol{u}\, dx = (q^+ - q^-) \int_\Gamma \boldsymbol{u} \cdot \boldsymbol{n}\, dx. \tag{2.22}$$

Since $\tilde{u}$ is a non-negative function in $[0, 1]^3$ that is not identically to zero, we can conclude

that the pressure q^+ has to be equal to q^-. Because of the fact that the neighboring elements were chosen arbitrarily, we can finally conclude that p is constant in M. $\quad\square$

Remark 2.7. Up to the point where we showed that an arbitrary $q \in N_M$ has to be elementwise constant the same proof works for the hexahedral Taylor-Hood element

$$
\begin{aligned}
\boldsymbol{V_h} &= \{\boldsymbol{v} \in H_0^1(\Omega)^d : \boldsymbol{v}|_K \in \mathcal{Q}_{k+1}(K)^3 \quad \forall K \in \mathcal{T}_h\} \\
Q_h &= \{q \in L_0^2(\Omega) \cap C(\overline{\Omega}) : q|_K \in \mathcal{Q}_k(K) \quad \forall K \in \mathcal{T}_h\}.
\end{aligned}
\tag{2.23}
$$

We can then simply conclude that q has to be constant on M since q is continuous.

The next theorem is dedicated to the two-dimensional case.

Proposition 2.8. *Define a macroelement partition $\mathcal{M}_h$ by grouping together, for each internal vertex x_0, those vertex elements that touch x_0. Then for the two-dimensional case ($d = 2$) the space of spurious pressure modes N_M is one-dimensional, consisting of globally constant functions in M for each $M \in \mathcal{M}_h$.*

Proof. The proof works similar for the two-dimensional case although there are some simplifications. Consider again an arbitrary internal vertex x_0 and the associated macroelement $M \in \mathcal{M}_h$. Furthermore, we choose two neighboring elements K^+ and K^- in M. Additionally, choose a coordinate system such that the common edge e_1 lies on the x-axis. Let $\boldsymbol{F}_\pm$ be an invertible bilinear mapping from the reference cell to $K^\pm$ that leaves the x-direction invariant and maps vertices onto vertices. Then we define for a generic $q \in N_M$ a function $\boldsymbol{w}$ in M by

$$
\boldsymbol{w}|_{K^\pm} = \left(\tilde{w} \circ \boldsymbol{F}_\pm^{-1} \frac{\partial q}{\partial x}, 0\right)
\tag{2.24}
$$

$$
\boldsymbol{w}|_K = \boldsymbol{0} \qquad \forall K \in M \setminus \{K^+, K^-\}.
\tag{2.25}
$$

where $\tilde{w}$ is defined by $\tilde{w} = x(x-1)(1-y) \in \mathcal{Q}_2$. Since $\frac{\partial q}{\partial x}$ is continuous on e_1 and $\tilde{w} \circ \boldsymbol{F}_\pm^{-1}$ vanishes on $\partial K^\pm \setminus e_1$, the function $\boldsymbol{w}$ is continuous in M. Furthermore, $\tilde{w}$ is quadratic in x and linear in y and $q \circ \boldsymbol{F}_\pm \in \mathcal{Q}_k$. Thus, we achieve the inclusions

$$
(\tilde{w} \circ \boldsymbol{F}_\pm^{-1} \frac{\partial q}{\partial x}) \circ \boldsymbol{F}_\pm \in \mathcal{Q}_{k+1}
\tag{2.26}
$$

$$
\boldsymbol{w} \in V_{0,M}.
\tag{2.27}
$$

This means that we can test the macroelement condition (2.12) with $\boldsymbol{w}$.

$$
0 = \int_M q \operatorname{div} \boldsymbol{w} \, dx = \int_{e_1} q \, \boldsymbol{w} \cdot \boldsymbol{n} \, dx - \int_{K^+ \cup K^-} \nabla q \cdot \boldsymbol{w} \, dx
\tag{2.28}
$$

$$= \int_{K^+} (\tilde{w} \circ \boldsymbol{F_+^{-1}}) \left(\left.\frac{\partial q}{\partial x}\right|_{K_+} \right)^2 dx + \int_{K^-} (\tilde{w} \circ \boldsymbol{F_-^{-1}}) \left(\left.\frac{\partial q}{\partial x}\right|_{K_-} \right)^2 dx \qquad (2.29)$$

where $\int_{e_1} q\, \boldsymbol{w} \cdot \boldsymbol{n}\, dx$ disappears due to the choice of $\boldsymbol{w}$. Since $\tilde{w}$ is a non-negative function that is not identically to zero, we conclude that the first component of ∇q vanishes on $K^\pm$. It can be shown analogously that the second component vanishes. So q is elementwise constant in M.

Finally, it has to be shown that these constants are in fact the same.

Again, we consider two neighboring elements K^+ and K^- and choose a coordinate system as before. The constants on the elements $K^\pm$ are denoted by $q^\pm$ respectively. Then we can define a function $\boldsymbol{u} \in \mathcal{Q}_2(K^+ \cup K^-)$ by

$$\begin{aligned}
\boldsymbol{u}|_{K^\pm} &= \left(0, \tilde{w} \circ \boldsymbol{F_\pm^{-1}}\right) \\
\boldsymbol{u}|_K &= \boldsymbol{0} \qquad\qquad \forall K \in M \setminus (K^+ \cup K^-).
\end{aligned} \qquad (2.30)$$

By the same argument as before $\boldsymbol{w}$ is continuous and vanishes on ∂M, giving $\boldsymbol{u} \in V_{0,M}$. Applying the macroelement condition (2.12) then yields

$$0 = \int_M q \operatorname{div} \boldsymbol{u}\, dx = q^+ \int_{K^+} \operatorname{div} \boldsymbol{u}\, dx + q^- \int_{K^-} \operatorname{div} \boldsymbol{u}\, dx = (q^+ - q^-) \int_\Gamma \boldsymbol{u} \cdot \boldsymbol{n}\, dx. \quad (2.31)$$

$\tilde{w}$ is a non-negative function that does not vanish identically on e_1 and thus q^+ and q^- are the same. Since K^+ and K^- were chosen arbitrarily, q has to be constant in M. $\square$

Remark 2.9. Up to the point where we showed that an arbitrary $q \in N_M$ has to be elementwise constant the same proof works for the quadrilateral Taylor-Hood element

$$\begin{aligned}
\boldsymbol{V_h} &= \{\boldsymbol{v} \in H_0^1(\Omega)^d : \boldsymbol{v}|_K \in \mathcal{Q}_{k+1}(K)^2 \quad \forall K \in \mathcal{T}_h\} \\
Q_h &= \{q \in L_0^2(\Omega) \cap C(\overline{\Omega}) : q|_K \in \mathcal{Q}_k(K) \quad \forall K \in \mathcal{T}_h\}.
\end{aligned} \qquad (2.32)$$

We can then simply conclude that q has to be constant on M since q is continuous.

After these extensive preparations the inf-sup condition follows quite easily.

Theorem 2.10. *Let $\mathcal{T}_h$ be a regular family of quadrilateral ($d = 2$) or hexahedral ($d = 3$) decompositions of Ω. Then the following spaces*

$$\begin{aligned}
\boldsymbol{V_h} &= \{\boldsymbol{v} \in H_0^1(\Omega)^d : \boldsymbol{v}|_K \in \mathcal{Q}_{k+1}(K) \quad \forall K \in \mathcal{T}_h\} \\
Q_h &= \{q \in L_0^2(\Omega) : q = q_k + q_0, q_k \in C(\overline{\Omega}), q_k|_K \in \mathcal{Q}_k(K), q_0|_K \in \mathcal{Q}_0(K) \quad \forall K \in \mathcal{T}_h\}
\end{aligned}$$

with $d \in \{2,3\}$ and $k \in \mathbb{N}_{>0}$ satisfy the inf-sup condition (2.3).

Proof. Due to Theorem 2.5 we have to check the five hypotheses (H1)-(H5).
(H1) was proved in Proposition 2.8 respectively Proposition 2.6. (H2) and (H4) hold due to the choice of the macroelements. (H3) is a consequence of the regularity assumption. It is well known that the choice of spaces

$$
\begin{aligned}
\boldsymbol{V_h} &= \{\boldsymbol{v} \in H_0^1(\Omega)^d : \boldsymbol{v}|_K \in \mathcal{Q}_{k+1}(K) \quad \forall K \in \mathcal{T}_h\} \\
P_h &= \{q \in L_0^2(\Omega) : q|_K \in \mathcal{P}_k(K) \quad \forall K \in \mathcal{T}_h\}
\end{aligned} \tag{2.33}
$$

satisfies the inf-sup condition for each $k \in \mathbb{N}_{>0}$ as shown in [MT02]. In particular, this means that the inf-sup condition between $\boldsymbol{V_h}$ and the space of elementwise constant functions holds true due to

$$
\mathcal{Q}_0(K) \subset \mathcal{P}_k(K) \quad \forall k \in \mathbb{N}_0. \tag{2.34}
$$

Therefore, (H5) is fulfilled.   □

Remark 2.11. Conditions (H2)-(H5) do not depend on the choice of the pressure space Q_h and for the case of the two- and three-dimensional Taylor-Hood element Remark 2.9 and Remark 2.7 show (H1) respectively. This means, that in this way we can prove the inf-sup condition for the Taylor-Hood element.

2.2 Approximation results

Now that we proved the inf-sup stability we can use the usual results for the discretized Stokes problem.

The existence and uniqueness result Theorem 2.1 has a discrete counterpart.

Theorem 2.12. *Let $(\boldsymbol{u}, p) \in \boldsymbol{V} \times Q$ be the solution to (2.2) and suppose that $(\boldsymbol{V_h}, Q_h)$ fulfills the inf-sup condition (2.10). Then there exists a unique solution $(\boldsymbol{u_h}, p_h) \in \boldsymbol{V_h} \times Q$ to the discretized Stokes problem and the following estimate holds*

$$
\|\boldsymbol{u} - \boldsymbol{u_h}\|_{\boldsymbol{V}} + \|p - p_h\|_Q \le C \inf_{\substack{\boldsymbol{v_h} \in \boldsymbol{V_h} \\ q_h \in Q_h}} \{\|\boldsymbol{u} - \boldsymbol{u_h}\|_{\boldsymbol{V}} + \|p - q_h\|_Q\} \tag{2.35}
$$

Proof. cf. [GR86, p. 114].   □

In combination with the approximation result we achieve the following convergence result.

Theorem 2.13. *Let $\Omega \subset \mathbb{R}^d$ be a bounded domain with Lipschitz-continuous boundary and $\mathcal{T}_h$ a regular triangulation of Ω.*

If the solution to the Stokes problem (2.2) satisfies the regularity assumptions

$$\boldsymbol{u} \in [H^{k+1}(\Omega) \cap H_0^1(\Omega)]^d, \quad p \in H^k(\Omega) \cap L_0^2(\Omega) \tag{2.36}$$

for some $k \in \mathbb{N}_{>0}$, then for the discrete solution $(\boldsymbol{u_h}, p_h)$

$$\|\boldsymbol{u} - \boldsymbol{u_h}\|_V + \|p - p_h\|_Q \le C_1 h^{k+1}(\|\boldsymbol{u}\|_{[H^{k+1}(\Omega)]^d} + \|p\|_{H^k(\Omega)}) \tag{2.37}$$

holds where C_1 is a constant independent of the maximal cell diameter h. If the domain Ω is furthermore convex, the error of the velocity can be limited by

$$\|\boldsymbol{u} - \boldsymbol{u_h}\|_{0,\Omega} \le C_2 h^{k+2}(\|\boldsymbol{u}\|_{[H^{k+1}(\Omega)]^d} + \|p\|_{H^k(\Omega)}), \tag{2.38}$$

where also C_2 does not depend on h.

Proof. cf. [GR86, p. 125-127]. □

2.3 Implementation

The first part of the following subsection is devoted to some remarks about the problems that have to be faced when implementing and using the $\mathcal{Q}_k + \mathcal{Q}_0$ element. In the second part we discuss the actual implementation of the Stokes problem.

2.3.1 The discontinuous element

We implemented the element $\mathcal{Q}_k + \mathcal{Q}_0$ in the finite element library `deal.II`([BHK], [BHK07]) as `FE_Q_DG0`. This was mainly done by extending the existing polynomial class `TensorProductPolynomialSpace` to `TensorProductPolynomialSpaceConstant` by adding an additional constant function. Furthermore, the class `FE_Q` was modified to suit the new polynomial space. This implementation and its documentation can be found in version 7.3 of the previous mentioned library (see [FEQ12]).

When using this element one has to be aware that the sum $\mathcal{Q}_k + \mathcal{Q}_0$ is not direct since a global constant function can be represented by functions in $\mathcal{Q}_k$ and $\mathcal{Q}_0$ separately. Therefore, a mass matrix $A_{ij} = \int_\Omega \phi_i \phi_j \, dx$ formed with this element has exactly one zero eigenvalue. One possibility to ensure the invertibility is to impose an additional constraint, e.g. setting the sum of the values of the discontinuous functions to zero. In order to reduce the coupling between discontinuous nodes, we set just the sum of the discontinuous functions on the boundary to zero in our implementations.

In the case of a stiffness matrix $A_{ij} = \int_\Omega \nabla \phi_i \cdot \nabla \phi_j \, dx$ the number of additional zero eigenvalues equals the number of cells in the triangulation. This is due to the fact that a (weak) solution to a Poisson equation remains a solution after changing it by a constant on one element. In order to deal with this behavior, one has to introduce some connectivity information between the cells in the problem. We discuss a suitable approach in Section 3.

2.3.2 The Stokes equation

For solving the Stokes equation in `deal.II` the tutorial program step-22 was modified by the author. This modification may be found in the test suite in the `deal.II` subversion repository[1].

For the implementation we use $2(\boldsymbol{S}(\boldsymbol{u}), \boldsymbol{S}(\boldsymbol{v}))_{[L^2(\Omega)]^d}$ with the symmetric gradient tensor $\boldsymbol{S}(\boldsymbol{u})$ instead of the diffusion term $(\nabla \boldsymbol{u}, \nabla \boldsymbol{v})_{[L^2(\Omega)]^d}$. The following lemma gives us the equivalence of these two formulations.

Lemma 2.14. *Let $\boldsymbol{u}, \boldsymbol{v} \in [H_0^1(\Omega)]^d$ be two solenoidal functions. Then*

$$(\boldsymbol{S}(\boldsymbol{u}), \boldsymbol{S}(\boldsymbol{v}))_{[L^2(\Omega)]^d} = (\nabla \boldsymbol{u}, \nabla \boldsymbol{v})_{[L^2(\Omega)]^d} \tag{2.39}$$

where the symmetric strain rate tensor $\boldsymbol{S}$ is given by $\boldsymbol{S}(\boldsymbol{u}) = \frac{1}{2}\left[\nabla \boldsymbol{u} + (\nabla \boldsymbol{u})^T\right]$.

Proof.

$$
\begin{aligned}
2(\boldsymbol{S}(\boldsymbol{u}), \boldsymbol{S}(\boldsymbol{v}))_{[L^2(\Omega)]^d} &= \sum_{i,j=1}^d \frac{1}{2} \int_\Omega \left(\frac{\partial u_i}{\partial x_j} \frac{\partial u_j}{\partial x_i}\right)\left(\frac{\partial v_i}{\partial x_j} + \frac{\partial v_j}{\partial x_i}\right) dx \\
&= \frac{1}{2} \sum_{i,j=1}^d \int_\Omega \frac{\partial u_i}{\partial x_j}\frac{\partial v_i}{\partial x_j} + \frac{\partial u_j}{\partial x_i}\frac{\partial v_j}{\partial x_i} + \frac{\partial u_i}{\partial x_j}\frac{\partial v_j}{\partial x_i} + \frac{\partial u_j}{\partial x_i}\frac{\partial u_i}{\partial x_j} \, dx \\
&= \sum_{i,j=1}^d \int_\Omega \frac{\partial u_i}{\partial x_j}\frac{\partial v_i}{\partial x_j} \, dx + \sum_{i,j=1}^d \int_\Omega \frac{\partial u_i}{\partial x_j}\frac{\partial v_j}{\partial x_i} \, dx \\
&= (\nabla \boldsymbol{u}, \nabla \boldsymbol{v})_{[L^2(\Omega)]^d} + \int_\Omega \sum_{i=1}^d \frac{\partial u_i}{\partial x_i} \sum_{j=1}^d \frac{\partial v_j}{\partial x_j} \, dx \\
&= (\nabla \boldsymbol{u}, \nabla \boldsymbol{v})_{[L^2(\Omega)]^d} + \int_\Omega \operatorname{div} \boldsymbol{u} \operatorname{div} \boldsymbol{v} \, dx = (\nabla \boldsymbol{u}, \nabla \boldsymbol{v})_{[L^2(\Omega)]^d}
\end{aligned}
$$

$\square$

---

[1] `https://svn.dealii.org/trunk/tests/fe/fe_q_dg0`

Starting from the weak formulation of the Stokes equations (2.5), the implemented discretization reads

Find $(\boldsymbol{u_h}, p_h) \in \boldsymbol{V_h} \times Q_h$:

$$2\nu(\boldsymbol{S}(\boldsymbol{u_h}), \boldsymbol{S}(\boldsymbol{v_h}))_{[L^2(\Omega)]^d} - (p_h, \operatorname{div} \boldsymbol{v_h})_{L^2(\Omega)} = (\boldsymbol{f}, \boldsymbol{v_h})_{[L^2(\Omega)]^d} \quad \forall \boldsymbol{v_h} \in \boldsymbol{V_h} \qquad (2.40)$$

$$(\operatorname{div} \boldsymbol{u_h}, q_h)_{L^2(\Omega)} = 0 \qquad\qquad \forall q_h \in Q_h.$$

This naturally leads to the following linear system for the nodal values of the velocity U and the pressure P

$$\begin{pmatrix} A & B^T \\ B & 0 \end{pmatrix} \begin{pmatrix} U \\ P \end{pmatrix} = \begin{pmatrix} F \\ 0 \end{pmatrix} \qquad (2.41)$$

that exhibits a saddle point structure. In order to solve this system, we make use of the Schur complement $S = -BA^{-1}B^T$. The first equation can then be transformed to $U = A^{-1}F - A^{-1}B^T P$. Inserting this into the second one eliminates the velocity and we obtain an equation for the pressure P alone

$$SP = -BA^{-1}B^T P = -BA^{-1}F. \qquad (2.42)$$

Then the velocity is retrieved by the equation

$$AU = F - B^T P. \qquad (2.43)$$

The interesting question that now arises is how to choose the solvers and preconditioners for these problems. The choice for the Schur complement is based on the following result from [ESW05, Theorem 5.22, p.270].

Theorem 2.15. *For a inf-sup stable finite element pair on a regular, quasi-uniform triangulation $\mathcal{T}_h$ the Schur complement $S = -BA^{-1}B^T$ is spectrally equivalent to the pressure mass matrix M_P:*

$$\beta^2 \le \frac{q^T BA^{-1}B^T q}{q^T M_p q} \le 1 \qquad \forall q \in \mathbb{R}^{n_p}, q \notin 0, 1 \qquad (2.44)$$

where n_p is the dimension of the pressure mass matrix M_p and $\beta > 0$ the inf-sup constant. Furthermore, the condition number satisfies $\operatorname{cond}(S) \le C/(c\beta^2)$ where c and C are constants that fulfill

$$ch^d \le \frac{q^T M_p q}{q^T q} \le Ch^d \qquad \forall q \in \mathbb{R}^{n_p}, q \ne 0. \qquad (2.45)$$

Due to the symmetry of A also the Schur complement is symmetric, i.e. $S^T = (-BA^{-1}B^T)^T = -BA^{-T}B^T = -BA^{-1}B^T = S$, and thus we can use a CG solver. Due to the previous result we use a pressure mass matrix for preconditioning.

Next we have to think about inverting A. This matrix is related to the Laplace operator because it is equivalent to the symmetric gradient tensor. The following theorem from [ESW05, Theorem 1.32., p.59] gives an upper bound for the condition of such a matrix.

Theorem 2.16. *On a regular, quasi-uniform triangulation $\mathcal{T}_h$ the Poisson matrix $A \in \mathbb{R}^{n_v \times n_v}$ given by $a_{ij} = \int \Omega \phi_j \phi_i \, dx$ satisfies*

$$ch^d \leq \frac{v^T A v}{v^T v} \leq Ch^{d-2} \qquad \forall v \in \mathbb{R}^{n_v}. \tag{2.46}$$

The condition is bounded by $\operatorname{cond}(A) \leq C/ch^{-2}$.

So the matrix is ill-conditioned. Since we have to solve with this matrix both in the Schur complement and for retrieving the velocity it is worth to spend more effort in the preconditioner. This is the reason why we choose a direct sparse LU decomposition. Since A is symmetric, we use a CG solver.

Remark 2.17. The described procedure using gradient methods is equivalent to Uzawa's algorithm [BF91, II.5.1]:

1. Let p^0 be chosen arbitrarily,

2. p^n being given, find $\boldsymbol{u}^{n+1}$ as solution of

$$a(\boldsymbol{u}^{n+1}, v) = f(\boldsymbol{v}) - b(\boldsymbol{v}, p^n) \qquad \forall \boldsymbol{v} \in \boldsymbol{V},$$

3. compute p^{n+1} using with ρ small enough

$$(p^{n+1} - p^n, q) = \rho \, b(\boldsymbol{u}^{n+1}, q) \qquad \forall q \in Q$$

4. stop whenever $\|p^{n+1} - p^n\|_Q$ is small enough, otherwise go to step 2.

Another idea for solving the coupled system is the use of a block solver and block preconditioner. We follow such an approach for solving the discretized Navier-Stokes problem in Section 4.

2.4 Numerical results

In this section we will investigate the numerical performance of the discussed element. Therefore, we consider the stationary Stokes equation with the following reference solution

$$\boldsymbol{u} = (\partial_y \psi_z, -\partial_x \psi_z), \tag{2.47}$$

$$p = \begin{cases} y(1-y)exp(x-1/2)^2 + 1/2 & x \leq 1/2, \\ y(1-y)exp(x-1/2)^2 - 1/2 & x > 1/2. \end{cases} \tag{2.48}$$

where ψ_z is determined by

$$\psi_z = x^2(x-1)^2 y^2(y-1)^2. \tag{2.49}$$

We choose the right-hand side in a way that the reference solution solves the Stokes problem

$$\boldsymbol{f} = -\Delta \boldsymbol{u} + \nabla p. \tag{2.50}$$

Furthermore, we like to have a discontinuity in the pressure solution. To obtain this we take the term

$$\langle \boldsymbol{f}, \boldsymbol{v} \rangle = \int_\Omega \boldsymbol{f} \cdot \boldsymbol{v} \, dx + \sum_{K \in \mathcal{T}_h} \frac{1}{2} \int_{\partial K} [\![p]\!] \cdot \boldsymbol{v} \, dx \tag{2.51}$$

in the variational formulation into account. Such a term appears in the continuum surface model [BKZ92] that makes it possible to solve two-phase flows in one equation.

2.5 Convergence results

We are interested in the difference between a solution that uses $\mathcal{Q}_k + \mathcal{Q}_0$ elements and one that uses $\mathcal{Q}_k$ elements for the pressure. In both cases $\mathcal{Q}_{k+1}$ elements are used for the velocity.

Figure 2.4 now shows as expected the difficulties the continuous elements has to approximate the reference pressure solution. Also the velocity solution shows artifacts at the discontinuous pressure edge (Figure 2.5). The discontinuity reduces the order of convergence for the pressure by a half as can be seen in Table 2.1. Even stronger affected are the velocity, the gradient and the divergence of the velocity. In all three cases the order of convergence is reduced by 1.5.

On the contrary, the discontinuous element does not suffer these problems. Figure 2.6 shows that even for a rather coarse grid the pressure approximation is quite good compared
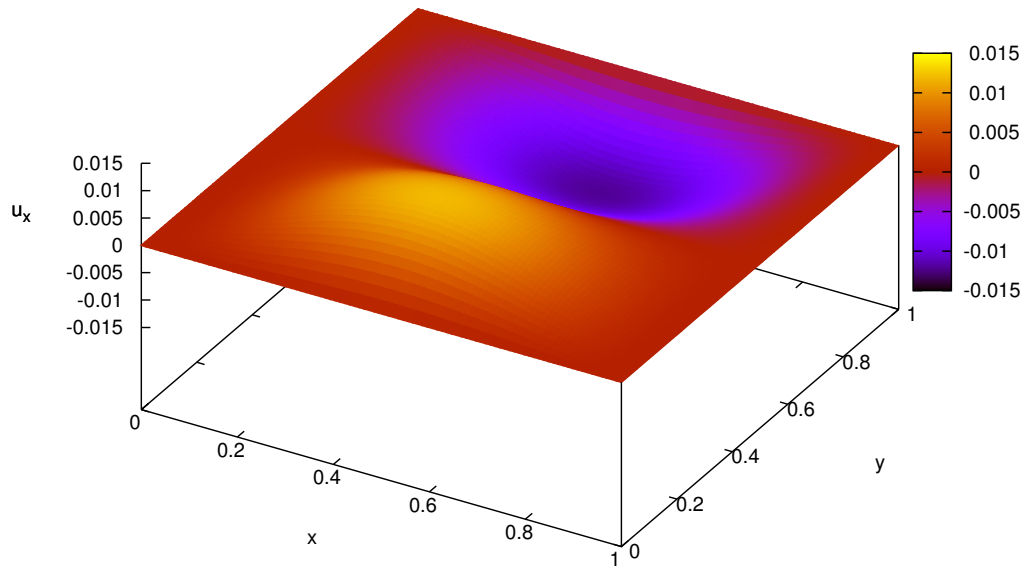
Figure 2.1: Reference velocity solution x-component
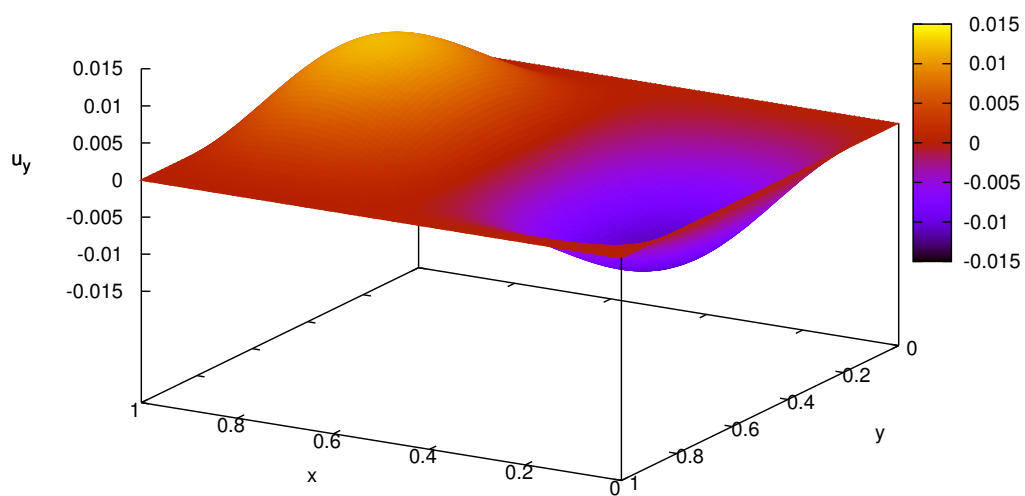
Figure 2.2: Reference velocity solution y-component
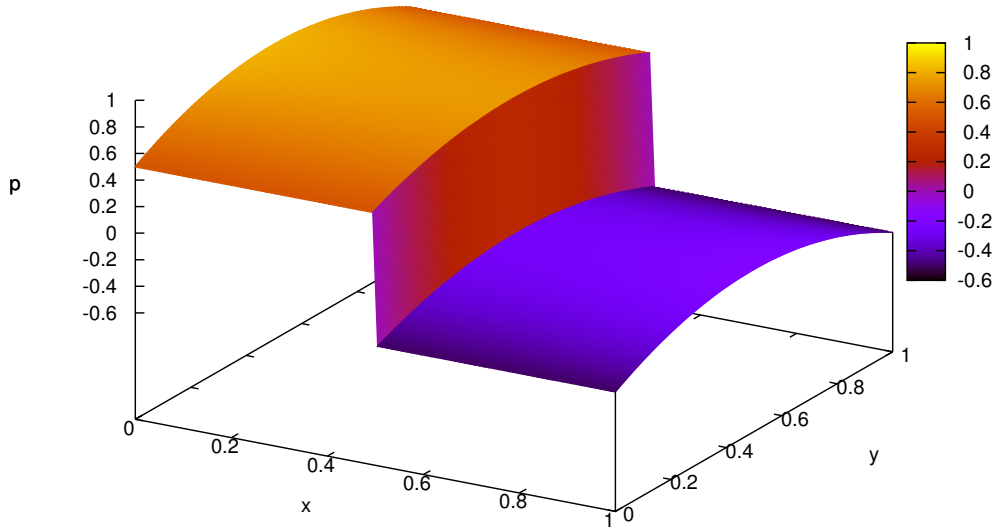
Figure 2.3: Reference pressure solution

Table 2.1: Spatial convergence for the $\mathcal{Q}_2/\mathcal{Q}_1$ element

#cells	$\|\boldsymbol{u} - \boldsymbol{u_h}\|_{L^2}$		$\|\boldsymbol{u} - \boldsymbol{u_h}\|_{H^1}$		$\|\operatorname{div}\boldsymbol{u_h}\|_{L^2}$		$\|p - p_h\|_{L^2}$	
4	1.026e-02	-	1.188e-01	-	1.114e-01	-	2.512e-01	-
16	4.852e-03	1.08	9.199e-02	0.37	8.847e-02	0.33	1.891e-01	0.41
64	1.820e-03	1.41	6.625e-02	0.47	6.500e-02	0.44	1.343e-01	0.49
256	6.537e-04	1.48	4.717e-02	0.49	4.673e-02	0.48	9.498e-02	0.50
1024	2.329e-04	1.49	3.347e-02	0.50	3.331e-02	0.49	6.716e-02	0.50
4096	8.265e-05	1.49	2.370e-02	0.50	2.365e-02	0.49	4.749e-02	0.50
16384	2.928e-05	1.50	1.678e-02	0.50	1.676e-02	0.50	3.358e-02	0.50
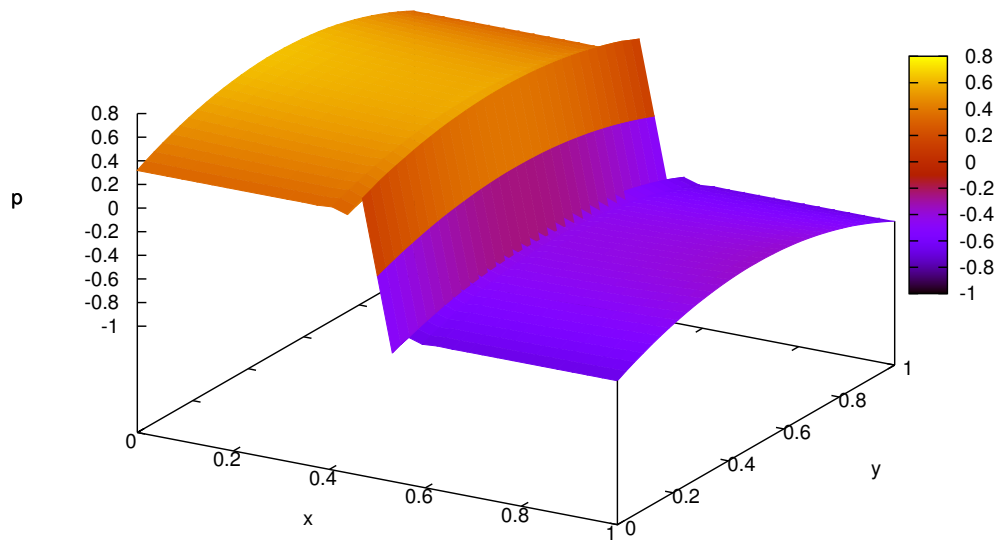
Figure 2.4: Pressure solution with the $\mathcal{Q}_2/\mathcal{Q}_1$ element
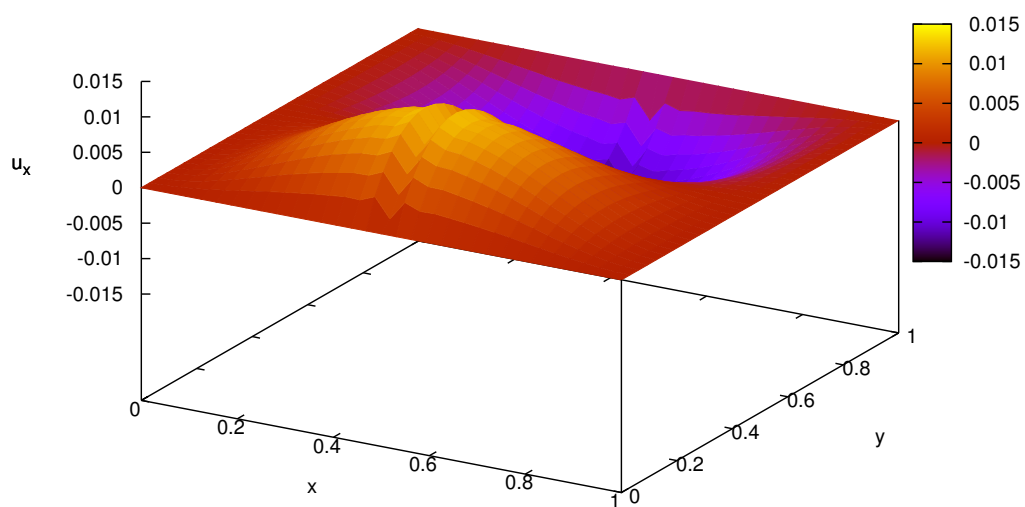
Figure 2.5: Solution of the first velocity component with the $\mathcal{Q}_2/\mathcal{Q}_1$ element

to the continuous case. Additionally, no artifacts can be seen in the velocity solution(2.7. Table 2.2 also reveals that none of the convergence rates for pressure and velocity are affected by the discontinuity in the reference solution. This result is confirmed by the results for a $\mathcal{Q}_3/(\mathcal{Q}_2 + \mathcal{Q}_0)$ discretization in Table 2.3.
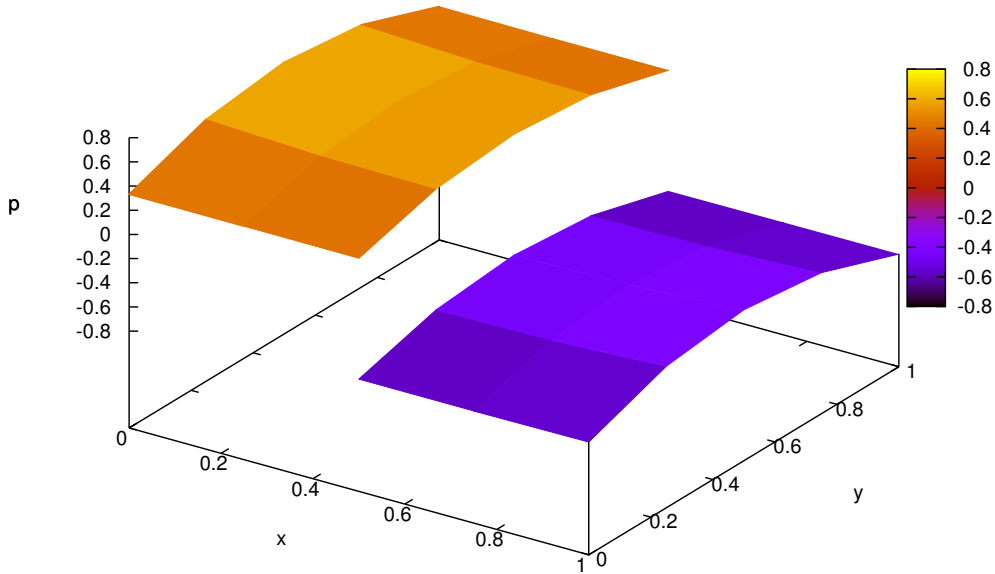
Figure 2.6: Pressure solution with the $\mathcal{Q}_2/(\mathcal{Q}_1 + \mathcal{Q}_0)$ element

Table 2.2: Spatial convergence for the $\mathcal{Q}_2/(\mathcal{Q}_1 + \mathcal{Q}_0)$ element

#cells	$\|\boldsymbol{u} - \boldsymbol{u_h}\|_{L^2}$		$\|\boldsymbol{u} - \boldsymbol{u_h}\|_{H^1}$		$\|\operatorname{div} \boldsymbol{u_h}\|_{L^2}$		$\|p - p_h\|_{L^2}$	
4	1.267e-03	-	1.783e-02	-	1.017e-02	-	2.085e-02	-
16	1.714e-04	2.89	4.500e-03	1.99	2.991e-03	1.77	5.231e-03	2.00
64	2.151e-05	2.99	1.118e-03	2.01	7.756e-04	1.95	1.304e-03	2.00
256	2.687e-06	3.00	2.787e-04	2.00	1.960e-04	1.98	3.258e-04	2.00
1024	3.357e-07	3.00	6.962e-05	2.00	4.916e-05	2.00	8.146e-05	2.00
4096	4.204e-08	3.00	1.740e-05	2.00	1.230e-05	2.00	2.037e-05	2.00
16384	6.026e-09	2.80	4.352e-06	2.00	3.078e-06	2.00	5.101e-06	2.00

Furthermore, Table 2.4 shows that the solution achieved by the $\mathcal{Q}_1 + \mathcal{Q}_0$ element is numerically local conservative, i.e.

$$\max_k |(\operatorname{div} \boldsymbol{u_h}, 1)_{L^2(K)}| \approx 0. \tag{2.52}$$
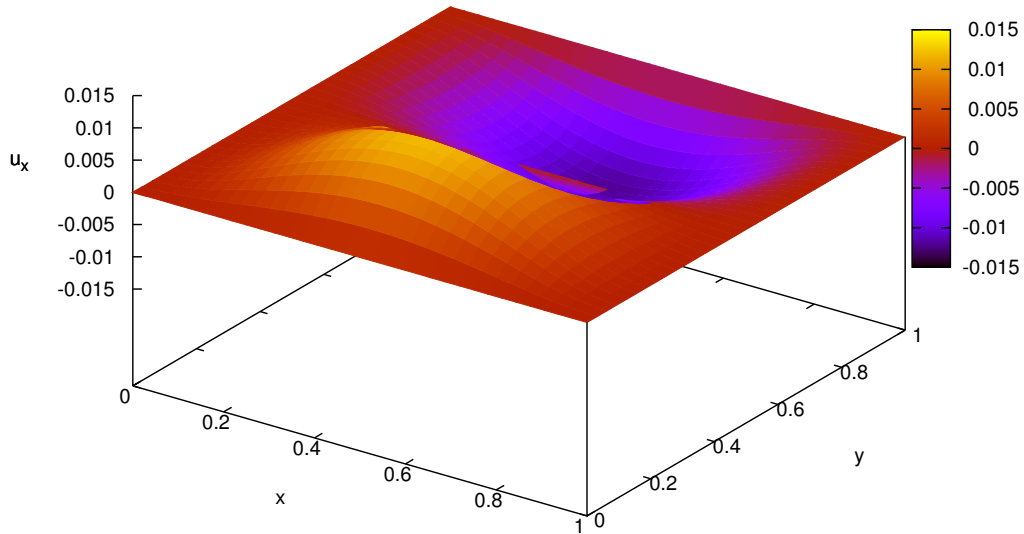
Figure 2.7: Solution of the first velocity component with the $\mathcal{Q}_2/(\mathcal{Q}_1 + \mathcal{Q}_0)$ element

Table 2.3: Spatial convergence for the $\mathcal{Q}_3/(\mathcal{Q}_2 + \mathcal{Q}_0)$ element

#cells	$\|\boldsymbol{u} - \boldsymbol{u_h}\|_{L^2}$		$\|\boldsymbol{u} - \boldsymbol{u_h}\|_{H^1}$		$\|\operatorname{div} \boldsymbol{u_h}\|_{L^2}$		$\|p - p_h\|_{L^2}$	
4	1.002e-04	-	1.968e-03	-	1.795e-03	-	3.744e-04	-
16	6.154e-06	4.03	2.351e-04	3.07	2.281e-04	2.98	3.963e-05	3.24
64	3.815e-07	4.01	2.898e-05	3.02	2.872e-05	2.99	5.187e-06	2.93
256	2.378e-08	4.00	3.609e-06	3.01	3.600e-06	3.00	6.610e-07	2.97
1024	1.486e-09	4.00	4.506e-07	3.00	4.503e-07	3.00	8.372e-08	2.98

Table 2.4: Local mass conservation

#cells	$\mathcal{Q}_2/\mathcal{Q}_1$	$\mathcal{Q}_2/(\mathcal{Q}_1 + \mathcal{Q}_0)$	$\mathcal{Q}_3/(\mathcal{Q}_2 + \mathcal{Q}_0)$
4	1.30500e-02	1.35106e-17	2.22681e-09
16	5.54285e-03	1.21998e-08	6.62999e-09
64	1.42973e-03	2.45045e-09	1.54363e-09
256	3.57486e-04	5.50899e-09	1.37852e-09
1024	8.93714e-05	7.64287e-10	9.66402e-10
4096	2.23428e-05	1.83063e-10	4.39099e-10
16384	5.58570e-06	1.38260e-10	1.75149e-10

However, this does not mean that the pressure solution is pointwise solenoidal. Figure 2.8 clearly shows that the divergence is discontinous across element boundaries and vanishes only in average on each element.
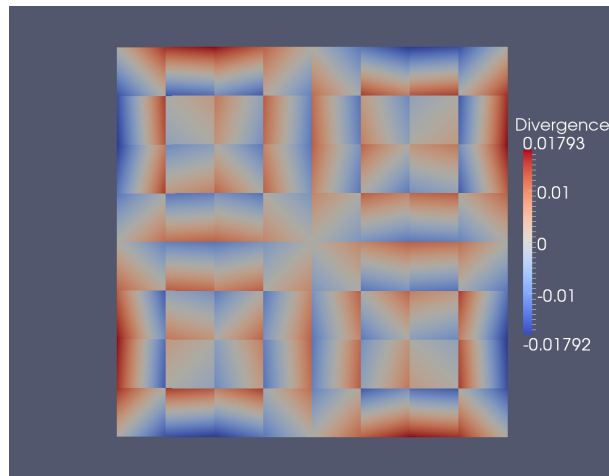
Figure 2.8: Pointwise divergence for the $\mathcal{Q}_2/(\mathcal{Q}_1 + \mathcal{Q}_0)$ pair

2.6 Computational costs

Finally, we compare the computational effort that has to be used for the element pairs $\mathcal{Q}_2/(\mathcal{Q}_1 + \mathcal{Q}_0)$ and $\mathcal{Q}_2/\mathcal{Q}_1$.

In Table 2.5 the number of degrees of freedom for both solution components is listed. Since both pairs use a $\mathcal{Q}_2$-approximation for the velocity the number of dofs are the same. The used pressure spaces differ by exactly one degree of freedom per cell. Therefore there are as many dofs more for the discontinuous approximation as there are cells in the triangulation. In our case of a first order approximation this number nearly doubles.

Table 2.5: Number of degrees of freedom (dofs) for the $\mathcal{Q}_2/(\mathcal{Q}_1 + \mathcal{Q}_0)$ element and the $\mathcal{Q}_2/\mathcal{Q}_1$ element

# cells	4	16	64	256	1024	4096	16384
# velocity dofs	50	162	578	2178	8450	33282	132098
# pressure dofs $\mathcal{Q}_2/(\mathcal{Q}_1 + \mathcal{Q}_0)$	13	41	145	545	2113	8321	33025
# pressure dofs $\mathcal{Q}_2/\mathcal{Q}_1$	9	25	81	289	1089	4225	16641

Nevertheless, the number of degrees of freedom for the pressure is in both cases much smaller than the number of dofs for the velocity. Therefore, it is not surprising that the assembling does not take much more time using the discontinuous elements (Table 2.6). However, for solving the linear equations there seems to be a significant difference between the two approximations. Whereas the solver time is comparable for the coarsest triangulations, solving takes nearly twice the time for a discontinuous approximation on the finest mesh. Apart from that Table 2.6 shows that the preconditioner for the Schur complement is well chosen. The number of needed iterations is nearly the same for all mesh sizes and both approximations.

Table 2.6: Comparison of running time and solver iterations between the $\mathcal{Q}_2/\mathcal{Q}_1$ pair and the $\mathcal{Q}_2/(\mathcal{Q}_1 + \mathcal{Q}_0)$ pair

	time for assembling		time for solving		solver iterations	
#cells	$\mathcal{Q}_2/(\mathcal{Q}_1 + \mathcal{Q}_0)$	$\mathcal{Q}_2/\mathcal{Q}_1$	$\mathcal{Q}_2/(\mathcal{Q}_1 + \mathcal{Q}_0)$	$\mathcal{Q}_2/\mathcal{Q}_1$	$\mathcal{Q}_2/(\mathcal{Q}_1 + \mathcal{Q}_0)$	$\mathcal{Q}_2/\mathcal{Q}_1$
4	$6.3 \cdot 10^{-4}$	$8.4 \cdot 10^{-4}$	$3.7 \cdot 10^{-4}$	$3.5 \cdot 10^{-4}$	6	5
16	$1.3 \cdot 10^{-3}$	$2.1 \cdot 10^{-3}$	$1.0 \cdot 10^{-3}$	$1.4 \cdot 10^{-3}$	9	9
64	$5.9 \cdot 10^{-3}$	$8.8 \cdot 10^{-3}$	$5.3 \cdot 10^{-3}$	$4.3 \cdot 10^{-3}$	10	9
256	$2.6 \cdot 10^{-2}$	$2.8 \cdot 10^{-2}$	$2.2 \cdot 10^{-2}$	$1.5 \cdot 10^{-2}$	9	9
1024	$1.2 \cdot 10^{-1}$	$1.2 \cdot 10^{-1}$	$1.6 \cdot 10^{-1}$	$1.0 \cdot 10^{-1}$	10	9
4096	$7.3 \cdot 10^{-1}$	$7.3 \cdot 10^{-1}$	$1.1 \cdot 10^{0}$	$7.3 \cdot 10^{-1}$	10	10
16384	$4.0 \cdot 10^{0}$	$4.0 \cdot 10^{0}$	$5.5 \cdot 10^{0}$	$3.2 \cdot 10^{0}$	10	10

Summarizing the numerical results, the use of the $\mathcal{Q}_2/(\mathcal{Q}_1 + \mathcal{Q}_0)$ improves the mass conservation much. Furthermore, the order of convergence in cases, where the pressure is discontinuous, benefits significantly by the choice of the new element pair. Of course, the computational costs using the discontinuous are higher. Surprisingly, only the solver but not the assembling was affected.

3 Discontinuous Galerkin methods for the Poisson equation

Up to now we have considered only problems where the pressure is approximated by functions in $L^2(\Omega)$. In particular we imposed no differentiability assumptions on the discrete pressure space. However, when using projection methods for solving incompressible flow problems one needs to solve a Poisson equation for the pressure. We will face the same problem for the construction of a suitable preconditioner for our Navier-Stokes solver in 4.2. In these cases obviously at least weak differentiability of the discrete pressure is needed. Although the spaces $\nabla \mathcal{Q}_k$ and $\nabla(\mathcal{Q}_k + \mathcal{Q}_0)$ are the same, some difficulties arise when moving from continuous to discontinuous elements.

In this section we discuss suitable approaches for solving a Poisson equation with discontinuous ansatz functions. We roughly follow the paper [ABCM02] by Arnold and the presentation in [Har08] by Hartmann.

3.1 Notations

In order to be able to work on a non-discrete level with functions that are potentially discontinuous, we have to define a space that allows us to use Sobolov space function on each element of a finite element triangulation.

Definition 3.1 (Broken Sobolev space)**.** Let $\mathcal{T}_h$ be a triangulation for the domain Ω. We define by $H^k(\mathcal{T}_h)$ the *broken Sobolev space* whose restriction to each element $K \in \mathcal{T}_h$ belongs to the Sobolev space $H^k(K)$, i.e.

$$H^k(\mathcal{T}_h) := \{f \in L^2(\Omega) : v|_K \in H^k(K) \quad \forall K \in \mathcal{T}_h\}.$$

Function in this space are typically discontinuous across element borders and therefore double-valued on the interior boundaries. The following definition gives the necessary notation for this situation.

Definition 3.2 (Traces)**.** For a function $f \in H^1(\mathcal{T}_h)$ we denote by $f^\pm$ the *traces* from within and from without of a considered element K on the boundary ∂K. The traces of functions in $H^1(\mathcal{T}_h)$ then belong to $T(\Gamma) := \prod_{K \in \mathcal{T}_h} L^2(\partial K)$ where Γ is the union of the boundaries of the elements K. Note that the traces are single-valued on $\partial \Omega$ and $f^- = f^+$.

3.2 Primal flux formulation

The aim of this section is to solve a Poisson problem on a domian Ω using Neumann conditions on Γ_N and Dirichlet boundary conditions on $\Gamma_D = \partial\Omega \setminus \Gamma_N$. In the given setup the problem reads in

$$
\begin{aligned}
\text{Find } u \in H^1(\mathcal{T}_h) \text{ such that} \\
-\Delta u(x) = f(x) \quad &\forall x \in \Omega \\
\nabla u(x) \cdot \boldsymbol{n}(x) = g(x) \quad &\forall x \in \Gamma_N \\
u(x) = h(x) \quad &\forall x \in \Gamma_D.
\end{aligned}
\tag{3.1}
$$

By introducing a new variable $\boldsymbol{\sigma} \in [H^1(\Omega)]^d$ these equations can be rewritten as the first-order system

$$
\begin{aligned}
\text{Find } (u, \boldsymbol{\sigma}) \in H^1(\mathcal{T}_h) \times [H^1(\Omega)]^d \text{ such that} \\
\boldsymbol{\sigma}(\boldsymbol{x}) = \nabla u(x) \quad &\forall x \in \Omega \\
-\nabla \cdot \boldsymbol{\sigma}(x) = f(x) \quad &\forall x \in \Omega \\
\nabla u(x) \cdot \boldsymbol{n}(x) = g(x) \quad &\forall x \in \Gamma_N \\
u(x) = h(x) \quad &\forall x \in \Gamma_D.
\end{aligned}
\tag{3.2}
$$

where $\boldsymbol{n}(x)$ denotes the unit normal vector. The variational formulation is then given by multiplying the equations with $\boldsymbol{\tau} \in [H^1(\mathcal{T}_h)]^d$ resp. $v \in H^1(\mathcal{T}_h)$ and integrating over an element $K \subset \Omega$

$$
\begin{aligned}
\int_K \boldsymbol{\sigma} \cdot \boldsymbol{\tau}\, dx &= -\int_K u \nabla \cdot \boldsymbol{\tau}\, dx + \int_{\partial K} u \boldsymbol{\tau} \cdot \boldsymbol{n}\, dx \\
\int_K \boldsymbol{\sigma} \cdot \nabla v\, dx &= \int_K f\, v\, dx + \int_{\partial K} \boldsymbol{\sigma} \cdot \boldsymbol{n} v\, dx.
\end{aligned}
\tag{3.3}
$$

Since the functions we consider here are discontinuous, the boundary terms do not cancel out when we sum over all elements. The resulting *system flux formulation* reads

$$
\int_\Omega \boldsymbol{\sigma} \cdot \boldsymbol{\tau}\, dx = -\int_\Omega u \nabla \cdot \boldsymbol{\tau}\, dx + \sum_{K \in \mathcal{T}_h} \int_{\partial K} \hat{u} \boldsymbol{\tau} \cdot \boldsymbol{n}\, dx \qquad \forall \boldsymbol{\tau} \in [H^1(\mathcal{T}_h)]^d \tag{3.4}
$$

$$
\int_\Omega \boldsymbol{\sigma} \cdot \nabla v\, dx = \int_\Omega f\, v\, dx + \sum_{K \in \mathcal{T}_h} \int_{\partial K} \hat{\boldsymbol{\sigma}} \cdot \boldsymbol{n} v\, dx \qquad \forall v \in H^1(\mathcal{T}_h). \tag{3.5}
$$

where $\hat{u}$ is a scalar numerical flux function and $\hat{\boldsymbol{\sigma}}$ is a vector-valued numerical flux function. All the in this section considered models differ only by the choice of these two functions and hence all properties of the discretizations depend on the fluxes.

Definition 3.3 (Consistency, conservativity). The numerical fluxes $\hat{u}$ and $\hat{\boldsymbol{\sigma}}$ are called *consistent* if

$$\hat{u}(v) = v, \qquad \hat{\boldsymbol{\sigma}}(v, \nabla v) = \nabla v \qquad \text{on } \Gamma \tag{3.6}$$

whenever v is a smooth function. Furthermore, we say that $\hat{u}$ and $\hat{\boldsymbol{\sigma}}$ are *conservative* if they are single-valued on Γ.

Now we want to reduce the size of the problem by eliminating the variable $\boldsymbol{\sigma}$. Therefore, we perform another integration by parts in (3.4) and set $\boldsymbol{\tau} = \nabla v$

$$\int_\Omega \boldsymbol{\sigma} \cdot \nabla v \, dx = \int_\Omega \nabla u \cdot \nabla v \, dx + \sum_{K \in \mathcal{T}_h} \int_{\partial K} (\hat{u} - u) \boldsymbol{n} \cdot \nabla v \, dx. \tag{3.7}$$

Substituting (3.7) into (3.5) gives with the bilinear form $\hat{B}(\cdot, \cdot) : H^2(\mathcal{T}_h) \times H^2(\mathcal{T}_h) \to \mathbb{R}$

$$\hat{B}(u, v) = \int_\Omega \nabla u \cdot \nabla v \, dx - \sum_{K \in \mathcal{T}_h} \int_{\partial K} \hat{\boldsymbol{\sigma}} \cdot \boldsymbol{n} v \, dx + \sum_{K \in \mathcal{T}_h} \int_{\partial K} (\hat{u} - u) \boldsymbol{n} \cdot \nabla v \, dx \tag{3.8}$$

the *element-based primal flux formulation*

$$\hat{B}(u, v) = \int_\Omega f \, v \, dx \qquad \forall v \in H^2(\mathcal{T}_h). \tag{3.9}$$

Next we want to have a *face-based* form, i.e. a formulation in terms of $\int_\Gamma$, instead of the *element-based* form, i.e. the formulation in terms of $\int_{\partial K}$ in which every interior face occurs twice. Before doing this we again need to describe some operators on boundaries of elements.

Definition 3.4 (Mean value and jump operator). Let $e \in \Gamma \setminus \partial\Omega := \Gamma \setminus \partial\Omega$ be an interior face between two adjacent elements K^+ and K^- with unit outward normal vectors, $\boldsymbol{n}^+, \boldsymbol{n}^- \in \mathbb{R}^d$. Let $q \in T(\mathcal{T}_h)$ and $\boldsymbol{\phi} \in [T(\mathcal{T}_h)]^d$ be the traces of a scalar and a vector valued function. Then, we define the *mean value* and the *jump operator*, $\{\!\{\cdot\}\!\}$ and $[\![\cdot]\!]$, as follows

$$\begin{aligned}
\{\!\{q\}\!\} &= \frac{1}{2}(q^+ + q^-) & [\![q]\!] &= q^+ \boldsymbol{n}^+ + q^- \boldsymbol{n}^- \\
\{\!\{\boldsymbol{\phi}\}\!\} &= \frac{1}{2}(\boldsymbol{\phi}^+ + \boldsymbol{\phi}^-) & [\![\boldsymbol{\phi}]\!] &= \boldsymbol{\phi}^+ \cdot \boldsymbol{n}^+ + \boldsymbol{\phi}^- \cdot \boldsymbol{n}^-.
\end{aligned} \tag{3.10}$$

On boundary edges $e \in \partial\Omega$ the mean value and jump operators are defined by

$$\begin{aligned}
\{\!\{q\}\!\} &= q^+ & [\![q]\!] &= q^+ \boldsymbol{n}^+ \\
\{\!\{\boldsymbol{\phi}\}\!\} &= \boldsymbol{\phi}^+ & [\![\boldsymbol{\phi}]\!] &= \boldsymbol{\phi}^+ \cdot \boldsymbol{n}^+.
\end{aligned} \tag{3.11}$$

Now we are able to express the discretization in terms of integrals over the interior faces Γ. The equivalence of these two formulations is proved in the following Lemma.

Lemma 3.5. *The element-based primal flux form (3.9) is equivalent to the* face-based primal flux form

$$
\begin{aligned}
&Find\ u \in H^2(\mathcal{T}_h)\ such\ that\\
&\hat{C}(u,v) = \int_\Omega f\,v\,dx \qquad \forall v \in H^2(\mathcal{T}_h)
\end{aligned}
\tag{3.12}
$$

where $C(\cdot,\cdot)$ is defined by

$$
\begin{aligned}
\hat{C}(u,v) := &\int_\Omega \nabla u \cdot \nabla v\,dx + \int_\Gamma \left(\llbracket \hat{u} - u \rrbracket \cdot \{\!\{\nabla v\}\!\} - \{\!\{\hat{\boldsymbol{\sigma}}\}\!\} \cdot \llbracket v \rrbracket\right) dx\\
&+ \int_{\Gamma\setminus\partial\Omega} \left(\{\!\{\hat{u} - u\}\!\}\llbracket \nabla v \rrbracket - \llbracket \hat{\boldsymbol{\sigma}} \rrbracket\{\!\{v\}\!\}\right) dx.
\end{aligned}
\tag{3.13}
$$

Proof. Let $q \in T(\mathcal{T}_h)$ and $\boldsymbol{\phi} \in [T(\mathcal{T}_h)]^d$. Then we get

$$
\begin{aligned}
&\int_{\Gamma\setminus\partial\Omega} \{\!\{\boldsymbol{\phi}\}\!\} \cdot \llbracket q \rrbracket + \llbracket \boldsymbol{\phi} \rrbracket\{\!\{q\}\!\}\,dx\\
&= \frac{1}{2}\int_{\Gamma\setminus\partial\Omega} \left(\boldsymbol{\phi}^+ + \boldsymbol{\phi}^-\right)\cdot\left(q^+\boldsymbol{n}^+ + q^-\boldsymbol{n}^-\right) + \left(\boldsymbol{\phi}^+ \cdot \boldsymbol{n}^+ + \boldsymbol{\phi}^- \cdot \boldsymbol{n}^-\right)\left(q^+ + q^-\right)dx\\
&= \frac{1}{2}\int_{\Gamma\setminus\partial\Omega} \boldsymbol{\phi}^+ \cdot \boldsymbol{n}^+ q^+ + \boldsymbol{\phi}^+ \cdot \boldsymbol{n}^- q^- + \boldsymbol{\phi}^- \cdot \boldsymbol{n}^+ q^+ + \boldsymbol{\phi}^- \cdot \boldsymbol{n}^- q^-\,dx\\
&\quad + \frac{1}{2}\int_{\Gamma\setminus\partial\Omega} \boldsymbol{\phi}^+ \cdot \boldsymbol{n}^+ q^+ + \boldsymbol{\phi}^+ \cdot \boldsymbol{n}^+ q^- + \boldsymbol{\phi}^- \cdot \boldsymbol{n}^- q^+ + \boldsymbol{\phi}^- \cdot \boldsymbol{n}^- q^-\,dx\\
&= \int_{\Gamma\setminus\partial\Omega} \boldsymbol{\phi}^+ \cdot \boldsymbol{n}^+ q^+ + \boldsymbol{\phi}^- \cdot \boldsymbol{n}^- q^-\,dx\\
&= \sum_{K\in\mathcal{T}_h} \int_{\partial K\setminus\partial\Omega} \boldsymbol{\phi}^+ \cdot \boldsymbol{n}^+ q^+\,dx
\end{aligned}
\tag{3.14}
$$

On $\partial\Omega$ we have $\{\!\{\boldsymbol{\phi}\}\!\} \cdot \llbracket q \rrbracket = \boldsymbol{\phi}^+ \cdot \boldsymbol{n}^+ q^+$ and therefore

$$
\int_\Gamma \{\!\{\boldsymbol{\phi}\}\!\} \cdot \llbracket q \rrbracket\,dx + \int_{\Gamma\setminus\partial\Omega} \llbracket \boldsymbol{\phi} \rrbracket\{\!\{q\}\!\}\,dx = \sum_{K\in\mathcal{T}_h} \int_{\partial K} \boldsymbol{\phi}^+ \cdot \boldsymbol{n}^+ q^+\,dx
\tag{3.15}
$$

holds.

We now apply (3.15) twice (once with $\boldsymbol{\phi} = \hat{\boldsymbol{\sigma}}$ and $q = v$, once with $\boldsymbol{\phi} = \nabla v$ and $q = \hat{u} - u$)

to the element-based form (3.9)

$$
\begin{aligned}
\hat{B}(u,v) &= \int_{\Omega} \nabla u \cdot \nabla v \, dx - \sum_{K \in \mathcal{T}_h} \int_{\partial K} \hat{\boldsymbol{\sigma}} \cdot \boldsymbol{n} v \, dx + \sum_{K \in \mathcal{T}_h} \int_{\partial K} (\hat{u} - u) \boldsymbol{n} \cdot \nabla v \, dx \\
&= \int_{\Omega} \nabla u \cdot \nabla v \, dx - \int_{\Gamma} \{\!\!\{\hat{\boldsymbol{\sigma}}\}\!\!\} \cdot [\![v]\!] \, dx - \int_{\Gamma \setminus \partial \Omega} [\![\hat{\boldsymbol{\sigma}}]\!] [\![v]\!] \, dx \\
&\quad + \int_{\Gamma} \{\!\!\{\nabla v\}\!\!\} \cdot [\![\hat{u} - u]\!] \, dx + \int_{\Gamma \setminus \partial \Omega} [\![\nabla v]\!] \{\!\!\{\hat{u} - u\}\!\!\} \, dx.
\end{aligned}
\tag{3.16}
$$

Rearranging terms then gives

$$
\begin{aligned}
\hat{B}(u,v) &= \int_{\Omega} \nabla u \cdot \nabla v \, dx + \int_{\Gamma} \left([\![\hat{u} - u]\!] \cdot \{\!\!\{\nabla v\}\!\!\} - \{\!\!\{\hat{\boldsymbol{\sigma}}\}\!\!\} \cdot [\![v]\!] \right) dx \\
&\quad + \int_{\Gamma \setminus \partial \Omega} \left(\{\!\!\{\hat{u} - u\}\!\!\} [\![\nabla v]\!] - [\![\hat{\boldsymbol{\sigma}}]\!] \{\!\!\{v\}\!\!\} \right) dx \\
&= \hat{C}(u,v)
\end{aligned}
\tag{3.17}
$$

and consequently the equivalence of the two formulations. $\qquad\square$

3.3 Examples of Discontinous Galerkin methods

Up to now we did not specify the flux functions $\hat{u}$ and $\hat{\sigma}$. We consider three different models here.

1. **The symmetric interior penalty method (SIPG)**
   The fluxes $\hat{u}$ and $\hat{\boldsymbol{\sigma}}$ are chosen according to

$$
\begin{aligned}
\hat{u} &= \{\!\!\{u\}\!\!\} & \hat{\boldsymbol{\sigma}} &= \{\!\!\{\nabla u\}\!\!\} - \delta^{ip}(u) & &\text{on } \Gamma \setminus \partial \Omega \\
\hat{u} &= g_D & \hat{\boldsymbol{\sigma}} &= \nabla u - \delta_{\Gamma}^{ip}(u) & &\text{on } \Gamma_D \\
\hat{u} &= u & \hat{\boldsymbol{\sigma}} &= g_N \boldsymbol{n} & &\text{on } \Gamma_N
\end{aligned}
\tag{3.18}
$$

   where the penalty terms are defined by

$$
\begin{aligned}
\delta^{ip}(u) &= \delta [\![u]\!] & &\text{on } \Gamma \setminus \partial \Omega \\
\delta_{\Gamma}^{ip}(u) &= \delta(u - g_D)\boldsymbol{n} & &\text{on } \Gamma_D.
\end{aligned}
\tag{3.19}
$$

   As it turns out later, a suitable choice for the penalty parameter δ is given by $\delta = C\, p^2/h$ where p is the polynomial degree of the used approximation space and h the mean value of the adjoining cells' diameter.

2. **The non-symmetric interior penalty method (NIPG)**
   The fluxes for the NIPG model only differ from the SIPG choices by the definition

of the boundaries $\hat{u}$ on $\Gamma \setminus \partial\Omega$ and Γ_D:

$$
\begin{aligned}
\hat{u} &= \{\!\{u\}\!\} + \boldsymbol{n}^+ \cdot [\![u]\!] & \hat{\boldsymbol{\sigma}} &= \{\!\{\nabla u\}\!\} - \delta^{ip}(u) & &\text{on } \Gamma \setminus \partial\Omega \\
\hat{u} &= 2u - g_D & \hat{\boldsymbol{\sigma}} &= \nabla u - \delta_\Gamma^{ip}(u) & &\text{on } \Gamma_D \\
\hat{u} &= u & \hat{\boldsymbol{\sigma}} &= g_N \boldsymbol{n} & &\text{on } \Gamma_N
\end{aligned}
\tag{3.20}
$$

The penalty terms $\delta^{ip}(u)$ and $\delta_\Gamma^{ip}(u)$ are chosen as before.

3. **The method of Baumann-Oden (BO)**
   The BO method is a special case of the NIPG model in which the penalty parameter vanishes. In particular, the numerical flux function $\hat{u}$ is unchanged:

$$
\begin{aligned}
\hat{u} &= \{\!\{u\}\!\} + \boldsymbol{n}^+ \cdot [\![u]\!] & \hat{\boldsymbol{\sigma}} &= \{\!\{\nabla u\}\!\} & &\text{on } \Gamma \setminus \partial\Omega \\
\hat{u} &= 2u - g_D & \hat{\boldsymbol{\sigma}} &= \nabla u & &\text{on } \Gamma_D \\
\hat{u} &= u & \hat{\boldsymbol{\sigma}} &= g_N \boldsymbol{n} & &\text{on } \Gamma_N
\end{aligned}
\tag{3.21}
$$

These three models can be unified into one equation

$$
\begin{aligned}
B(u, v) &= \int_\Omega \nabla u \cdot \nabla v \, dx + \int_{\Gamma_\mathcal{I} \cup \Gamma_D} \left(\theta [\![u]\!] \cdot \{\!\{\nabla v\}\!\} - \{\!\{\nabla u\}\!\} \cdot [\![v]\!] \right) dx \\
&\quad + \int_{\Gamma_\mathcal{I} \cup \Gamma_D} \delta [\![u]\!] \cdot [\![v]\!] \, dx \\
F(v) &= \int_\Omega f \, v \, dx + \int_{\Gamma_D} \theta g_D \boldsymbol{n} \cdot \nabla v \, dx + \int_{\Gamma_D} \delta g_D v \, dx + \int_{\Gamma_N} g_N v \, dx.
\end{aligned}
\tag{3.22}
$$

where the parameters corresponding to the considered methods are given by

$$
\begin{array}{lll}
\text{SIPG:} & \theta = -1 & \delta > 0 \\
\text{NIPG:} & \theta = 1 & \delta > 0 \\
\text{Baumann-Oden:} & \theta = 1 & \delta = 0.
\end{array}
$$

3.4   Uniqueness and approximation results

Now the question arises whether the considered methods yield a unique solution when applied to the Poisson equation and furthermore what kind of approximation results can be obtained.

First of all we check whether a solution to the original Poisson problem also solves the variational formulation proposed by SIPG, NIPG or Baumann-Oden.

Theorem 3.6 (Consistency). *A discontinuous Galerkin discretization of the form (3.12) is consistent, i.e. a solution $u \in H^2(\Omega)$ to the original Poisson problem (3.1) satisfies*

$$\hat{B}(u,v) = F(v) \qquad \forall v \in H^2(\mathcal{T}_h), \tag{3.23}$$

if and only if the numerical fluxes $\hat{u}$ and $\hat{\boldsymbol{\sigma}}$ are consistent (cf. Definition 3.3).

Proof. Let $u \in H^2(\Omega)$ be a solution to the original Poisson problem. Then $\{\!\{u\}\!\} = u$ and $[\![u]\!] = 0$ and we can conclude

$$
\begin{aligned}
\hat{B}(u,v) &= \int_\Omega \nabla u \cdot \nabla v \, dx + \int_\Gamma [\![\hat{u} - u]\!] \cdot \{\!\{\nabla v\}\!\} - \{\!\{\hat{\boldsymbol{\sigma}}\}\!\} \cdot [\![v]\!] \, dx \\
&\quad + \int_{\Gamma \backslash \partial\Omega} \{\!\{\hat{u} - u\}\!\} [\![\nabla v]\!] - [\![\hat{\boldsymbol{\sigma}}]\!] \{\!\{v\}\!\} \, dx \\
&= -\int_\Omega \Delta u v \, dx + \sum_{K \in \mathcal{T}_h} \int_{\partial K} \nabla u \cdot \boldsymbol{n} v \, dx \\
&\quad + \int_\Gamma [\![\hat{u}]\!] \cdot \{\!\{\nabla v\}\!\} - \{\!\{\hat{\boldsymbol{\sigma}}\}\!\} \cdot [\![v]\!]) \, dx + \int_{\Gamma \backslash \partial\Omega} (\{\!\{\hat{u}\}\!\} - u)[\![\nabla v]\!] - [\![\hat{\boldsymbol{\sigma}}]\!]\{\!\{v\}\!\} \, dx \\
&= \int_\Omega fv \, dx + \int_\Gamma \{\!\{\nabla u\}\!\} \cdot [\![v]\!] \, dx + \int_{\Gamma \backslash \partial\Omega} [\![\nabla u]\!]\{\!\{v\}\!\} \, dx \\
&\quad + \int_\Gamma [\![\hat{u}]\!] \cdot \{\!\{\nabla v\}\!\} - \{\!\{\hat{\boldsymbol{\sigma}}\}\!\} \cdot [\![v]\!]) \, dx + \int_{\Gamma \backslash \partial\Omega} (\{\!\{\hat{u}\}\!\} - u)[\![\nabla v]\!] - [\![\hat{\boldsymbol{\sigma}}]\!]\{\!\{v\}\!\} \, dx \\
&= \int_\Omega fv \, dx + \int_\Gamma (\nabla u - \{\!\{\hat{\boldsymbol{\sigma}}\}\!\}) \cdot [\![v]\!] + [\![\hat{u}]\!] \cdot \{\!\{\nabla v\}\!\} \, dx \\
&\quad + \int_{\Gamma \backslash \partial\Omega} (\{\!\{\hat{u}\}\!\} - u)[\![\nabla v]\!] - [\![\hat{\boldsymbol{\sigma}}]\!]\{\!\{v\}\!\} \, dx.
\end{aligned}
\tag{3.24}
$$

If the numerical fluxes are consistent $\{\!\{\hat{\boldsymbol{\sigma}}\}\!\} = \nabla u$, $\{\!\{\hat{u}\}\!\} = u$, $[\![\hat{\boldsymbol{\sigma}}]\!] = 0$ and $[\![\hat{u}]\!] = 0$. This gives

$$\hat{B}(u,v) = \int_\Omega fv \, dx. \tag{3.25}$$

and the discretization is consistent.

Conversely, if the discretization is consistent, (3.24) implies

$$
\begin{aligned}
\{\!\{\hat{\boldsymbol{\sigma}}\}\!\} = \nabla u \quad & [\![\hat{\boldsymbol{\sigma}}]\!] = 0 \\
\{\!\{\hat{u}\}\!\} = u \quad & [\![\hat{u}]\!] = 0
\end{aligned}
\tag{3.26}
$$

and thus $\hat{\boldsymbol{\sigma}}(u, \nabla u) = \nabla u$ and $\hat{u}(u) = u$, i.e. the fluxes are consistent. $\qquad\square$

It can now be easily validated that the numerical fluxes chosen in SIPG, NIPG and

Baumann-Oden are indeed consistent.

In order to use standard techniques for the existence and uniqueness of a solution, we need the bilinear form to be continuous and coercive.

Lemma 3.7 (Continuity). *Consider the case of SIPG, NIPG or Baumann-Oden. Then there exists a constant $1 < C \leq 2$ such that*

$$|B(u,v)| \leq C \|\|u\|\|_\delta \|\|v\|\|_\delta \qquad \forall u, v \in H^2(\mathcal{T}_h) \tag{3.27}$$

where the norm $\|\|\cdot\|\|_\delta$ is defined by

$$\|\|u\|\|_\delta^2 = \|\nabla u\|_{L^2(\Omega)}^2 + \int_{\Gamma_\mathcal{I} \cup \Gamma_D} \delta^{-1}(\boldsymbol{n} \cdot \{\!\!\{\nabla u\}\!\!\})^2 \, dx + \int_{\Gamma_\mathcal{I} \cup \Gamma_D} \delta [\![v]\!]^2 \, dx. \tag{3.28}$$

Proof. cf. [Har08, p. 46f.]. □

Next we discuss the coercivity of the three proposed methods. For Baumann-Oden we just get

$$B(u,u) = \|\nabla u\|_{L^2(\Omega)}^2 \tag{3.29}$$

so this method is not coercive unless we use homogeneous Dirichlet boundary conditions. The coercivity of the remaining two methods is discussed in the following theorem.

Theorem 3.8 (Coercivity). *In the case of NIPG or SIPG there exists a constant $C_{IP}^0 \geq 0$ such that for all $C_{IP} > C_{IP}^0$*

$$|B(u,u)| \geq \gamma \|\|u\|\|_\delta^2 \qquad \forall u \in H^2(\mathcal{T}_h) \tag{3.30}$$

with a constant $\gamma > 0$. For the NIPG method $C_{IP} = 0$ holds.

Proof. cf. [Har08, p. 50f.] □

Due to the coercivity, the resulting linear system in a finite element ansatz is non-singular and there is a unique numerical solution $u_h \in X_h$ for the SIPG and NIPG method where X_h is a finite dimensional subspace of the broken Sobolev space $H^1(\mathcal{T}_h)$. In this thesis we choose $X_h = \mathcal{Q}_k + \mathcal{Q}_0$.

Combining the coercivity and continuity results with interpolation properties of the finite subspace X_h gives the following convergence result.

Theorem 3.9. *Let $u \in H^{k+1}(\Omega)$ be the solution to the Poisson equation (3.1) and let $u_h \in U_h^k$ be the solution to the variational formulation given by SIPG or NIPG where $C_{IP} > C_{IP}^0$. Furthermore assume that X_h has the approximation property*

$$\forall v \in L^2(\Omega) \, \exists v_I \in X_h : \|v - v_I\|_{L^2(K)} \leq C h_K^{k+1} |v|_{H^{k+1}(K)} \qquad \forall K \in \mathcal{T}_h. \tag{3.31}$$

Then for NIPG we get the L^2-approximation

$$\|u - u_h\|_{L^2(\Omega)} \leq C h^k |u|_{H^{k+1}(\Omega)} \tag{3.32}$$

and for SIPG

$$\|u - u_h\|_{L^2(\Omega)} \leq C h^{k+1} |u|_{H^{k+1}(\Omega)} \tag{3.33}$$

holds.

Proof. cf. [Har08, Lemma 5.29, p. 52] □

This result and the symmetry of $B(\cdot, \cdot)$ are the reasons why we prefer the SIPG method to the NIPG method in this thesis.

4 Navier-Stokes equations

In this section we want to examine the discretized Navier-Stokes equations using the element pair $\mathcal{Q}_{k+1}/(\mathcal{Q}_k + \mathcal{Q}_0)$. After a short general introduction we turn over to the actual discretization of theses equations in Subsection 4.1. Afterwards we have a closer look onto the solution process where we especially are interested in the choice of preconditioners and solvers. In particular we use the results of Section 3 for the construction of the preconditioner. Since we are interested in modelling turbulent flow, we describe the LES approach and state the used turbulence model by Vreman in Subsection 4.3. As testcase for this setting we want to consider a three-dimensional channel flow that we describe in Subsection 4.4. Finally, we present numerical results and compare the resulting statistics to those obtained with a Taylor-Hood element pair.

The time-dependent, incompressible Navier-Stokes equations

$$
\begin{aligned}
\frac{\partial \boldsymbol{u}}{\partial t} + (\boldsymbol{u} \cdot \nabla)\boldsymbol{u} - \nu \Delta \boldsymbol{u} + \nabla p &= \boldsymbol{f} \quad \text{in } \Omega \times (0, T), \\
\operatorname{div} \boldsymbol{u} &= 0 \quad \text{in } \Omega \times (0, T), \\
\boldsymbol{u} &= \boldsymbol{0} \quad \text{on } \partial\Omega \times (0, T), \\
\boldsymbol{u}(\cdot, 0) &= \boldsymbol{u_0} \quad \text{in } \Omega
\end{aligned}
\tag{4.1}
$$

describe the motion of an incompressible fluid in the domain Ω. Compared to the Stokes equations (2.1) we have here to deal with an additional nonlinearity and a time derivative. The weak formulation of the incompressible Navier-Stokes equations then reads

$$
\begin{aligned}
\left(\frac{\partial \boldsymbol{u}}{\partial t}, \boldsymbol{v}\right) + (\nu \nabla \boldsymbol{u}, \nabla \boldsymbol{v}) + ((\boldsymbol{u} \cdot \nabla)\boldsymbol{u}, \boldsymbol{v}) - (\operatorname{div} \boldsymbol{u}, p) &= (\boldsymbol{f}, \boldsymbol{v}) \quad \forall \boldsymbol{v} \in \boldsymbol{V}, t \in (0, T] \\
(\operatorname{div} \boldsymbol{u}, q) &= 0 \qquad \forall q \in Q, t \in (0, T]
\end{aligned}
\tag{4.2}
$$

We now formulate an existence and uniqueness result with the choices

$$
\begin{aligned}
\boldsymbol{V} &= \{\boldsymbol{v} \in [H_0^1(\Omega)]^d : \operatorname{div} \boldsymbol{v} = 0\} \\
\boldsymbol{H} &= \{\boldsymbol{v} \in [L_0^2(\Omega)]^d : \operatorname{div} \boldsymbol{v} = 0\}.
\end{aligned}
\tag{4.3}
$$

Theorem 4.1. *If $\boldsymbol{f} \in [L^2(0, T; \boldsymbol{V}')]^d$ and $\boldsymbol{u}_0 \in \boldsymbol{H}$, there exists a weak solution to the Navier-Stokes equations (4.2) that satisfies*

$$
\boldsymbol{u} \in L^2(0, T; \boldsymbol{V}) \cap L^\infty(0, T; \boldsymbol{H}).
\tag{4.4}
$$

In the case of space dimension $d = 2$ this solution is unique and

$$
\begin{aligned}
\boldsymbol{u} &\in \mathcal{C}(0, T; \boldsymbol{H}), \\
\boldsymbol{u}' &\in L^2(0, T; \boldsymbol{V}').
\end{aligned}
\tag{4.5}
$$

Proof. cf. [Tem95, Theorem 3.1, p. 21]. □

In three dimensions $(d = 3)$ uniqueness is an open question.

4.1 Time discretization

In order to deal with the time-derivative in the Navier-Stokes equations, we first semi-discretize the Navier-Stokes equations in time. This means that we only solve the equations for the discrete time steps $0 = t_0 < t_1 < \cdots < t_N = T$. We denote the velocity at time step t_n by $\boldsymbol{u}^n$ and the pressure by p^n.

A fully implicit discretization then takes the form

$$
\begin{aligned}
c\boldsymbol{u}^n + (\boldsymbol{u}^n \cdot \nabla)\boldsymbol{u}^n - \nu \Delta \boldsymbol{u}^n + \nabla p^n &= \tilde{\boldsymbol{f}}^n \quad \text{in } \Omega \\
\operatorname{div} \boldsymbol{u}^n &= 0 \quad \text{in } \Omega.
\end{aligned}
\tag{4.6}
$$

and the time-derivative transforms into a reaction term. Due to the nonlinearity $(\boldsymbol{u}^n \cdot \nabla)\boldsymbol{u}^n$ the stationary system (4.6) is still nonlinear and thus hard to solve. On the other hand a fully explicit discretization leads to strong restrictions on the time step which are also not desirable.

A remedy is then to linearize (4.6) by treating the nonlinearity $(\boldsymbol{u} \cdot \nabla)\boldsymbol{u}$ semi-explicitly as $(\boldsymbol{u}^{n-1} \cdot \nabla)\boldsymbol{u}^n$ and all the other terms implicitly. This approach is called IMEX and we use it here with Runge-Kutta methods. The corresponding Butcher schemes read

$$
\begin{array}{c|c}
\mathbf{c} & \mathbf{A} \\ \hline
& \mathbf{b^T}
\end{array}
=
\begin{array}{c|cc}
\gamma & \gamma & 0 \\
1 & 1-\gamma & \gamma \\ \hline
& 1-\gamma & \gamma
\end{array}
\qquad\qquad
\begin{array}{c|c}
\mathbf{\hat{c}} & \mathbf{\hat{A}} \\ \hline
& \mathbf{\hat{b}^T}
\end{array}
=
\begin{array}{c|ccc}
0 & 0 & 0 & 0 \\
\gamma & \gamma & 0 & 0 \\
1 & \delta & 1-\delta & 0 \\ \hline
& \delta & 1-\delta & 0
\end{array}
\tag{4.7}
$$

where $\gamma = 1 - \sqrt{1/2}$ and $\delta = 1 - 1/(2\gamma)$.

This leads to the following Oseen-like problem that we have to solve in each time step

$$
\begin{aligned}
-\nu \Delta \boldsymbol{u}^n + c\boldsymbol{u}^n + (\boldsymbol{b} \cdot \nabla)\boldsymbol{u}^n + \nabla p^n &= \tilde{\boldsymbol{f}} \\
\operatorname{div} \boldsymbol{u}^n &= 0
\end{aligned}
\tag{4.8}
$$

where div $\boldsymbol{b} = 0$. The variational form then reads

$$\nu(\nabla\boldsymbol{u}^n, \nabla\boldsymbol{v}) + (c\boldsymbol{u}^n, \boldsymbol{v}) + ((\boldsymbol{b}\cdot\nabla)\boldsymbol{u}^n, \boldsymbol{v}) - (\mathrm{div}\,\boldsymbol{v}, p) = \tilde{\boldsymbol{f}} \quad \forall \boldsymbol{v} \in \boldsymbol{V}$$
$$(\mathrm{div}\,\boldsymbol{u}^n, q) = 0 \quad \forall q \in Q. \tag{4.9}$$

According to [RST08, Theorem 1.5, p. 452] this equation is uniquely solvable if the spaces $\boldsymbol{V}$ and Q satisfy the inf-sup condition, i.e.

$$\inf_{\substack{q\in Q \\ q\neq 0}} \sup_{\substack{\boldsymbol{v}\in\boldsymbol{V} \\ \boldsymbol{v}\neq 0}} \frac{b(\boldsymbol{v}, q)}{\|\boldsymbol{v}\|_{\boldsymbol{V}}\|q\|_Q} \geq \beta. \tag{4.10}$$

In the proof the bilinear form $\tilde{a}(\cdot, \cdot)$ given by

$$\tilde{a}(\boldsymbol{u}, \boldsymbol{v}) = \nu(\nabla\boldsymbol{u}^n, \nabla\boldsymbol{v}) + (c\boldsymbol{u}^n, \boldsymbol{v}) + ((\boldsymbol{b}\cdot\nabla)\boldsymbol{u}^n, \boldsymbol{v}) \tag{4.11}$$

is considered. Due to the coercivity of $\tilde{a}$ in $\boldsymbol{V}_{div} = \{\boldsymbol{v} \in \boldsymbol{V} : (\mathrm{div}\,\boldsymbol{v}, q) = 0 \quad \forall q \in Q\}$

$$\begin{aligned}
\tilde{a}(\boldsymbol{u}, \boldsymbol{u}) &= \nu(\nabla\boldsymbol{u}, \nabla\boldsymbol{u}) + (c\boldsymbol{u}, \boldsymbol{u}) + ((\boldsymbol{b}\cdot\nabla)\boldsymbol{u}, \boldsymbol{u}) \\
&= \nu(\nabla\boldsymbol{u}, \nabla\boldsymbol{u}) + (c\boldsymbol{u}, \boldsymbol{u}) - ((\nabla\cdot\boldsymbol{b})\boldsymbol{v}, \boldsymbol{v}) \\
&= \nu\|\nabla\boldsymbol{u}\|^2 + c\|\boldsymbol{u}\|^2 \geq (C\nu + c)\|\boldsymbol{u}\|^2,
\end{aligned} \tag{4.12}$$

the same argumentation as for the solvability of the Stokes problem can be used. Analogously, the discretized problem

$$\nu(\nabla\boldsymbol{u}^n, \nabla\boldsymbol{v}) + c(\boldsymbol{u}^n, \boldsymbol{v}) + ((\boldsymbol{b}\cdot\nabla)\boldsymbol{u}^n, \boldsymbol{v}) = \tilde{\boldsymbol{f}} \quad \forall \boldsymbol{v} \in \boldsymbol{V}_h$$
$$(\mathrm{div}\,\boldsymbol{u}^n, q) = 0. \quad \forall q \in Q_h \tag{4.13}$$

is uniquely solvable if the spaces $\boldsymbol{V}_h$ and Q_h satisfy the discrete inf-sup condition (2.10). Due to Theorem 2.10, the pair $\mathcal{Q}_{k+1}/(\mathcal{Q}_k + \mathcal{Q}_0)$ fulfills this requirement and we expect no difficulties using the considered elements.

4.2 Assembling and solving the linear system

Up to now all considerations were not restricted to a specific choice of finite element pair. In this subsection, however, we are only interested in the treatment of the $\mathcal{Q}_{k+1}/(\mathcal{Q}_k + \mathcal{Q}_0)$ pair that we discussed in Section 2 for the Stokes problem.

In order to obtain a numerical solution for the Navier-Stokes equations in the discussed approach, we have to assemble the Oseen-like problem (4.9). This results in a linear system

of the form

$$\begin{pmatrix} A & B^T \\ B & 0 \end{pmatrix} \begin{pmatrix} u \\ p \end{pmatrix} = \begin{pmatrix} F \\ 0 \end{pmatrix} \tag{4.14}$$

where in A diffusion ($\nu \Delta \boldsymbol{u}$), advection (($\boldsymbol{b} \cdot \nabla)\boldsymbol{u}$) and reaction ($c\boldsymbol{u}$) are taken into account. B corresponds to the divergence operator (div $\boldsymbol{u}$) and B^T to the gradient operator (∇p). For solving this saddle point problem, we basically do the same as proposed in [Hei11]. As solver FGMRES is chosen and the used preconditioning matrix is

$$P = \begin{pmatrix} \tilde{A} & B^T \\ 0 & \tilde{S} \end{pmatrix} \tag{4.15}$$

where $\tilde{A}$ resp. $\tilde{S}$ is a approximation to A resp. the Schur complement $S = -BA^{-1}B^T$. This leads to the following iteration matrix

$$\begin{aligned} \begin{pmatrix} A & B^T \\ B & 0 \end{pmatrix} P^{-1} &= \begin{pmatrix} A & B^T \\ B & 0 \end{pmatrix} \begin{pmatrix} \tilde{A}^{-1} & -\tilde{A}^{-1}B^T\tilde{S}^{-1} \\ 0 & \tilde{S}^{-1} \end{pmatrix} \\ &= \begin{pmatrix} A\tilde{A}^{-1} & (I - A\tilde{A}^{-1})B^T\tilde{S}^{-1} \\ B\tilde{A}^{-1} & S\tilde{S}^{-1} \end{pmatrix}. \end{aligned} \tag{4.16}$$

If the approximations are exact, the iteration matrix simplifies to

$$\begin{pmatrix} I & 0 \\ BA^{-1} & I \end{pmatrix}. \tag{4.17}$$

This matrix has just eigenvalues equal to one and Krylov subspace method converges in two steps. Therefore, we expect a fast convergence if the approximations are chosen well enough.

Since A is a matrix corresponding to the velocity, we do not have to change this part of the implementation compared to $\mathcal{Q}_2/\mathcal{Q}_1$ elements. In that case it turned out that even a quite coarse approximation yields good approximations. Therefore, we choose BiCGStab with a rather large relative tolerance of 10^{-2} as solver and BlockJacobi(ILU) as preconditioner.

The more interesting part now is S^{-1}. Due to the turbulence models we have to choose a rather small time step size. This means that our problem is reaction dominant and we can approximate the inverse of the Schur complement S^{-1} by

$$S^{-1} = (-BA^{-1}B^T)^{-1} \approx (-\operatorname{div} c^{-1}I\nabla)^{-1} \approx -c\Delta^{-1}. \tag{4.18}$$

Therefore, it is appropriate to solve a Poisson problem in order to approximate the inverse of S. In the Navier-Stokes problem no boundary conditions for the pressure appear. So we have to use homogeneous Neumann boundary conditions to be consistent.

A naive ansatz using just a CG method without any regularization leads to some difficulties: If we take a solution and simply change it on one element by a constant, the result is still a solution. That means that the resulting linear system has as many zero eigenvalues as there are cells in the discretization of Ω. A first idea to circumvent this problem might be to set all discontinuous degrees of freedom to zero. Then we would have to solve a Poisson problem with continuous elements. Unfortunately, this approach leads to the same solutions as with the Taylor-Hood pair $\mathcal{Q}_2/\mathcal{Q}_1$ because we also have to apply these constraints on the pressure in order to be consistent.

The remedy here is to use the Symmetric Interior Penalty Galerkin (SIPG) that we introduced and discussed in Section 3. There we considered the Poisson problem with partly Neumann and partly Dirichlet boundary conditions. In our case where only Neumann boundary conditions are present the formulation (3.22) reduces to

$$B(u,v) = \int_\Omega \nabla u \cdot \nabla v \, dx + \int_{\Gamma_\mathcal{I}} \delta[\![u]\!] \cdot [\![v]\!] - \{\!\{\nabla u\}\!\} \cdot [\![v]\!] - [\![u]\!] \cdot \{\!\{\nabla v\}\!\} \, dx \qquad (4.19)$$

$$F(v) = \int_\Omega f \, v \, dx. \qquad (4.20)$$

Since the formulation is symmetric, we can choose here a CG solver with a rather small relative tolerance (10^{-5}) compared to the inversion of A. The choice of a suitable parallel preconditioner is quite a hard task here. We tried all of PETSc's [BBB$^+$12] preconditioners that were available in the `deal.II` version 7.2.0. In addition to the well-known algorithms we also used two preconditioners from the HYPRE suite [FJY06], namely BoomerAMG [HMY02] and ParaSails [Cho00]. BoomerAMG is a algebraic multi-grid preconditioner that showed very good performance for the Taylor-Hood pair in our program. ParaSails uses least-squares minimization to compute a sparse approximation inverse. Both algorithms are especially constructed for parallel usage.

In Table 4.1 we see different approaches on a $6 \times 6 \times 6$ and a $12 \times 12 \times 12$ mesh using one process. Nearly all of the preconditioners fail here because they do not show an improved performance compared to the identity. Just ParaSails seems to improve the calculation time. This is the reason why we choose it in our implementation. The number of FGMRES iterations is independent of the used preconditioner 35 for a $6 \times 6 \times 6$ mesh and 40 for a $12 \times 12 \times 12$ triangulation. In the case of a $\mathcal{Q}_2/\mathcal{Q}_1$ pair the preconditioner BoomerAMG showed extraordinary performance. On the $6 \times 6 \times 6$ mesh about 6 iteration steps are needed that take $0.01s$. On the $12 \times 12 \times 12$ each of the 7 iteration steps needs about $8s$.

Table 4.1: Average time and number of iterations for solving the Poisson problem

| Preconditioner | no periodicity | | | | periodicity | | | |
| | $6 \times 6 \times 6$ | | $12 \times 12 \times 12$ | | $6 \times 6 \times 6$ | | $12 \times 12 \times 12$ | |
	iters.	time	iters.	time	iters.	time	iters.	time
Identity	290	0.22 s	700	7.0 s	170	0.08 s	490	2.4 s
BoomerAMG [HMY02]	220	1.30 s	950	95.0 s	90	0.30 s	340	19.0 s
Jacobi	240	0.17 s	640	6.3 s	150	0.07 s	470	2.3 s
BlockJacobi(ILU)	30	0.05 s	330	6.5 s	80	0.07 s	200	2.1 s
BlockJacobi(ICC)	240	0.17 s	630	6.4 s	100	0.08 s	130	1.8 s
ParaSails [Cho00]	80	0.10 s	250	3.8 s	50	0.04 s	260	1.6 s

To solve for one time-step, 10 FGMRES iterations are required.

4.3 LES and the turbulence model

When the viscosity ν is getting smaller and smaller, typically the flow is becoming more and more turbulent. This means that there is a high sensitivity to small changes and additionally that there are very small structures (eddies) in the flow. Although these structures are quite small they have an important impact because this is where diffusion happens. So a very fine mesh has to be used in order to get a meaningful numerical solution due to the nonlinear term. Such an approach is called Direct Numerical Simulation (DNS). However, it is often not feasible to resolve all scales.

A remedy is to model the influence of the small scales and to compute the numerical solution on a coarse grid on which only large scales can be resolved. Such an approach, in which only big structures (large eddies) of he flow can be determined, is called Large Eddy Simulation (LES).

In order to solve only for the big scales, we have to change our equations a bit and separate the velocity

$$\boldsymbol{u} = \overline{\boldsymbol{u}} + \boldsymbol{u}' \tag{4.21}$$

into the resolved scales $\overline{\boldsymbol{u}}$ and the non-resolved scales $\boldsymbol{u}'$. The filter $\overline{\cdot}$ is in general given by

$$\overline{\phi(x,t)} = \int_{-\infty}^{\infty} \int_{-\infty}^{\infty} \phi(r,t') G(x-r,t-t') \, dt' \, dr \tag{4.22}$$

where G is a convolution. A homogeneous filter furthermore satisfies the following properties:

1. Conservation of constants

$$\int_{-\infty}^{\infty} \int_{-\infty}^{\infty} G(r, t')\, dt'\, dr = 1$$

2. Linearity

$$\overline{\phi + \psi} = \overline{\phi} + \overline{\psi}$$

3. Commutation with derivatives

$$\overline{\frac{\partial \phi}{\partial x_i}} = \frac{\partial \overline{\phi}}{\partial x_i} \quad i = 1, \ldots, d, \qquad\qquad \overline{\frac{\partial \phi}{\partial t}} = \frac{\partial \overline{\phi}}{\partial t}$$

The next step is to actually filter the Navier-Stokes equations. As we mentioned before, the small scales have an influence onto the large ones and therefore we expect $\boldsymbol{u'}$ to have some contribution when filtering the equations. The filtered Navier-Stokes equations then read

$$
\begin{aligned}
\frac{\partial \overline{\boldsymbol{u}}}{\partial t} + (\overline{\boldsymbol{u}} \cdot \nabla)\overline{\boldsymbol{u}} - \nu \Delta \overline{\boldsymbol{u}} + \nabla \overline{p} &= \overline{\boldsymbol{f}} - \operatorname{div} \boldsymbol{\tau} \quad && \text{in } \Omega \times (0, T), \\
\operatorname{div} \overline{\boldsymbol{u}} &= 0 \quad && \text{in } \Omega \times (0, T), \\
\overline{\boldsymbol{u}} &= \boldsymbol{0} \quad && \text{on } \partial\Omega \times (0, T), \\
\overline{\boldsymbol{u}}(\cdot, 0) &= \overline{\boldsymbol{u_0}} \quad && \text{in } \Omega.
\end{aligned}
\tag{4.23}
$$

where the residual stress tensor $\boldsymbol{\tau}$ is given by

$$\tau_{ij} = \overline{u_i \cdot u_j} - \overline{u_i} \cdot \overline{u_j}. \tag{4.24}$$

This means that the influence of the small scales comes in by the nonlinearity. In order to get a closed problem, in which only $\overline{\boldsymbol{u}}$ and $\overline{p}$ appear, we have to specify an approximation to $\boldsymbol{\tau}$. The most common choice is the *eddy viscosity hypothesis* that is given by

$$\boldsymbol{\tau}(\boldsymbol{u}) \approx -2\nu_e \boldsymbol{S}(\boldsymbol{u}) \tag{4.25}$$

with the symmetric strain rate tensor $\boldsymbol{S}(\boldsymbol{u}) = \frac{1}{2}(\nabla \boldsymbol{u} + (\nabla \boldsymbol{u})^T)$. We know note that $\Delta \overline{u} = 2 \operatorname{div} \boldsymbol{S}(\overline{\boldsymbol{u}})$ (see Lemma 2.14) and the filtered Navier-Stokes equations can be

rewritten as

$$\frac{\partial \overline{\boldsymbol{u}}}{\partial t} + (\overline{\boldsymbol{u}} \cdot \nabla)\overline{\boldsymbol{u}} - \nu\Delta\overline{\boldsymbol{u}} + \nabla\overline{p} = \overline{\boldsymbol{f}} - \operatorname{div}(2(\nu + \nu_e)\boldsymbol{S}(\boldsymbol{u})) \quad \text{in } \Omega \times (0, T),$$
$$\operatorname{div}\overline{\boldsymbol{u}} = 0 \qquad\qquad\qquad \text{in } \Omega \times (0, T),$$
$$\overline{\boldsymbol{u}} = \boldsymbol{0} \qquad\qquad\qquad \text{on } \partial\Omega \times (0, T),$$
$$\overline{\boldsymbol{u}}(\cdot, 0) = \overline{\boldsymbol{u_0}} \qquad\qquad\qquad \text{in } \Omega. \tag{4.26}$$

So the closure model introduces additional viscosity ν_e depending on the turbulence model. The model we consider in this thesis was introduced by Roel Verstappen in [Ver11] and analyzed by Helene Dallmann in [Dal12]. It is given by

$$\nu_e(\boldsymbol{v}) \sim \frac{|r(\boldsymbol{v})|}{q(\boldsymbol{v})}. \tag{4.27}$$

where r and q are two two invariants of the strain rate tensor

$$r(\boldsymbol{v}) := -\frac{1}{3}\operatorname{tr}\left(\boldsymbol{S}^3(\boldsymbol{v})\right)$$
$$q(\boldsymbol{v}) := \frac{1}{2}\operatorname{tr}\left(\boldsymbol{S}^2(\boldsymbol{v})\right).$$

4.4 Channel flow

The test case we want to consider is a flow between two parallel plates that are infinitely extended in x- and z-direction. On these plates homogeneous Dirichlet boundary conditions are imposed and the main flow direction is parallel to the x-axis. An example of
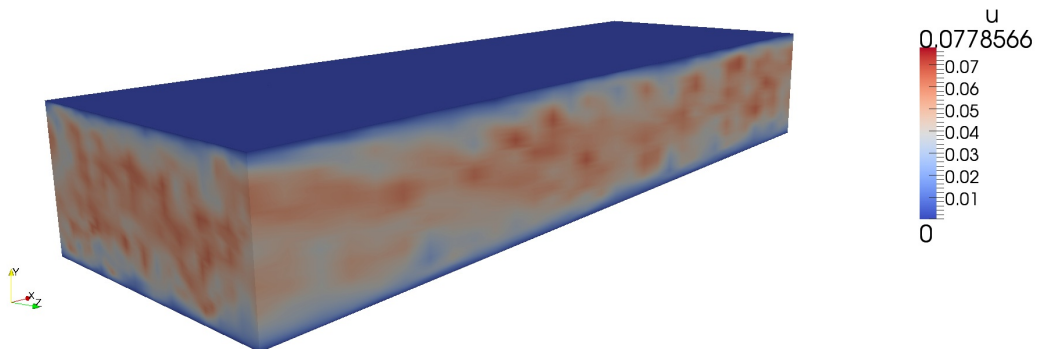
Figure 4.1: Turbulent channel flow

such an turbulent channel flow can be seen in Figure 4.1.

Since infinitely extended plates do not fit into the assumption of a bounded domain, we have to model them. We do this here by using periodic boundary conditions in y- and z-direction. In order to avoid influences by these boundaries, the lengths of the computational domain $\Omega = [0, L] \times [-H, H] \times [0, B]$ in the periodic directions have to be large enough. According to [BIL06] the choices $L = 4\pi$, $H = 1$ and $B = \frac{4}{3}\pi$ are appropriate for the Reynolds number $Re = 5600$ ($Re_\tau = 180$).

For the remainder of the problem's specification we need some quantities that are characteristic to the channel flow:

$$
\begin{aligned}
&\text{wall shear stress} &&\tau_W = \nu \left. \frac{\partial \langle u \rangle}{\partial y} \right|_{y=0} \\
&\text{friction velocity} &&u_\tau = \sqrt{\tau_W} \\
&\text{viscous length} &&y^+ = \frac{u_\tau y}{\nu} \\
&\text{friction Reynolds number} &&Re_\tau = \frac{u_\tau}{\nu}.
\end{aligned}
$$

Since we want to be able to capture dynamics of the flow near the walls, we choose a grid that is isotropic in x- and z-direction and is stretched in y-direction due to

$$
f : [0, 1] \to [-1, 1] : f(y) = \frac{\tanh(4y - 2)}{\tanh(2)}. \tag{4.28}
$$

This choice is recommended in [Zha07]. For the other parameters we refer to [Rö11] and just state them here.

- Right-hand side:

$$
\boldsymbol{f}(t_{n+1}) := \begin{pmatrix} \tau_W / H \\ 0 \\ 0 \end{pmatrix} + \frac{1}{\Delta t} \begin{pmatrix} U_{bulk} - U_{bulk}^{num}(t^n) \\ 0 \\ 0 \end{pmatrix} \tag{4.29}
$$

where U_{bulk}^{num} is the numerically computed bulk velocity.

- Initial value:

$$
\boldsymbol{u}_0 = \begin{pmatrix} U_R(y) + 0.1 U_{bulk} \Psi_{rand} \\ 0.1 U_{bulk} \Psi_{rand} \\ 0.1 U_{bulk} \Psi_{rand} \end{pmatrix} \tag{4.30}
$$

where U_{bulk} is given by

$$
U_{bulk} = \frac{1}{H} \int_0^H U_R(y) \, dy \tag{4.31}
$$

and $U_R(y) := U_R^+(y^+)u_\tau$ with

$$U_R^+(y^+) := \frac{1}{0.41} \ln(1 + 0.4y^+) + 7.8 \left(1 - \exp\left(-\frac{y^+}{11}\right) - \frac{y^+}{11} \exp\left(-\frac{y^+}{3}\right) \right). \quad (4.32)$$

$\Psi_{rand} \in [0,1]$ is a random number that perturbs the initial solution U_R in order to boost turbulence.

- Time step size: $\Delta t = 0.86$

4.5 Numerical results

In this section we observe the performance of the $\mathcal{Q}_2/(\mathcal{Q}_1 + \mathcal{Q}_0)$ pair for the channel flow problem described above. We first have a look onto a laminar example where we can compare the numerical results with an analytical solution. Afterwards we concentrate on the more interesting case of a turbulent flow.

4.5.1 Laminar flow

For validating the implementation we consider here a laminar flow. In this case we expect a stationary flow in x-direction. Inserting the ansatz $\boldsymbol{u} = (u_1(y), 0, 0)^T$ in the (stationary) Navier-Stokes equations, then gives

$$\frac{\partial p}{\partial y} = \frac{\partial p}{\partial z} = 0 \quad (4.33)$$

$$-\nu \Delta u_1 + \frac{\partial p}{\partial x} = 0. \quad (4.34)$$

So $\nu \Delta u_1 = \frac{\partial p}{\partial x} = C$ and the velocity is quadratic $\boldsymbol{u} = \left(-\frac{1}{\nu}\frac{\partial p}{\partial x}y(1-y), 0, 0\right)^T$.

In order to keep the flow laminar, we simply choose a quite low frictional Reynolds number $Re_\tau = 10$. The result that we get then after a few thousand time steps can be observed in Figure 4.2 and 4.3.
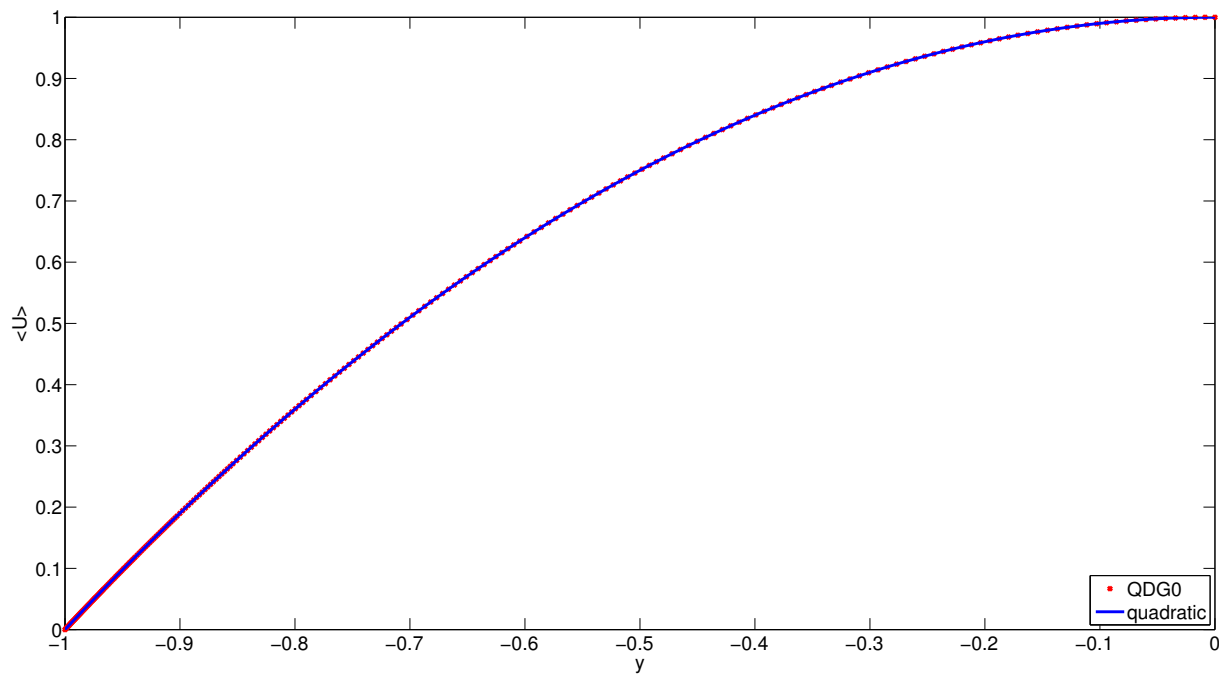
Figure 4.2: Numerical solution for the laminar channel flow
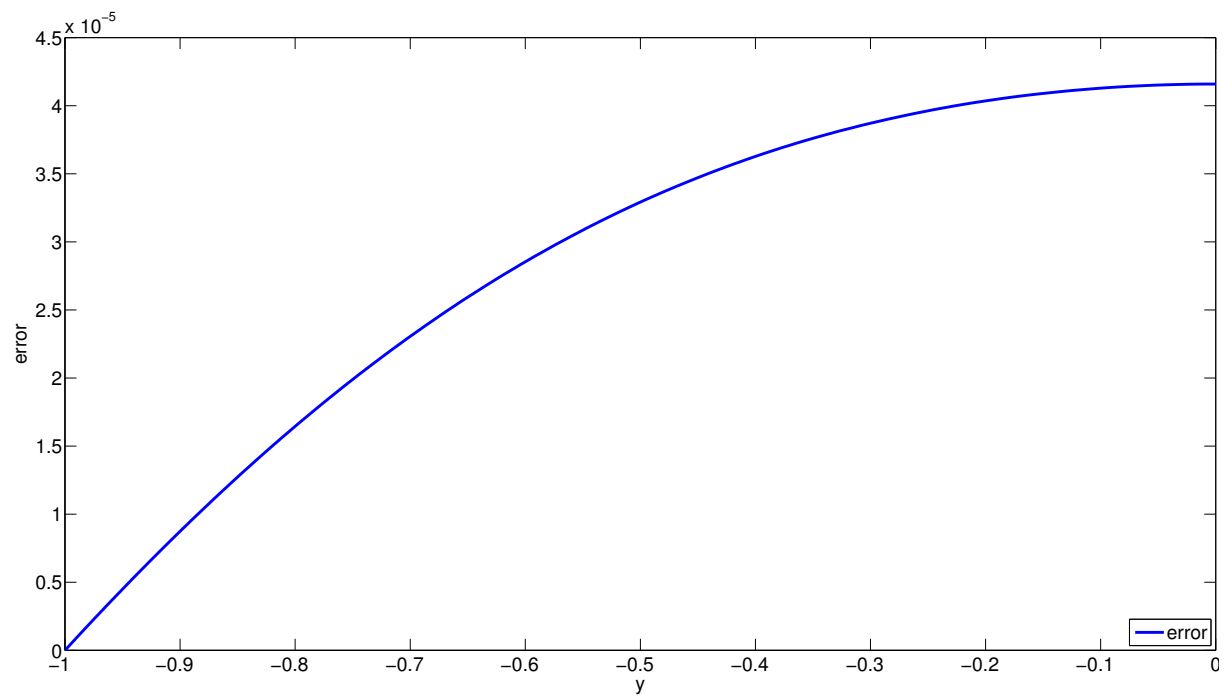
Figure 4.3: Error $|u_1 - u_h|$ for the laminar channel flow

The numerical result shows very good agreement with the analytical reference. So in the linear case we get exactly the expected behavior.

4.5.2 Turbulent flow

The only change we perform to make the flow turbulent is to change the frictional Reynolds number to the value we discussed before $Re_\tau = 180$. We compare our data with a Direct Numerical Simulation performed by Moser et al. in [MKM99] and with the results that were obtained with a Taylor-Hood $\mathcal{Q}_2/\mathcal{Q}_1$ pair.

The quantities that we are interested in are

- the mean velocities normalized with the friction velocity
  $\langle u \rangle^+ = \langle u \rangle / u_\tau$, $\langle v \rangle^+ = \langle v \rangle / u_\tau$, $\langle w \rangle^+ = \langle w \rangle / u_\tau$,

- the normalized Reynolds stresses $\langle u'u' \rangle^+$, $\langle u'v' \rangle^+$, $\langle v'v' \rangle^+$, $\langle w'w' \rangle^+$,

- the normalized turbulent kinetic energy $k^+ = \frac{1}{2} \left(\langle u'u' \rangle^+ + \langle v'v' \rangle^+ + \langle w'w' \rangle^+ \right)$,

- the root mean square velocity $u_{rms}^+ = \langle u'u' \rangle^+ - \frac{2}{3} k^+$

where we denote the velocity components according to $\boldsymbol{u} = (u, v, w)^T$.
Additionally to the already mentioned $16 \times 24 \times 16$ mesh, we consider a mesh with the resolution $16 \times 24 \times 24$ since we guess that this lead to significantly better results. Finally, we examine the behavior when we use Neumann boundary conditions everywhere instead of periodicity for the pressure.
The results on the $16 \times 24 \times 16$ mesh were obtained by averaging over 1500 time steps after a build-up time of 2000 time steps. On the $16 \times 24 \times 16$ mesh 600 developing time steps were used and the results were averaged over 750 time steps. In particular one has to be careful when comparing the results on these two meshes.

First order statistics

Concerning the first order statistics we are especially interested in the results in the main flow direction. Figure 4.5a and 4.5b clearly show that choosing $\mathcal{Q}_2/(\mathcal{Q}_1 + \mathcal{Q}_0)$ instead of the Taylor-Hood pair improves this quantity. The main difference to the reference solution remains in the interval $y^+ \in [10, 20]$. Interestingly the solution on the finer mesh shows exactly in this area better results than the solution on the coarser mesh.
In the wall normal direction we expect the velocity to be zero in average. This is confirmed by the results shown in Figure 4.6a and 4.6b. Near the wall both element pairs show a vanishing velocity v. However, when moving to the middle of the channel the approximation with the Taylor-Hood elements get worse. The new element does not suffer this problem. Although the velocity in z-direction should also be zero, both elements pairs exhibit more difficulties than in the previous case. Figure 4.7a shows that in the case of a discontinuous
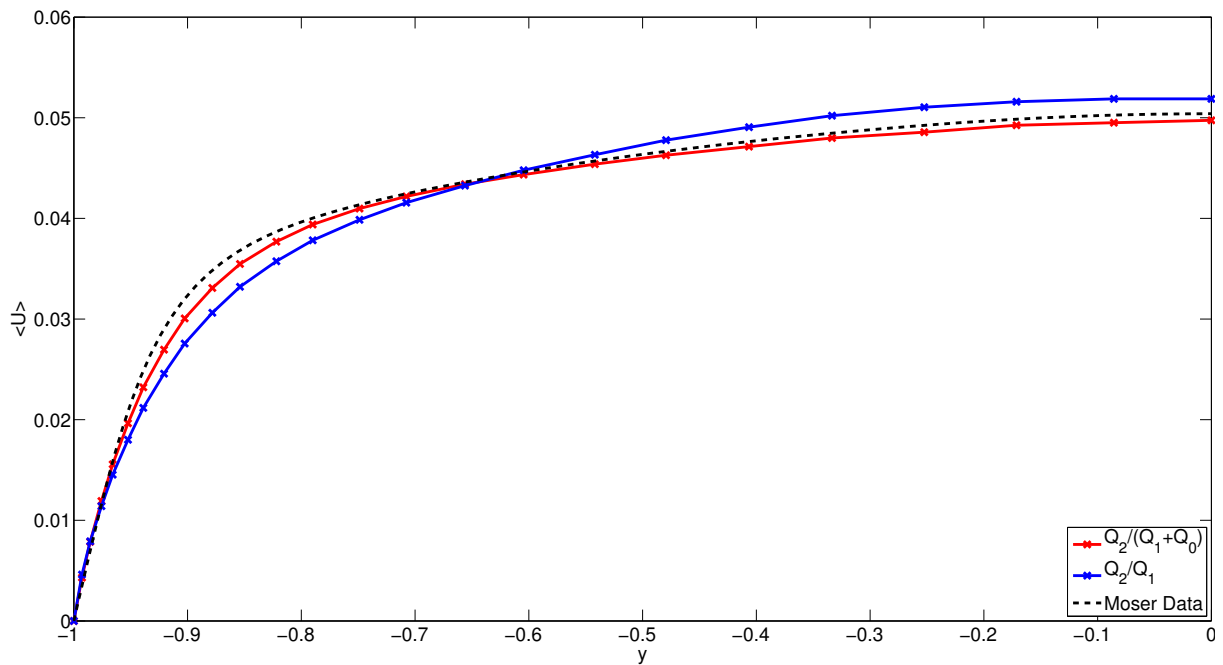
(a) Mesh resolution $16 \times 24 \times 16$
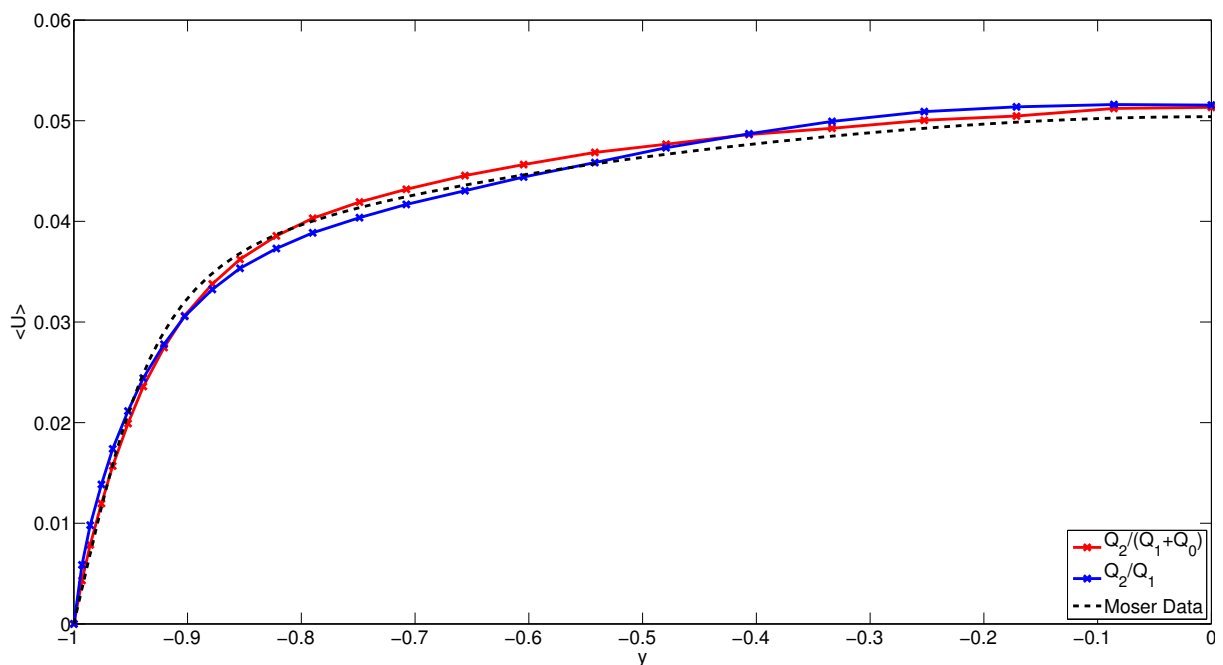
(b) Mesh resolution $16 \times 24 \times 24$

Figure 4.4: Mean velocity $\langle u \rangle$
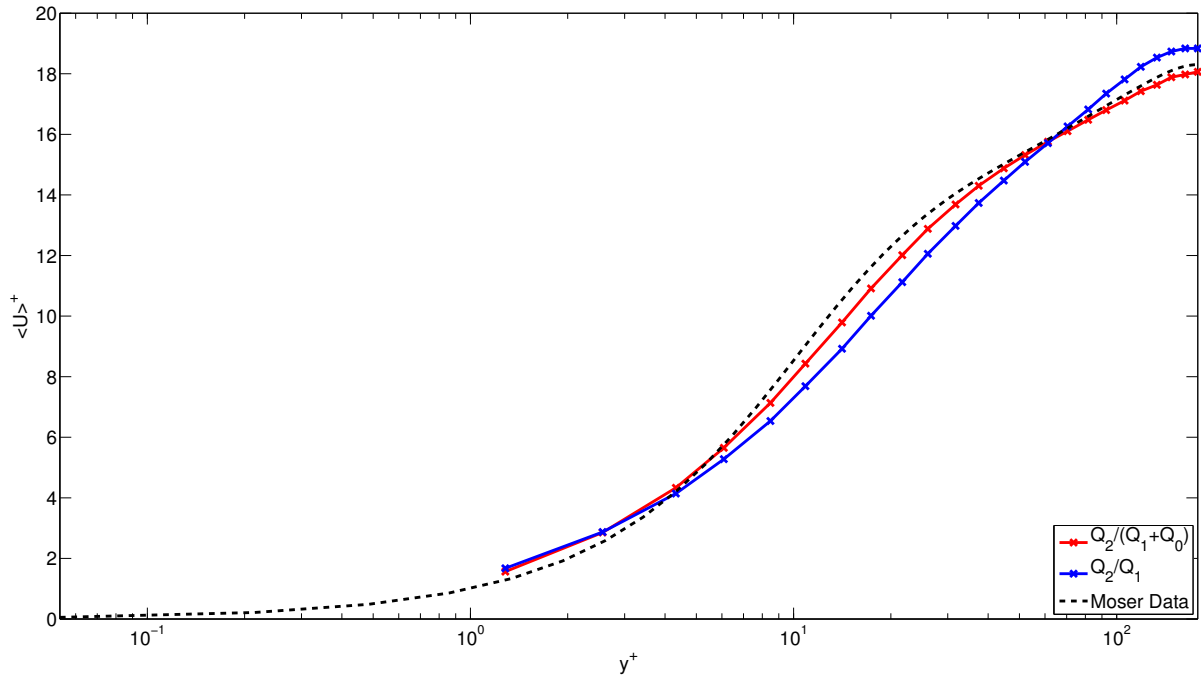
(a) Mesh resolution $16 \times 24 \times 16$
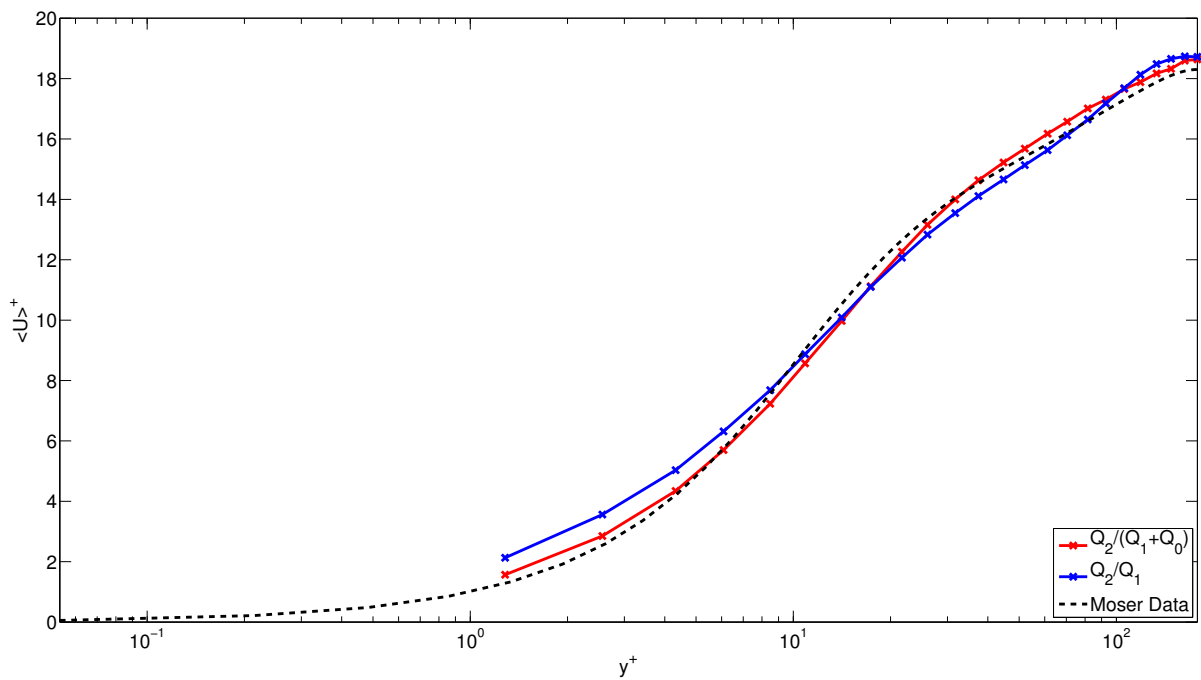
(b) Mesh resolution $16 \times 24 \times 24$

Figure 4.5: Mean velocity normalized $\langle u \rangle^+$
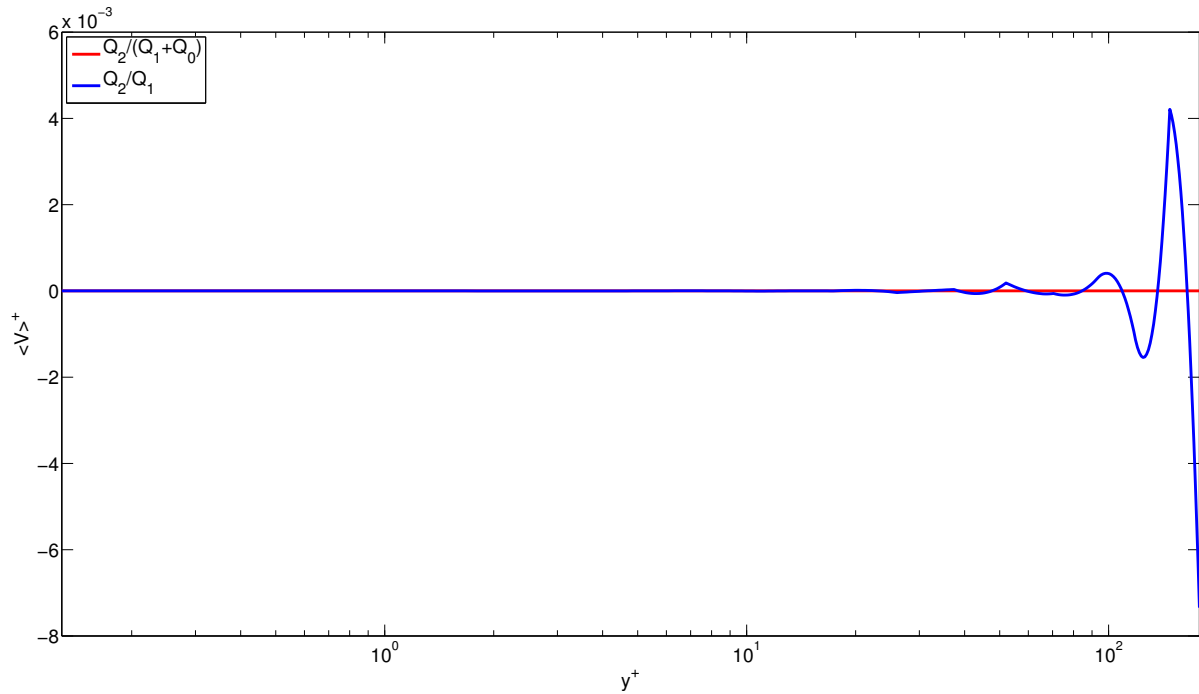
(a) Mesh resolution $16 \times 24 \times 16$
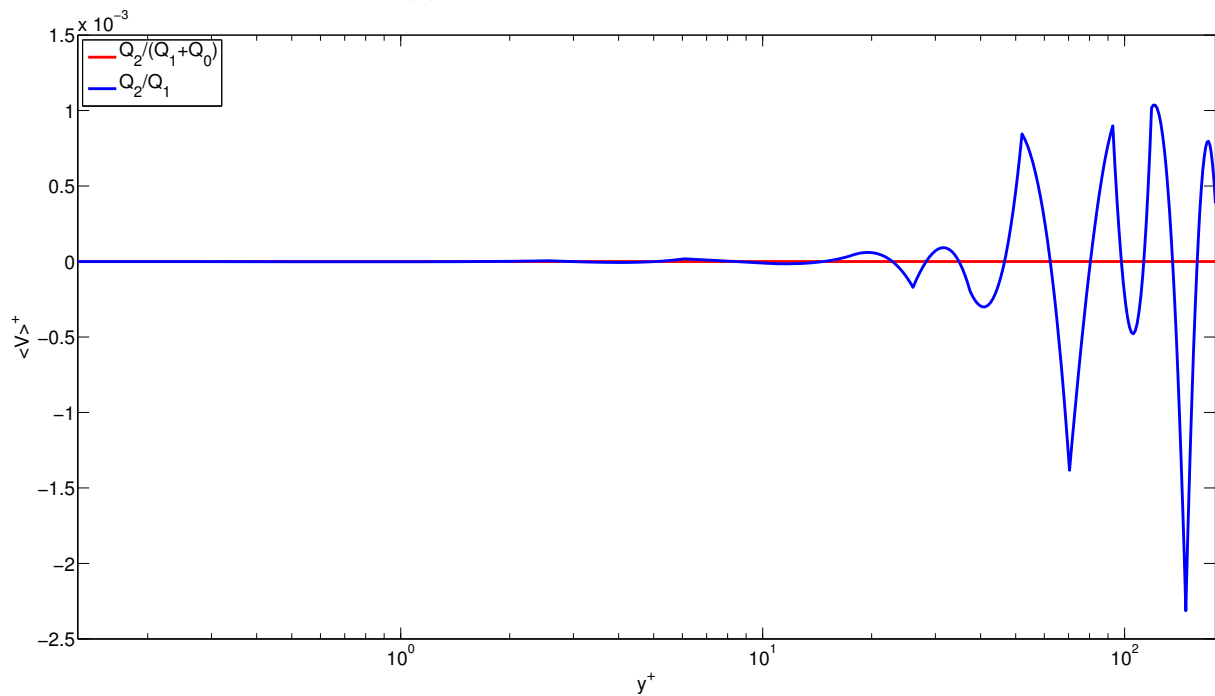
(b) Mesh resolution $16 \times 24 \times 24$

Figure 4.6: Second velocity component normalized $\langle v \rangle^+$

pressure w stays close to zero up to $y^+ = 20$. Such a limit cannot be given for the Taylor-Hood element. In both cases the velocity retreats from zero quite fast as can be seen in 4.7b. Previous computations have however shown that this behavior advances with more averaging steps. Choosing a better resolution in z-direction does not improve the results significantly.

A short summary for the first order statistics is that the using the new element in all cases lead to better results. Refining the mesh in z-direction did not improve the results much.

Second order statistics

Next we consider the second order statistics starting with $\langle u'u' \rangle^+$ in Figure 4.8a and 4.8b. The Taylor-Hood solution is in both refinement cases quite different from the reference solution as the profile is rather flat for $y^+ \in [20, 180]$. However, the $\mathcal{Q}_2/(\mathcal{Q}_1 + \mathcal{Q}_0)$ pair behaves strangely as well on the $16 \times 24 \times 16$ mesh. Up to $y^+ \approx 30$ at least the qualitative behavior is good. But further inside the flow the variance increases strongly instead of decreasing. On the refined mesh we observe a much better behavior. The profile has a clear maximum that almost agrees with the reference solution and also the decrease up to $y^+ \approx 50$ is in good agreement with the Direct Numerical Simulation. For higher values of y^+ however the variance is again increasing instead of declining.

The statistics for the variance of the v-component of the velocity (Figure 4.9a and 4.9b) are rather difficult to interpret. Both element pair give quite different results compared to the reference. Refining in z-direction does not improve this behavior.

Nearly the same holds true for the variance of the w-component of the velocity. Figure 4.10a and 4.10b show that the profiles are not similar to the reference when using a discontinuous pressure space. On the contrary, the Taylor-Hood pair shows a qualitative good result although the peak is at $y^+ \approx 80$ instead of $y^+ \approx 30$.

The profile for the covariance between u- and v-component in Figure 4.11a is reasonable for the Taylor-Hood pair. Figure 4.11b shows that the refinement in z-direction leads to a very good agreement with the reference data for the this pair. In contrary, there is almost no similarity between the $\mathcal{Q}_2/(\mathcal{Q}_1 + \mathcal{Q}_0)$ solution and the reference. Refining the mesh in z-direction at least seems to improve the capture of the peak.

The root mean square velocity u_{rms}^+ (Figure 4.12a and 4.12b) and the turbulent kinetic energy k^+ (Figure 4.13a and 4.13b) are linear combinations of the variances $\langle u'u' \rangle^+$, $\langle v'v' \rangle^+$ and $\langle w'w' \rangle^+$. Since both $\langle v'v' \rangle^+$ and $\langle w'w' \rangle^+$ are much smaller than $\langle u'u' \rangle^+$ we can basically refer to the variance of the first velocity component for a discussion.

Summarizing these results, a significant improvement is achieved when refining the mesh in z-direction for the case of $\mathcal{Q}_2/(\mathcal{Q}_1 + \mathcal{Q}_0)$ elements. There is no explanation so far what causes the problems in the middle of the channel ($y^+ > 50$).
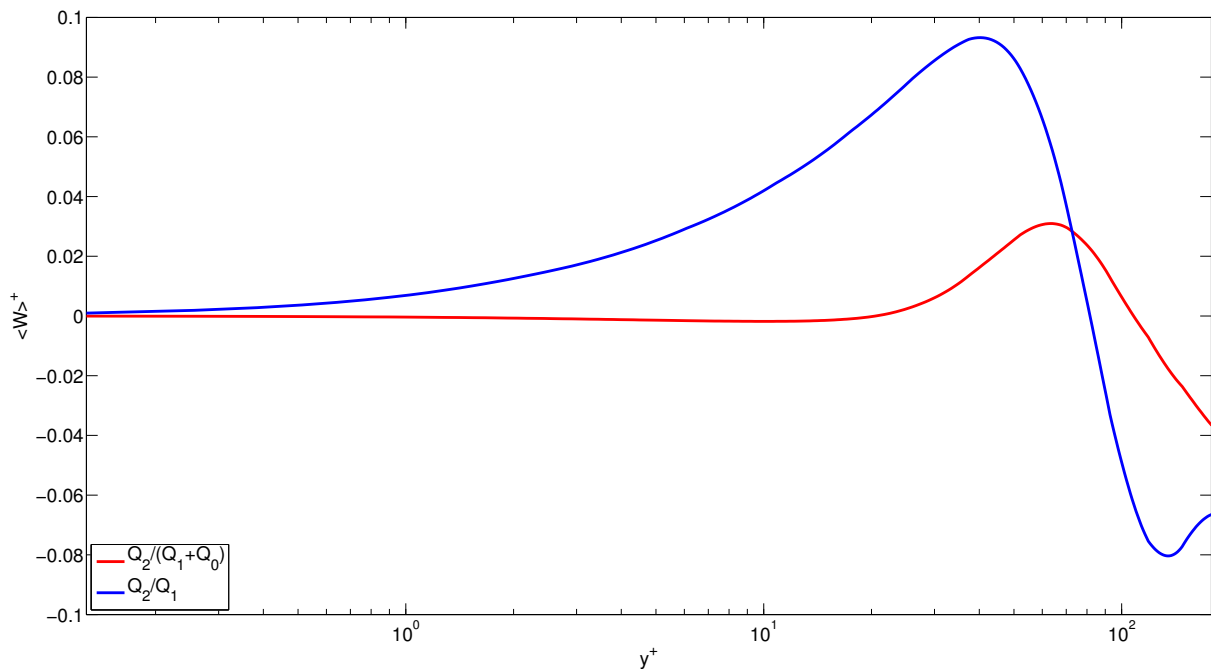
(a) Mesh resolution $16 \times 24 \times 16$
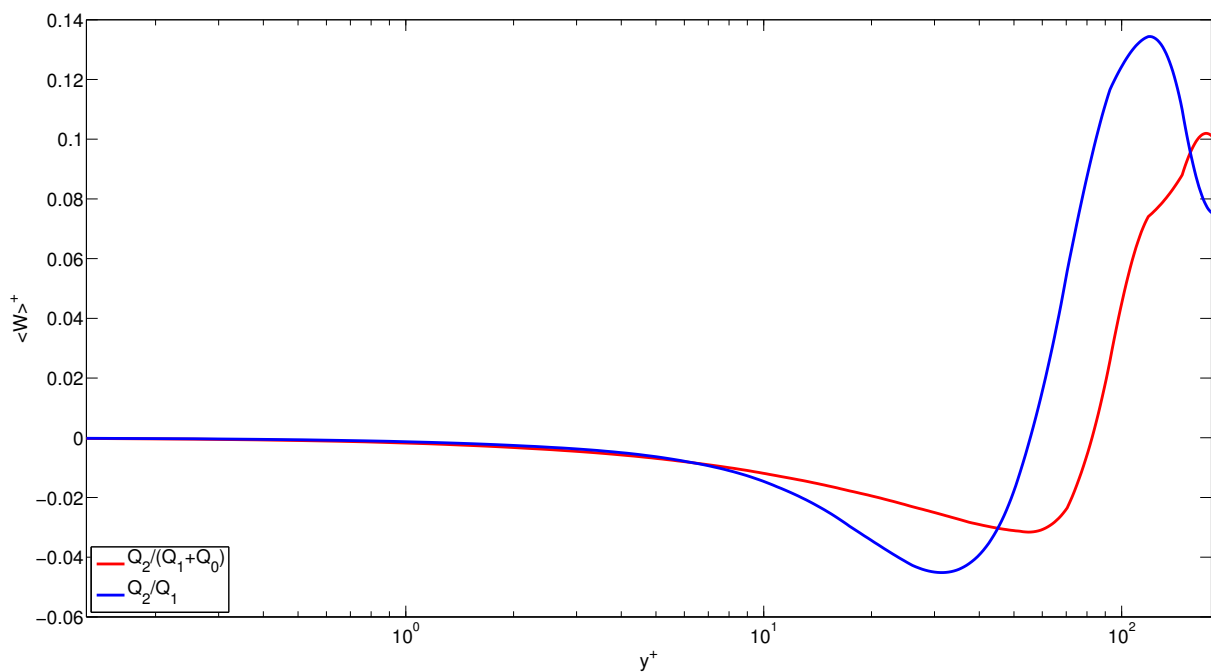
(b) Mesh resolution $16 \times 24 \times 24$

Figure 4.7: Third velocity component normalized $\langle w \rangle^+$
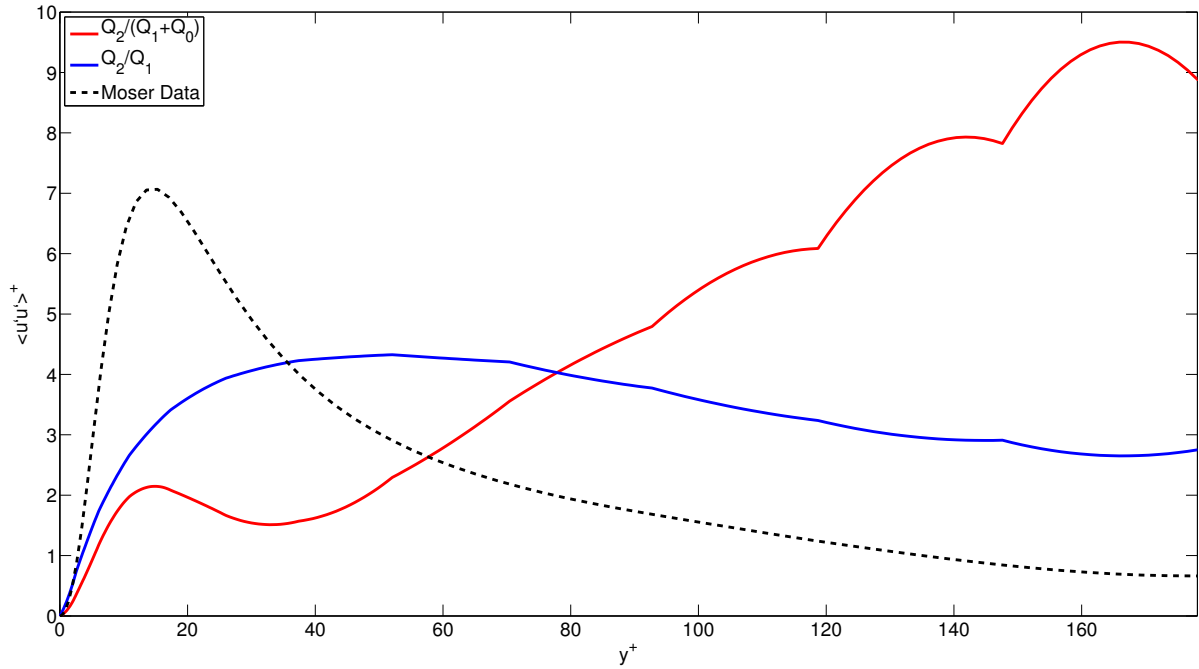
(a) Mesh resolution $16 \times 24 \times 16$
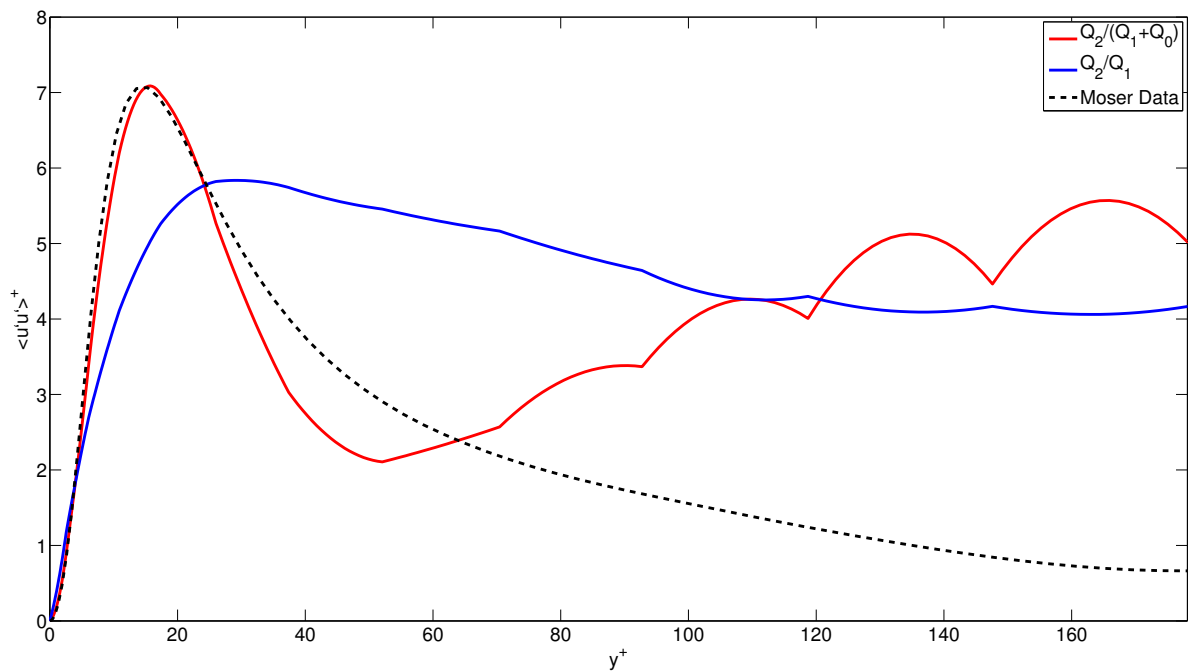
(b) [Mesh resolution $16 \times 24 \times 24$

Figure 4.8: Reynold stress $\langle u'u' \rangle^+$
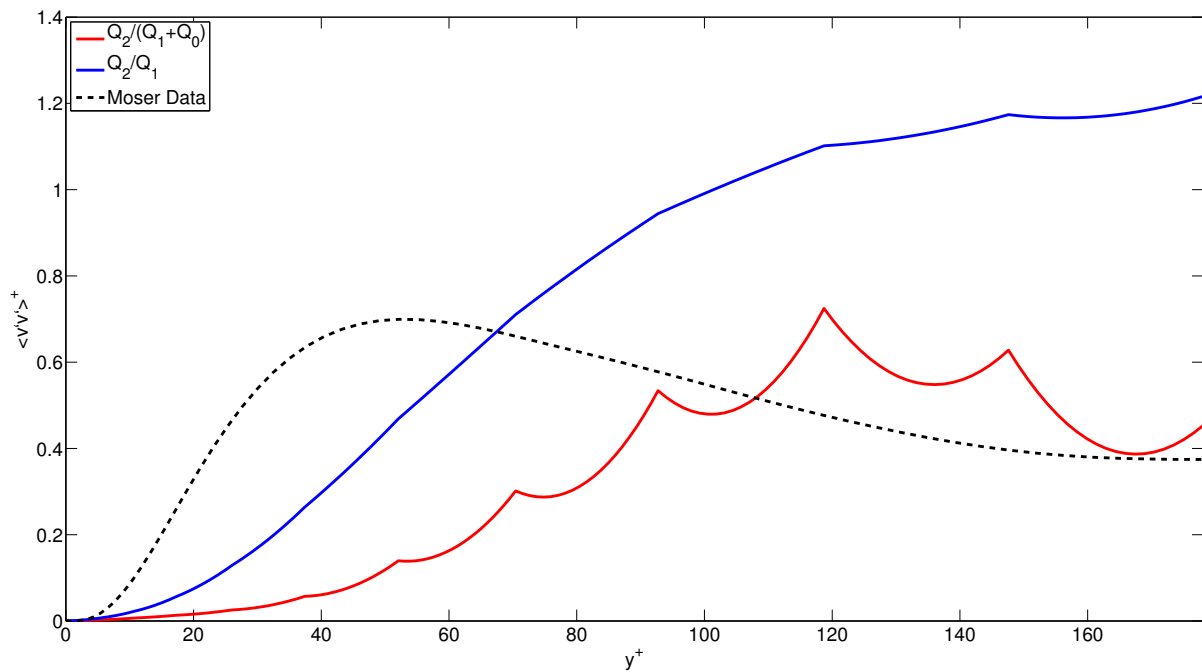
(a) Mesh resolution $16 \times 24 \times 16$
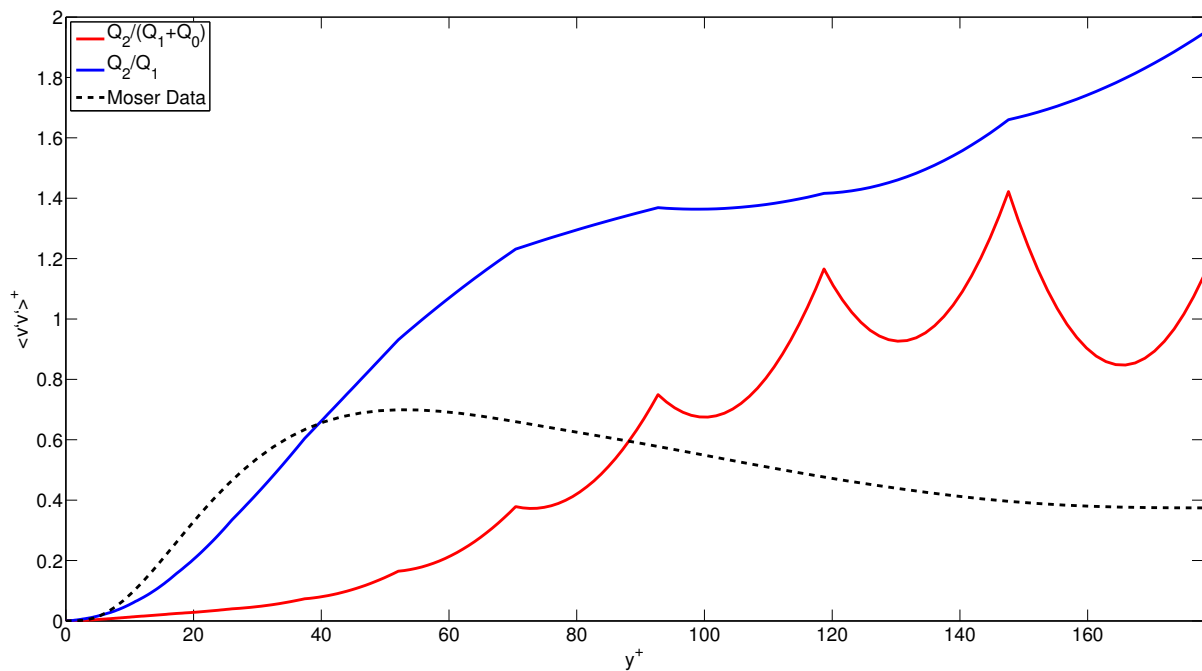
(b) Mesh resolution $16 \times 24 \times 24$

Figure 4.9: Reynold stress $\langle v'v' \rangle^+$
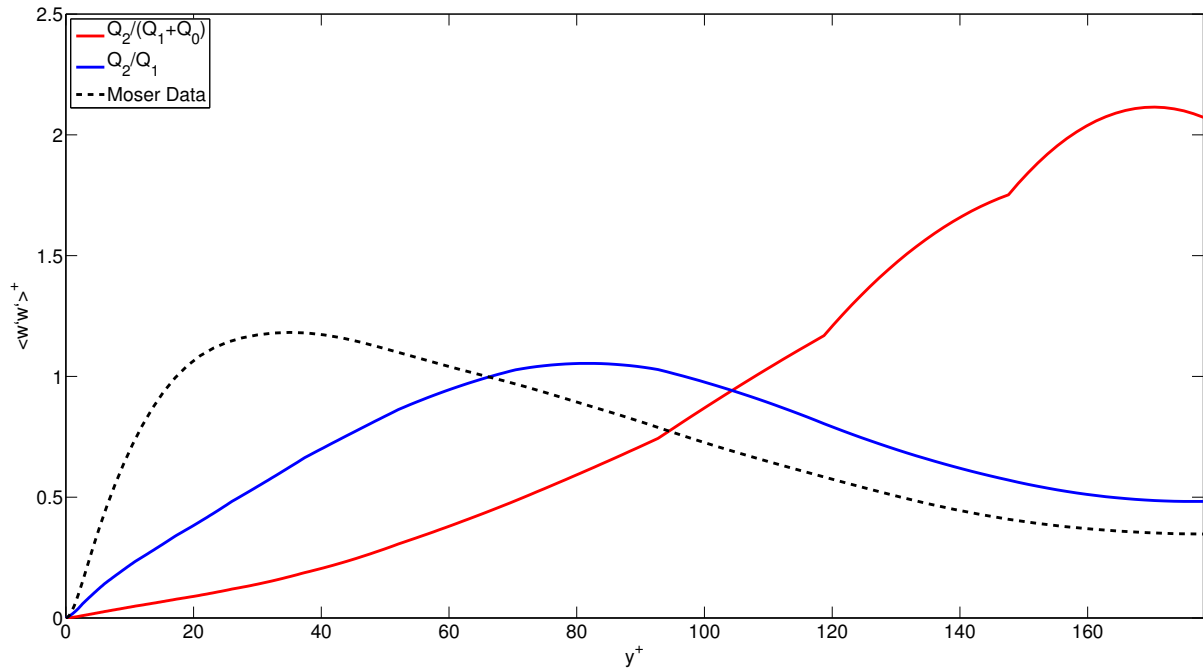
(a) Mesh resolution $16 \times 24 \times 16$
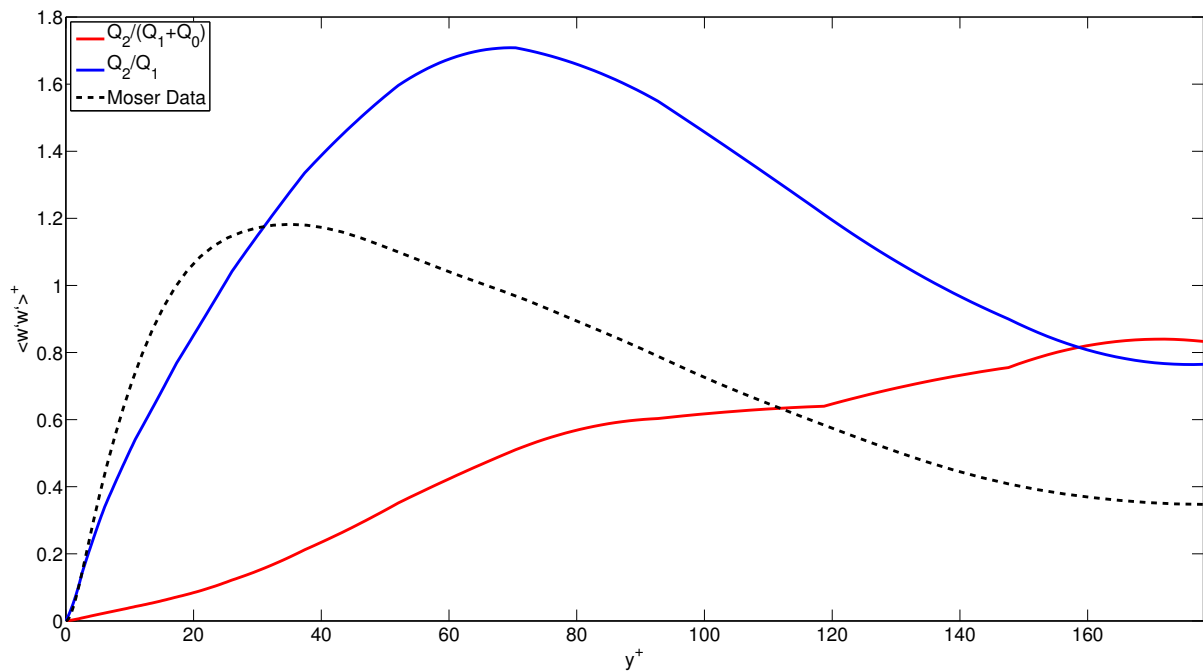
(b) Mesh resolution $16 \times 24 \times 24$

Figure 4.10: Reynold stress $\langle w'w' \rangle^+$
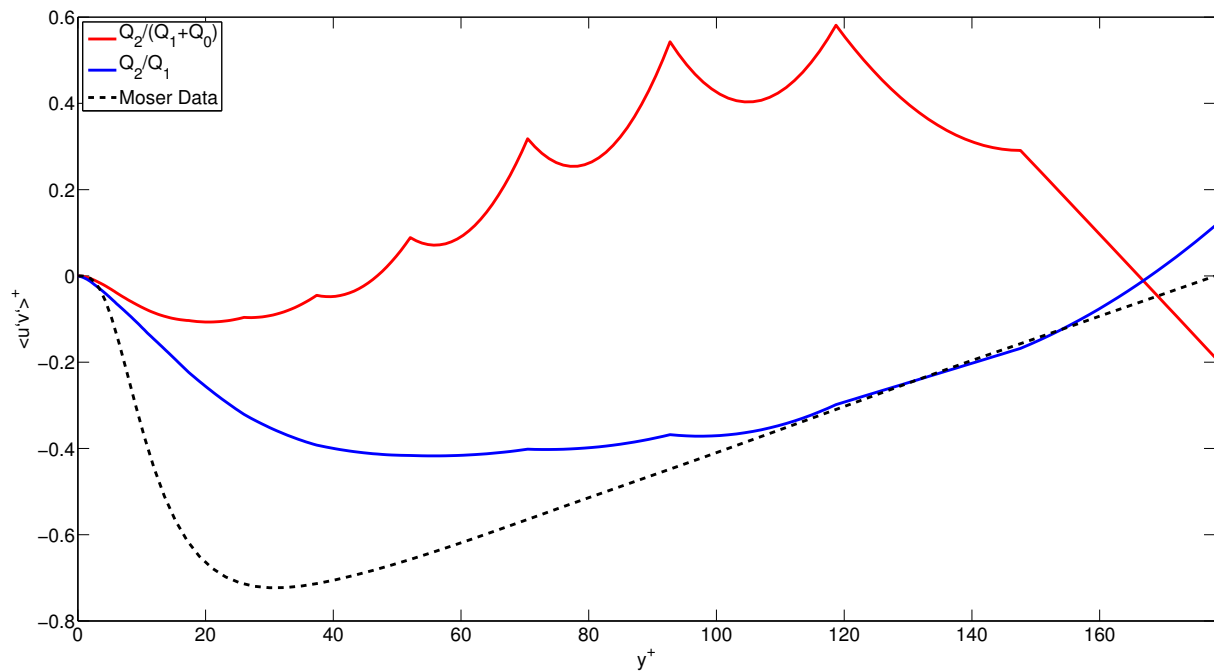
(a) Mesh resolution $16 \times 24 \times 16$
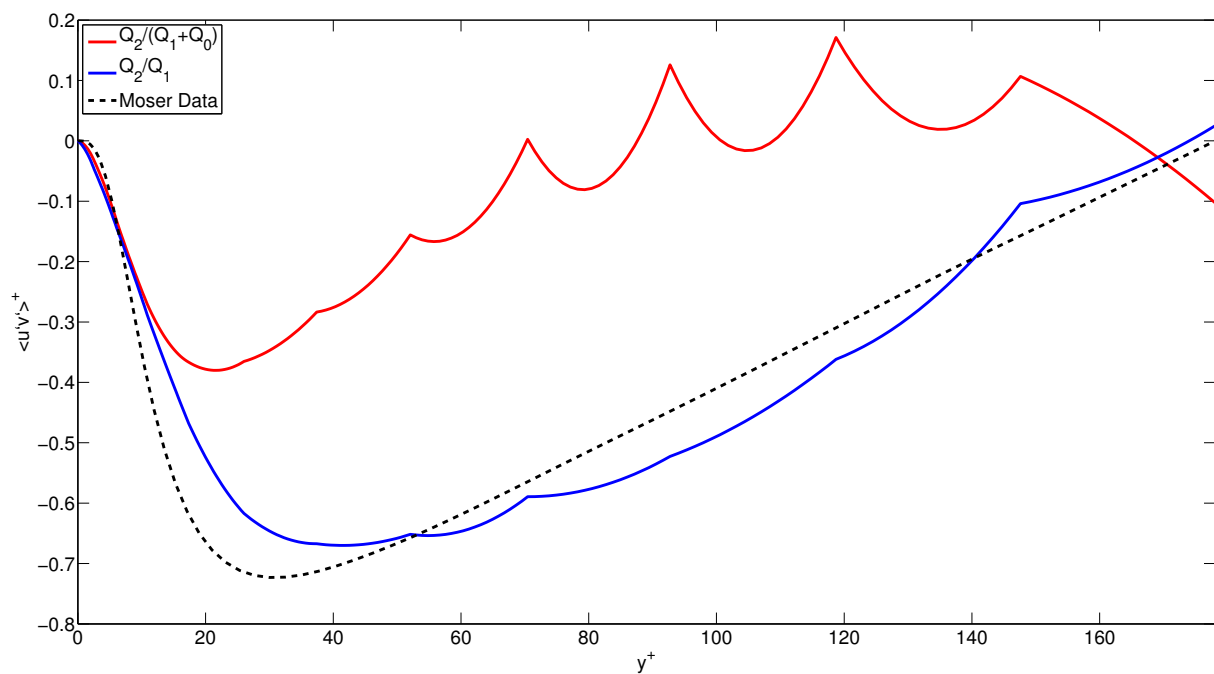
(b) Mesh resolution $16 \times 24 \times 24$

Figure 4.11: Reynold stress $\langle u'v' \rangle^+$
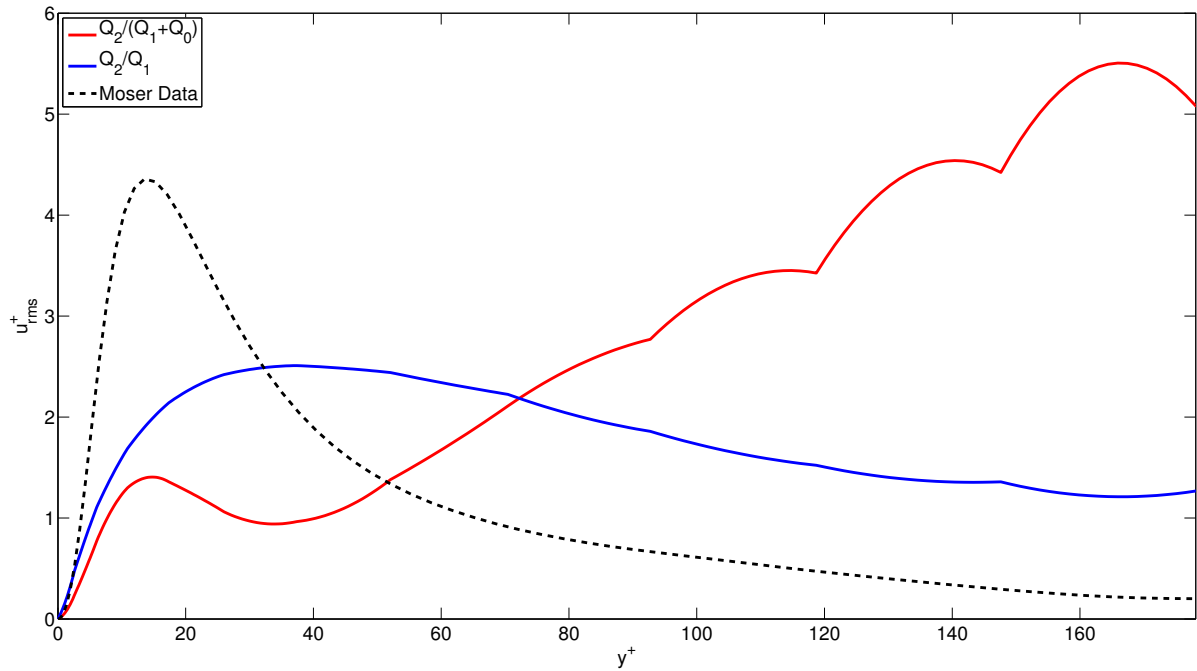
(a) Mesh resolution $16 \times 24 \times 16$
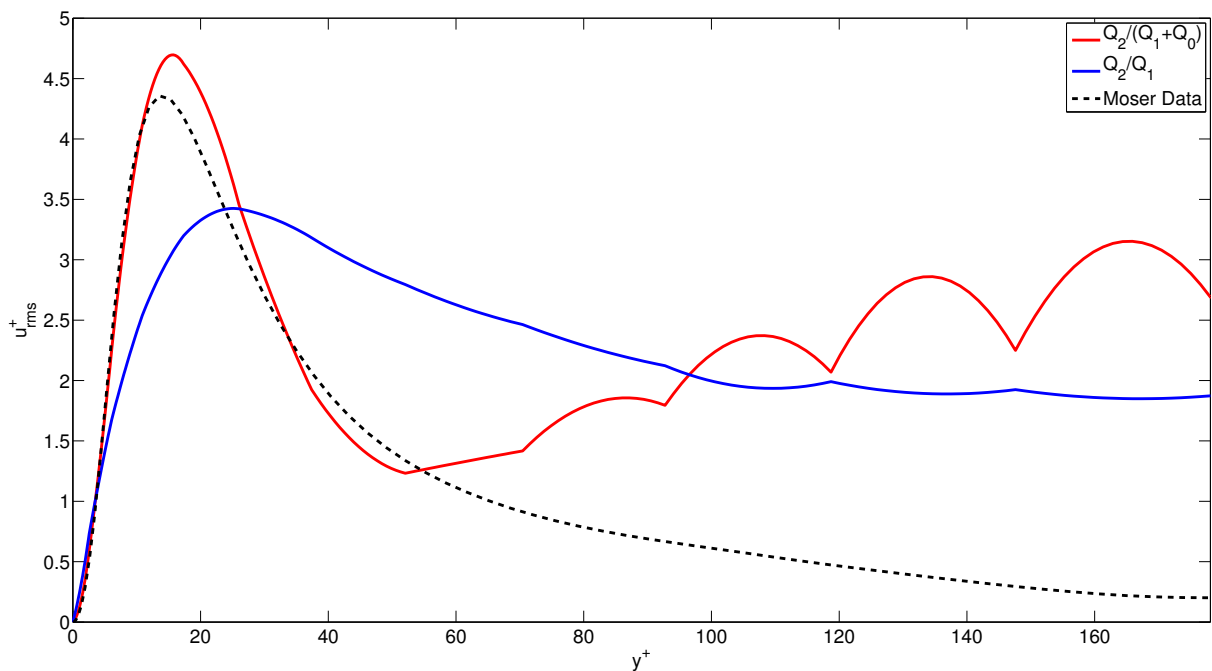
(b) Mesh resolution $16 \times 24 \times 24$

Figure 4.12: Root mean square velocity u_{rms}^+
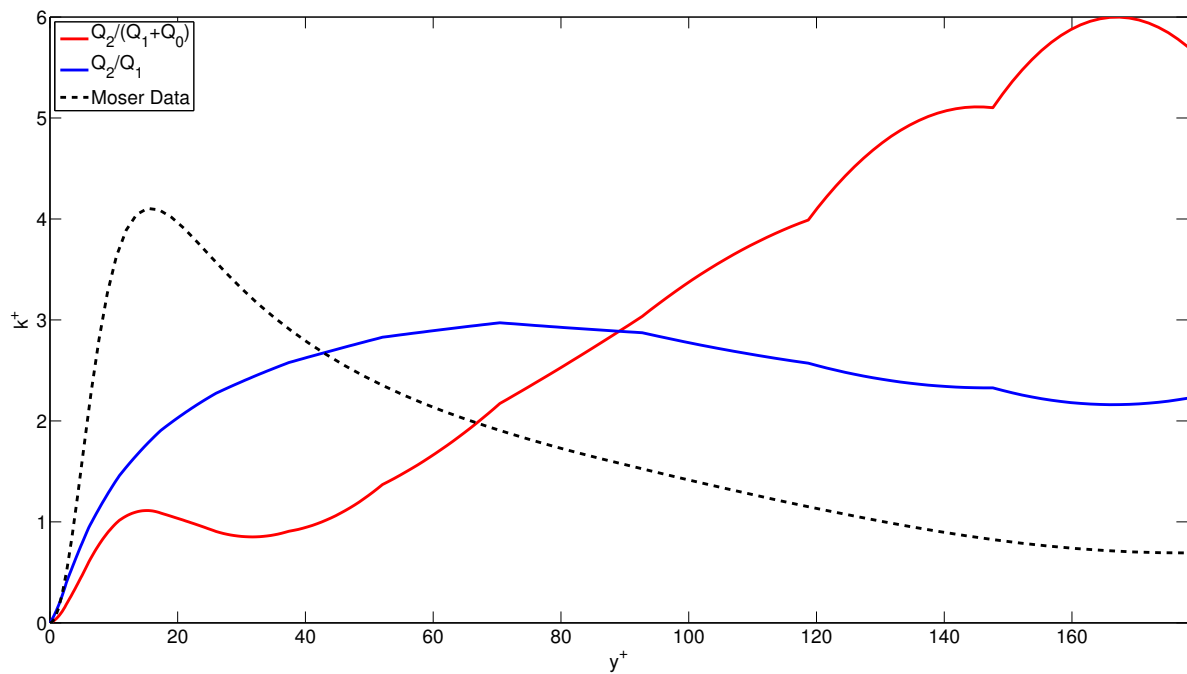
(a) Mesh resolution $16 \times 24 \times 16$
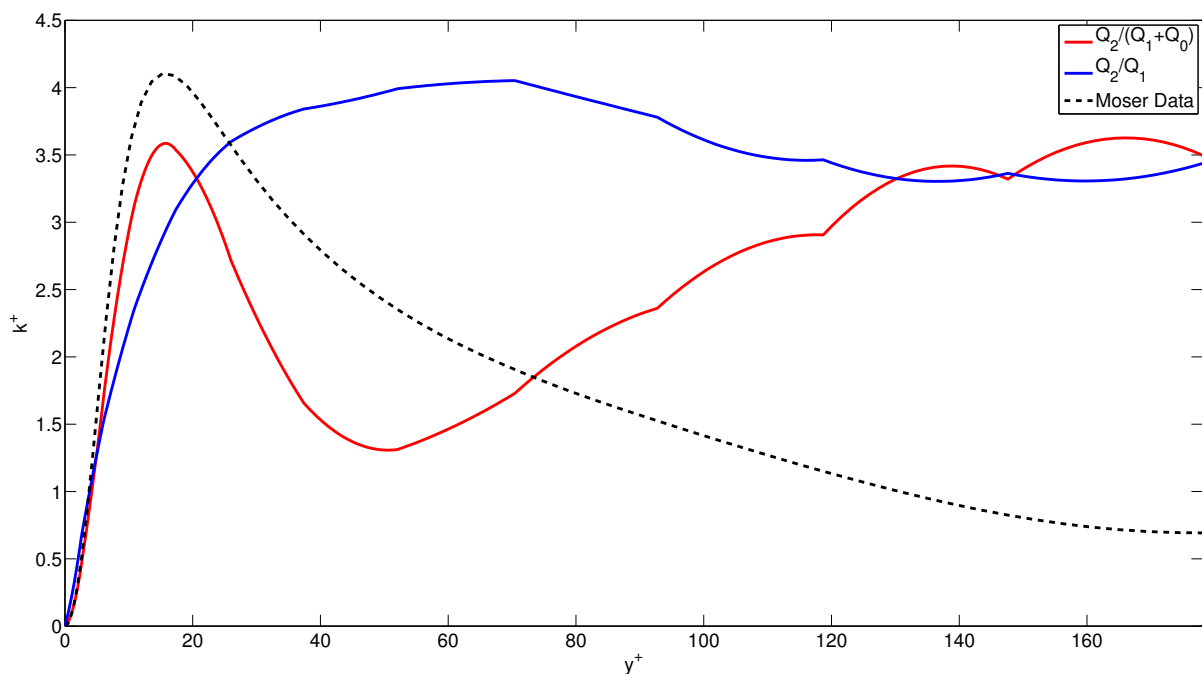
(b) Mesh resolution $16 \times 24 \times 24$

Figure 4.13: Turbulent kinetic energy k^+

Comparison between Neumann and partly periodic boundary conditions

Finally, we compare the impact of the boundary conditions on the solutions. The original implementation in [Hei11] uses for velocity and pressure the same periodicity constraints. This led to a significant improvement in terms of computation time. We observed the same effect for our $\mathcal{Q}_2/(\mathcal{Q}_1 + \mathcal{Q}_0)$ pair in Tale 4.1. However, since there are no boundary conditions for the pressure in the Navier-Stokes equations, the question arises whether this choice is appropriate. Therefore, we consider a $16 \times 24 \times 24$ mesh and compute the numerical solution using Neumann boundary conditions for the pressure everywhere.
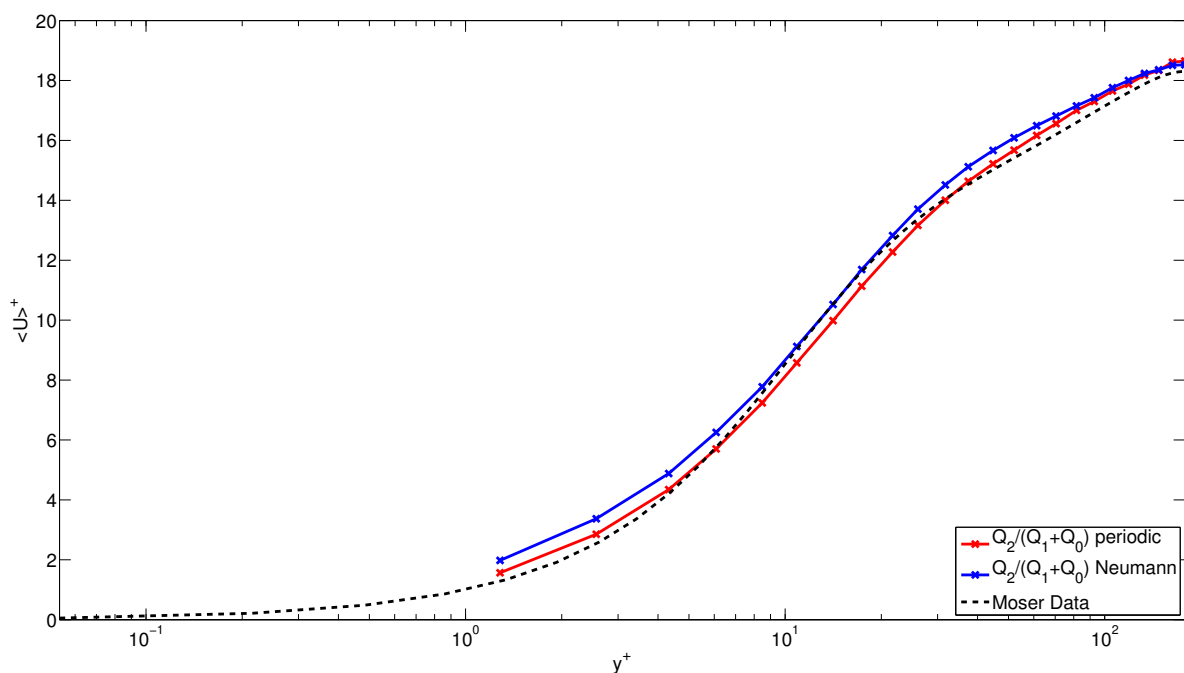
Figure 4.14: $\langle u \rangle^+$

Figure 4.14 shows that the mean velocity profile $\langle u \rangle$ even gets worse when changing from periodic to Neumann boundary conditions except for the interval $y^+ \in [10, 20]$ where the solution is in good agreement with the Moser data. In this interval all the previous considered cases showed worst behavior.

According to Figure 4.15 the results in the y-direction remain the same. This might not be surprising since the boundary conditions in that direction were not changed.

Concerning the last component of the velocity Figure 4.16 shows that the numerical solution stays longer close to zero when Neumann boundary condition are used. However, for $y^+ \geq 30$ in both cases there is a non-vanishing velocity component in z-direction.

For the statistics of second of order we first examine the variance $\langle u'u' \rangle^+$. In Figure 4.17 we observe that compared to the periodic boundary conditions the Neumann conditions yield a peak that is to high compared to the reference data. However, the behavior towards the
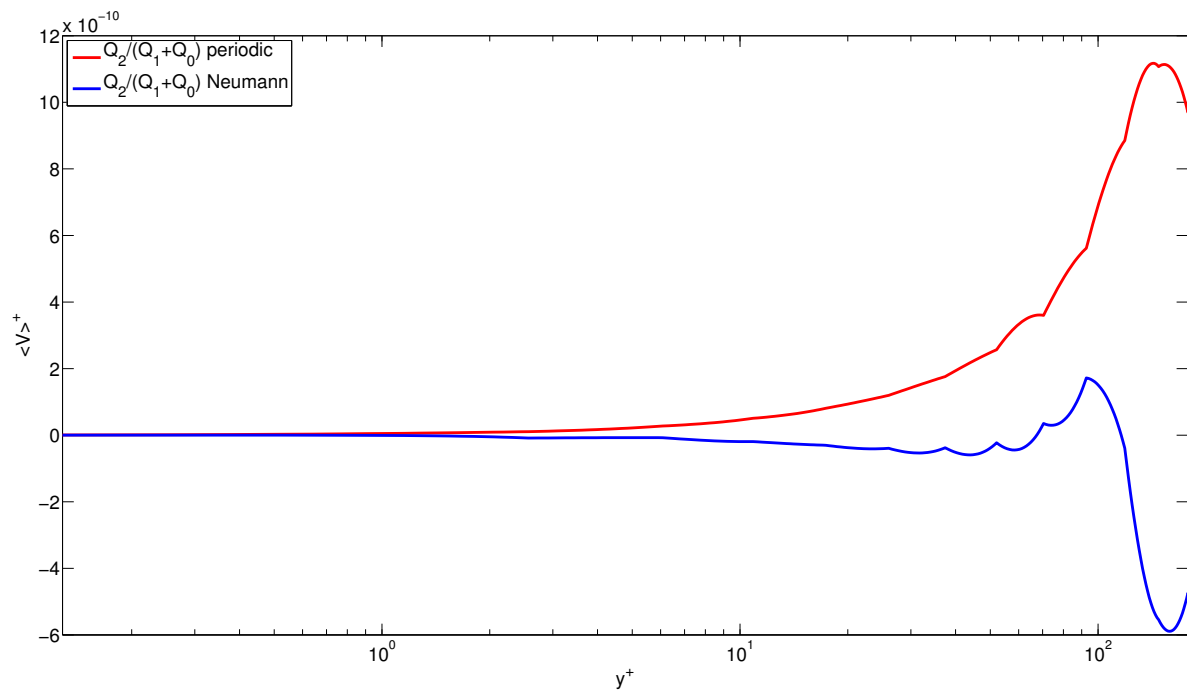
Figure 4.15: $\langle v \rangle^+$
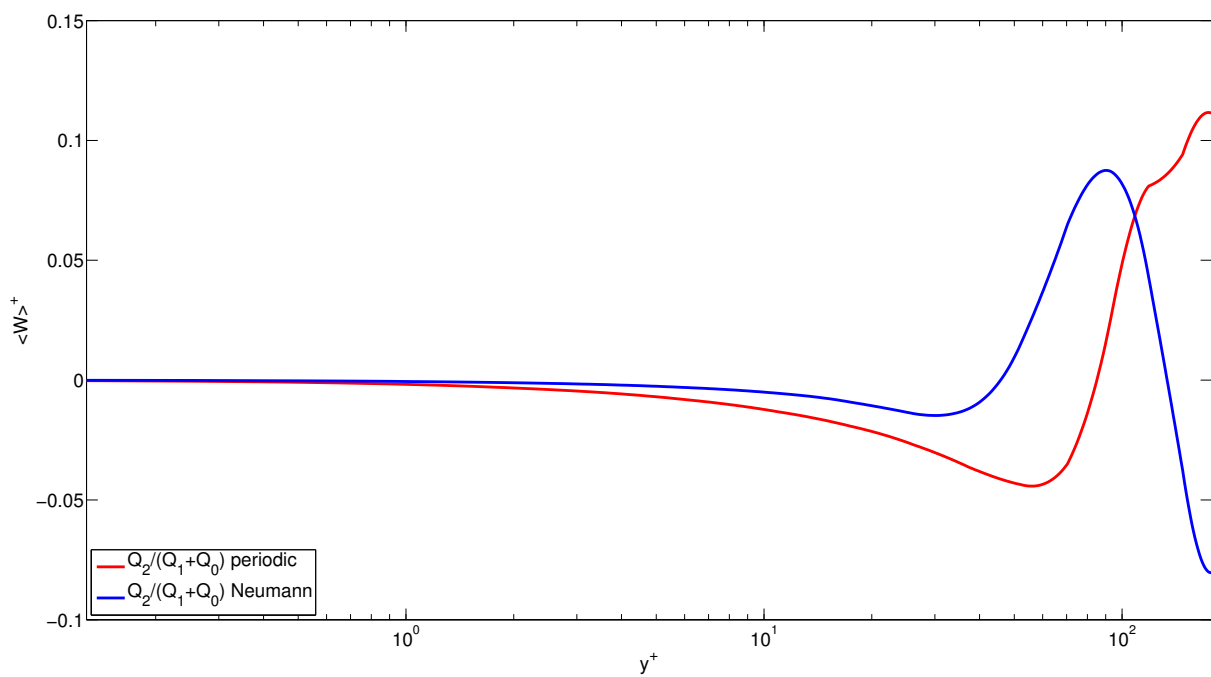
Figure 4.16: $\langle w \rangle^+$

middle of the flow improved. Although the variance is still increasing instead of declining, the quotient between the peak value and the value in the middle of the value is much better.
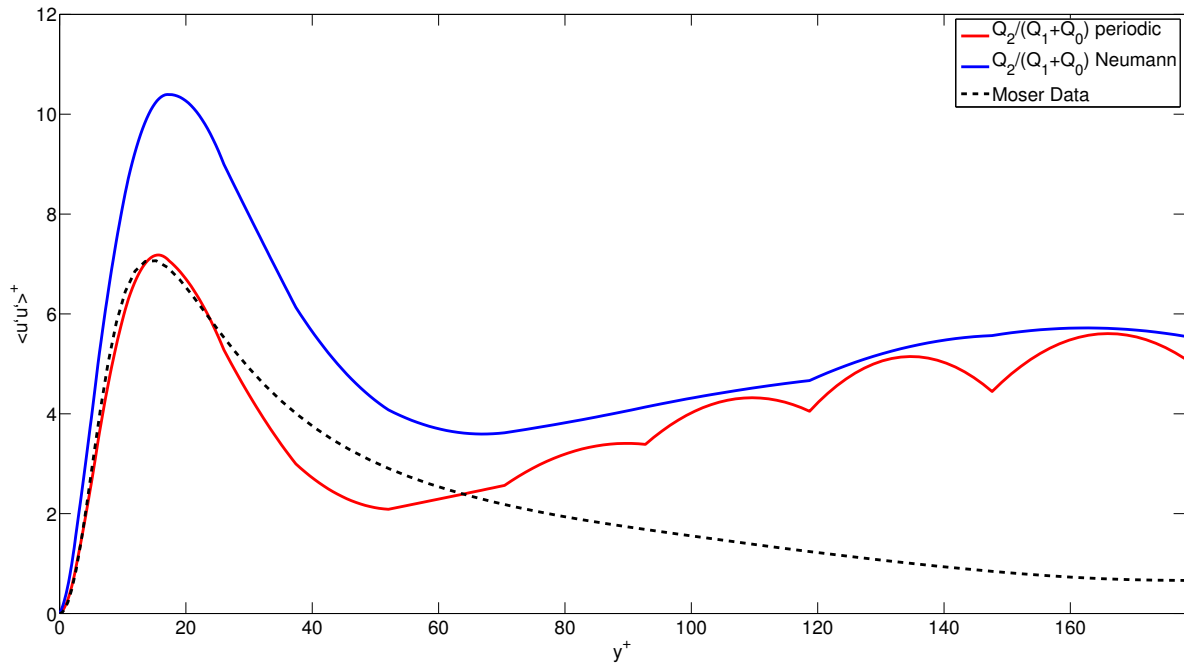
Figure 4.17: $\langle u'u' \rangle^+$
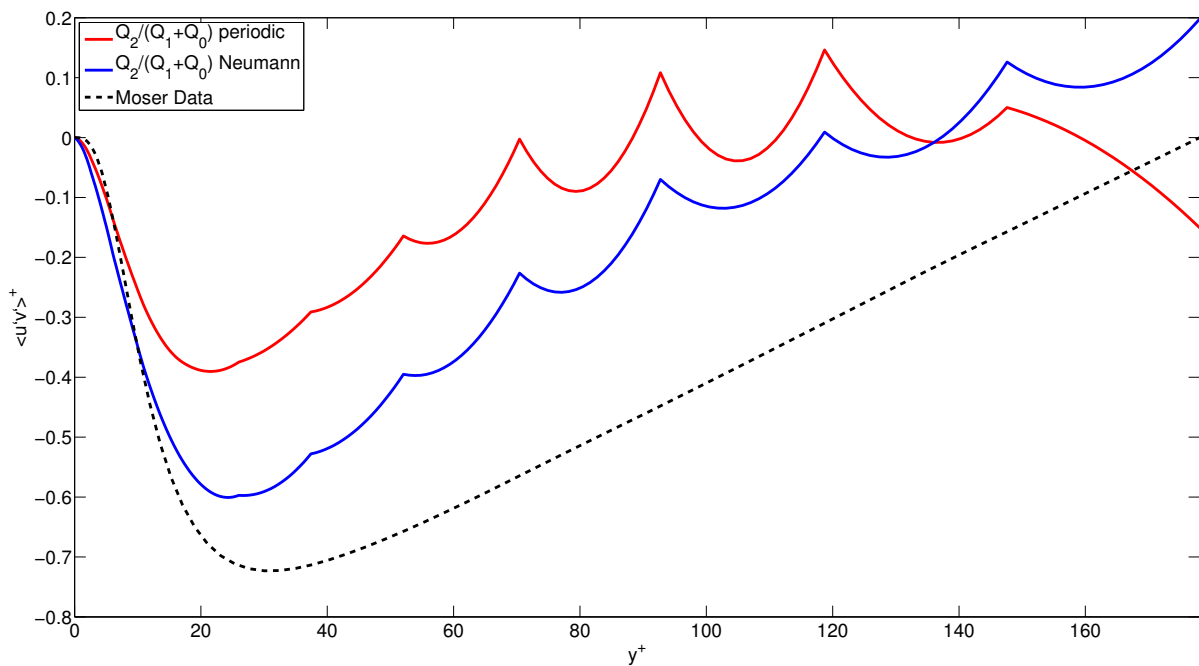
Figure 4.18: $\langle u'v' \rangle^+$

Next we compare the covariances $\langle u'v'\rangle^+$ in Figure 4.18. We already saw a significant improvement when refining the mesh in z-direction. This trend is continued when we switch form the periodicity constraints to the Neumann boundaries. The negative peak is met much better and also the quantitative trend towards the middle of the flow is right. In particular there is no decline towards the middle of the channel.

Unfortunately the results for the variance in y-direction $\langle v'v'\rangle$ and in z-direction does not improve. Both the profile in Figure 4.19 and Figure 4.20 differ much from the reference values.
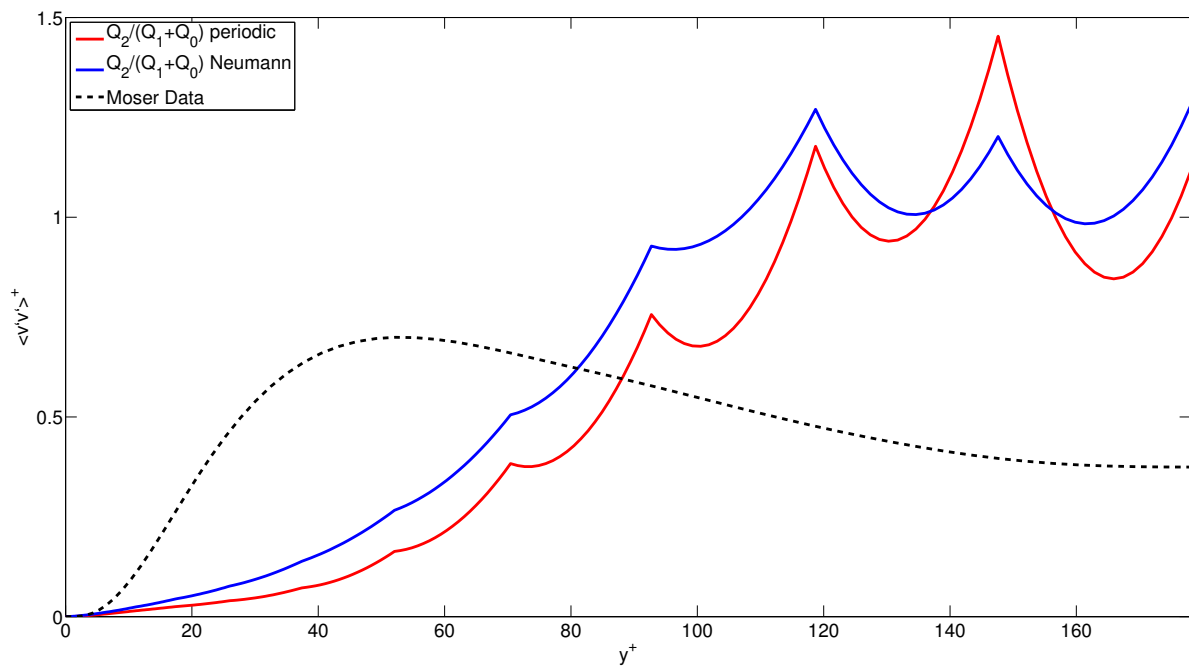
Figure 4.19: $\langle v'v'\rangle^+$

Concerning the turbulent kinetic energy k^+ we observe that for the Neumann conditions the peak is too high and too low for the periodicity constraints. The declining behavior towards the middle of the flow seems again to be better for the Neumann boundary conditions.

In summary there are no clear indications against using the same boundary conditions as for the velocity. Some quantities are significantly better using Neumann boundary conditions ($\langle u'v'\rangle^+$ and $\langle w\rangle^+$) and some other show improved behavior with periodicity constraints ($\langle u'u'\rangle^+$ and $\langle u\rangle^+$).

4.5.3 Computational costs

Similarly to the case of Stokes flow, we want to compare the computational effort that has to be spend when using the $\mathcal{Q}_2/\mathcal{Q}_1$ and the $\mathcal{Q}_2/(\mathcal{Q}_1 + \mathcal{Q}_0)$ element.
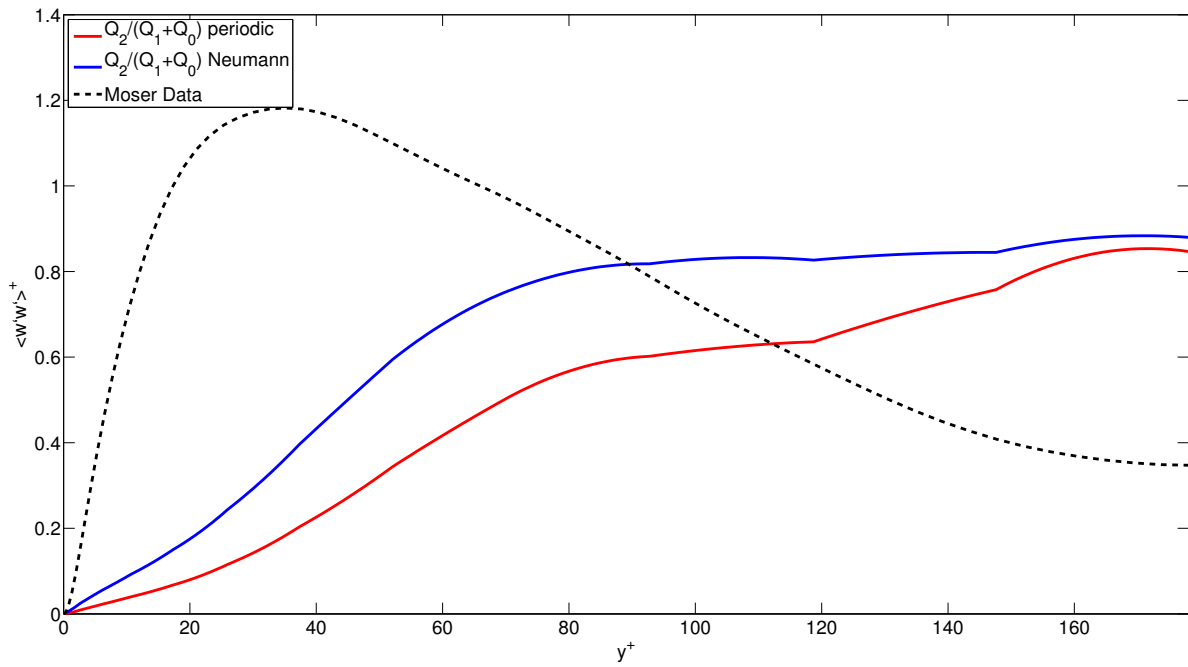
Figure 4.20: $\langle w'w' \rangle^+$
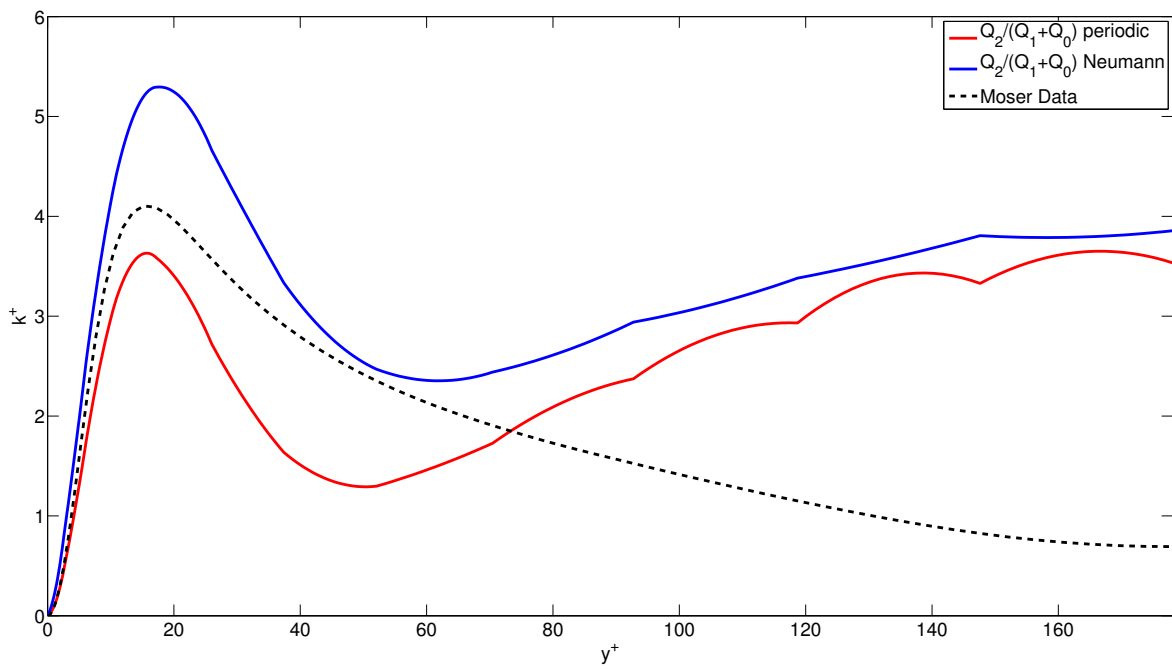
Figure 4.21: k^+

Again, the $\mathcal{Q}_2$-approximation for the velocity is the same and there are $(2n_1 + 1)(2n_2 + 1)(2n_3 + 1)$ dofs for each component assuming the mesh has a $n_1 \times n_2 \times n_3$ resolution. For the pressure we get $(n_1 + 1)(n_2 + 1)(n_3 + 1)$ resp. $(n_1 + 1)(n_2 + 1)(n_3 + 1) + n_1 n_2 n_3$ dofs. In particular the number of pressure nodes is in both cases much smaller then the number of velocity dofs. Compared to the implementation with the continuous pair the SIPG terms have to be assembled. According to our considerations this effort is clearly negligible in comparison to the remaining assembling time.

However, there is a huge difference in the duration of the solving process. This is mainly due to the fact that we did not find a preconditioner for the $\mathcal{Q}_2/(\mathcal{Q}_1 + \mathcal{Q}_0)$ element that leads to performance as impressive as the BoomerAMG algorithm for the $\mathcal{Q}_2/\mathcal{Q}_1$ Taylor-Hood pair. In particular this means that the current implementation is not as efficient as before.
Nevertheless, the numerical results, i.e. the statistics, show that the use of a the new element is worth the effort.

5 Summary

In this thesis we considered the finite element pair $\mathcal{Q}_{k+1}/(\mathcal{Q}_{k+1} + \mathcal{Q}_0)$ that is generated from the Taylor-Hood pair by adding elementwise constant functions to the pressure space. In particular we analyzed the behavior when applied to incompressible flow, namely the Stokes and Navier-Stokes equations.

Section 2 was devoted to the Stokes problem. We first of all proved that the considered finite element pair satisfies a discrete inf-sup condition for arbitrary regular quadrilateral and hexahedral meshes. From this result we got optimal convergence results by standard analysis. Afterwards we confirmed these observation with numerical results. Therefore, we chose a discontinuous reference solution and saw that no Gibbs phenomenon occurred in contrary to the observations with the Taylor-Hood pair. The optimality of the orders of convergence was then validated for $k \in \{1, 2\}$ and space dimension $d = 2$.

In the third section we constructed suitable methods for solving a Poisson equation using the element pair. Approximation results were given and the unique solvability of the proposed methods was proven. These kind of problems often occur when incompressible flow problems are discretized. As example may serve the projection step in a decoupled Navier-Stokes solver or the construction of a preconditioner for our implementation.

Finally, in the fourth chapter the full incompressible Navier-Stokes equations where considered. After some remarks to the implementation details a suitable preconditioner was constructed. For that in particular the results from the previous section were crucial. Then the proposed implementation was applied on the testcase of a turbulent channel flow. The results clearly showed that the element pair improves all the first order statistics compared to the Taylor-Hood element. For the second order statistics the observations are not that clear as there seems to be a strange behavior in the middle of the flow. Nevertheless these results could significantly be improved by refining the mesh in spanwise direction. There does not seem to be any serious indications against using partly periodic boundary conditions for the pressure.

A remaining problem clearly is the choice of a better preconditioner for the SIPG method that accelerates the CG solver sufficiently. In particular the rather slow solver prevents considering finer mesh resolutions. An additional approach to the already considered might be the use of geometric multi-grid methods. However, in the used library `deal.II` a parallel version is not yet available. The implementation is nontrivial since already partitioning the mesh over different processes is a difficult problem and an external package is used for this task.

Another problem that occurred in this thesis are the strange results in the second order statistics. The only cure so far seems to be to refine the mesh.

Acknowledgments

First of all, I would like to thank Prof. Dr. Gert Lube for supervising this thesis and proposing this very interesting topic to me. Further thanks go to Dr. Timo Heister who supported me especially in the numerical part of this thesis and was a discerning proofreader.

Additional acknowledgment deserves Dr. Lars Röhe who always had a sympathetic ear for me and my problems.

I am especially grateful to my family who supported me during my studies.

References

[ABCM02] Arnold, Douglas N. ; Brezzi, Franco ; Cockburn, Bernardo ; Marini, L.Donatella: Unified analysis of discontinuous Galerkin methods for elliptic problems. In: *SIAM J. Numer. Anal.* 39 (2002), Nr. 5, S. 1749–1779. `http://dx.doi.org/10.1137/S0036142901384162`. – DOI 10.1137/S0036142901384162

[Ape99] Apel, Thomas: *Anisotropic finite elements: Local estimates and applications.*, Chemnitz: TU Chemnitz, SFB 393, iv, 188 p. , Diss., 1999

[BBB+12] Balay, Satish ; Brown, Jed ; Buschelman, Kris ; Gropp, William D. ; Kaushik, Dinesh ; Knepley, Matthew G. ; McInnes, Lois C. ; Smith, Barry F. ; Zhang, Hong: *PETSc Web page.* `http://www.mcs.anl.gov/petsc`. Version: 2012

[BBF08] Boffi, Daniele ; Brezzi, Franco ; Fortin, Michel: Finite elements for the Stokes problem. In: *Boffi, Daniele (ed.) et al., Mixed finite elements, compatibility conditions, and applications. Lectures given at the C.I.M.E. summer school, Cetraro, Italy, June 26–July 1, 2006. Berlin: Springer; Florenz: Fondazione CIME Roberto Conti. Lecture Notes in Mathematics 1939, 45-100 (2008).* 1939 (2008), S. 45–100. `http://dx.doi.org/10.1007/978-3-540-78319-0`. – DOI 10.1007/978–3–540–78319–0

[BCGG12] Boffi, D ; Cavallini, N ; Gardini, F ; Gastaldi, L: Local Mass Conservation of Stokes Finite Elements. In: *Journal of scientific computing* 52 (2012), Nr. 2, S. 383–401

[BF91] Brezzi, Franco ; Fortin, Michel: *Mixed and hybrid finite element methods.* Springer Series in Computational Mathematics. 15. New York etc.: Springer-Verlag. ix, 350 p. , 1991

[BHK] Bangerth, W. ; Heister, T. ; Kanschat, G.: `deal.II` *Differential Equations Analysis Library, Technical Reference*, `http://www.dealii.org`. – `http://www.dealii.org`

[BHK07] Bangerth, W. ; Hartmann, R. ; Kanschat, G.: deal.II – a General Purpose Object Oriented Finite Element Library. In: *ACM Trans. Math. Softw.* 33 (2007), Nr. 4, S. 24/1–24/27

[BIL06] Berselli, L. C. ; Iliescu, T. ; Layton, W. J.: *Mathematics of large eddy simulation of turbulent flows.* Scientific Computation. Berlin: Springer. xvii,

348 p., 2006. `http://dx.doi.org/10.1007/b137408`. `http://dx.doi.org/10.1007/b137408`

[BKZ92]   BRACKBILL, J.U. ; KOTHE, D.B. ; ZEMACH, C.: A continuum method for modeling surface tension. In: *J. Comput. Phys.* 100 (1992), Nr. 2, S. 335–354. `http://dx.doi.org/10.1016/0021-9991(92)90240-Y`. – DOI 10.1016/0021–9991(92)90240–Y

[Cho00]   CHOW, Edmond: A priori sparsity patterns for parallel sparse approximate inverse preconditioners. In: *SIAM J. Sci. Comput.* 21 (2000), Nr. 5, S. 1804–1822. `http://dx.doi.org/10.1137/S106482759833913X`. – DOI 10.1137/S106482759833913X

[Dal12]   DALLMANN, Helene: *A Turbulence Model based on Invariants of the Strain Rate Tensor*, University of Göttingen, Institute for Numerical and Applied Mathematics, Master's Thesis, 2012

[ESW05]   ELMAN, Howard C. ; SILVESTER, David J. ; WATHEN, Andrew J.: *Finite elements and fast iterative solvers: with applications in incompressible fluid dynamics.* Numerical Mathematics and Scientific Computation. Oxford: Oxford University Press. xiii, 400 p., 2005

[FEQ12]   *FE_Q_DG0 Class Template Reference.* `http://www.dealii.org/developer/doxygen/deal.II/classFE__Q__DG0.html`. Version: 2012

[FJY06]   FALGOUT, Robert D. ; JONES, Jim E. ; YANG, Ulrike M.: *The design and implementation of hypre, a library of parallel high performance preconditioners.* Berlin: Springer, 2006

[Giv01]   GIVOLI, Dan: The Top 10 Computational Methods of the 20th Century. In: *IACM Expressions* 11 (2001), Nr. 11, S. 5–9

[GR86]   GIRAULT, Vivette ; RAVIART, Pierre-Arnaud: *Finite element methods for Navier-Stokes equations. Theory and algorithms.* Springer Series in Computational Mathematics, 1986

[GR07]   GROSS, Sven ; REUSKEN, Arnold: An extended pressure finite element space for two-phase incompressible flows with surface tension. In: *J. Comput. Phys.* 224 (2007), Nr. 1, S. 40–58. `http://dx.doi.org/10.1016/j.jcp.2006.12.021`. – DOI 10.1016/j.jcp.2006.12.021

[Har08]   HARTMANN, Ralf: Numerical Analysis of Higher Order Discontinuous Galerkin Finite Element Methods. In: *CFD - ADIGMA course on very high order discretization methods, Oct. 13-17, 2008, Rhode Saint Genese, Belgium* 2008-08 (2008), S. 1–107

[Hei11]   HEISTER, Timo: *A massively parallel finite element framework with application to incompressible flows.*, University of Göttingen, Diss., 2011

[HMY02]   HENSON, Van E. ; MEIER YANG, Ulrike: *BoomerAMG*: A parallel algebraic multigrid solver and preconditioner. In: *Appl. Numer. Math.* 41 (2002), Nr. 1, S. 155–177. `http://dx.doi.org/10.1016/S0168-9274(01)00115-5`. – DOI 10.1016/S0168–9274(01)00115–5

[MKM99]   MOSER, Robert D. ; KIM, John ; MANSOUR, Nagi N.: Direct numerical simulation of turbulent channel flow up to $Re_\tau = 590$. In: *Phys. Fluids* 11 (1999), Nr. 4, S. 943–945. `http://dx.doi.org/10.1063/1.869966`. – DOI 10.1063/1.869966

[MT02]   MATTHIES, G. ; TOBISKA, L.: The inf-sup condition for the mapped $Q_k - P_{k-1}^{\mathrm{disc}}$ element in arbitrary space dimensions. In: *Computing* 69 (2002), Nr. 2, S. 119–139. `http://dx.doi.org/10.1007/s00607-002-1451-3`. – DOI 10.1007/s00607–002–1451–3

[RST08]   ROOS, Hans-Görg ; STYNES, Martin ; TOBISKA, Lutz: *Robust numerical methods for singularly perturbed differential equations. Convection-diffusion-reaction and flow problems. 2nd ed.* Springer Series in Computational Mathematics 24. Berlin: Springer. xiv, 604 p., 2008. `http://dx.doi.org/10.1007/978-3-540-34467-4`. `http://dx.doi.org/10.1007/978-3-540-34467-4`

[Rö11]   RÖHE, Lars: *Turbulence Modelling by a Projection-Based Variational Multiscale Method for Incompressible Flow Problems*, University of Göttingen, Diss., 2011

[Ste84]   STENBERG, Rolf: Analysis of mixed finite element methods for the Stokes problem: A unified approach. In: *Math. Comput.* 42 (1984), S. 9–23. `http://dx.doi.org/10.2307/2007557`. – DOI 10.2307/2007557

[Tem95]   TEMAM, Roger: *Navier-Stokes equations and nonlinear functional analysis. 2nd ed.* CBMS-NSF Regional Conference Series in Applied Mathematics. 66. Philadelphia, PA: SIAM, Society for Industrial and Applied Mathematics. xiv, 141 p. \$ 26.50/pbk , 1995

[Ver11]   VERSTAPPEN, Roel: When does eddy viscosity damp subfilter scales sufficiently?   In: *J. Sci. Comput.* 49 (2011), Nr. 1, S. 94–110. `http://dx.doi.org/10.1007/s10915-011-9504-4`. – DOI 10.1007/s10915–011–9504–4

[Zha07]   ZHANG, Xiaoqin: *Identification of model and grid parameters for incompressible turbulent flows*, University of Göttingen, Diss., 2007

Erklärung nach §13(6) der Prüfungsordnung für den Master-Studiengang Mathematik an der Universität Göttingen:

Hiermit erkläre ich, dass ich diese Abschlussarbeit selbständig verfasst habe, keine anderen als die angegebenen Quellen und Hilfsmittel benutzt habe und alle Stellen, die wörtlich oder sinngemäß aus veröffentlichten Schriften entnommen wurden, als solche kenntlich gemacht habe. Darüberhinaus erkläre ich, dass diese Abschlussarbeit nicht, auch nicht auszugsweise, im Rahmen einer nichtbestandenen Prüfung an dieser oder einer anderen Hochschule eingereicht wurde.

Göttingen, den 11. März 2013

(Daniel Arndt)